UNIVERSIDADE ESTADUAL PAULISTA
"JÚLIO DE MESQUITA FILHO"

PROGRAMA DE PÓS-GRADUAÇÃO EM
FARMACOLOGIA E BIOTECNOLOGIA
(PPG-FARMATEC)

Instituto de Biociências de Botucatu - Unesp

Biosusceptometria AC e nanopartículas magnéticas para avaliação de parâmetros biofísicos: renais, cerebrais e efeito corona

ANDRÉ GONÇALVES PRÓSPERO

Tese de doutorado apresentada ao Instituto de Biociências, Universidade Estadual Paulista "Júlio de Mesquita Filho", Campus de Botucatu para obtenção do título de Doutor em Farmacologia e Biotecnologia.

Orientador: Prof. Dr. José Ricardo de Arruda Miranda

Co-Orientadora: Profa. Dra.Patrícia Fidelis de Oliveira

2019

UNIVERSIDADE ESTADUAL PAULISTA
"JÚLIO DE MESQUITA FILHO"

PROGRAMA DE PÓS-GRADUAÇÃO EM
FARMACOLOGIA E BIOTECNOLOGIA
(PPG-FARMATEC)

Instituto de Biociências de Botucatu - Unesp

Biosusceptometria AC e nanopartículas magnéticas para avaliação de parâmetros biofísicos: renais, cerebrais e efeito corona

ANDRÉ GONÇALVES PRÓSPERO

Tese de doutorado apresentada ao Instituto de Biociências, Universidade Estadual Paulista "Júlio de Mesquita Filho", Campus de Botucatu para obtenção do título de Doutor em Farmacologia e Biotecnologia.

Orientador: Prof. Dr. José Ricardo de Arruda Miranda

Co-Orientadora: Profa. Dra.Patrícia Fidelis de Oliveira

2019

FICHA CATALOGRÁFICA ELABORADA PELA SEÇÃO TÉC. AQUIS. TRATAMENTO DA INFORM.
DIVISÃO TÉCNICA DE BIBLIOTECA E DOCUMENTAÇÃO - CÂMPUS DE BOTUCATU - UNESP
BIBLIOTECÁRIA RESPONSÁVEL: ROSANGELA APARECIDA LOBO-CRB 8/7500

Próspero, André Gonçalves.
Biosusceptometria AC e nanopartículas magnéticas para avaliação de parâmetros biofísicos : renais, cerebrais e efeito corona / André Gonçalves Próspero. - Botucatu, 2019

Tese (doutorado) - Universidade Estadual Paulista "Júlio de Mesquita Filho", Instituto de Biociências de Botucatu
Orientador: José Ricardo de Arruda Miranda
Coorientador: Patrícia Fidelis de Oliveira
Capes: 20903006

1. Física médica. 2. Biofísica. 3. Biosusceptometria de Corrente Alternada. 4. Nanopartículas. 5. Perfusão isolada (Fisiologia). 6. Rins - Fisiologia. 7. Cérebro - Fisiologia.

Palavras-chave: biofísica cerebral; biofísica renal; biosusceptometria AC; efeito corona; nanopartículas magnéticas.

AGRADECIMENTOS

Agradeço em primeiro lugar à Deus, pela vida maravilhosa que tenho e por sempre estar presente e me guiar em todas as minhas decisões.

À minha companheira Sabrina Galetti Cherelli por estar sempre disponível e disposta a me ajudar no que for preciso nesses quase sete anos de relacionamento e quase cinco sob o mesmo teto, por me amar e ser a melhor companheira que eu poderia ter ao meu lado. Obrigado por me aturar, cuidar e zelar por mim. Agradeço também à sua família que sempre me acolhe e me trata como parte dela.

Agradeço aos meus pais, Alaor Eduardo Próspero e Marben Maria Gonçalves Próspero, que apesar das dificuldades sempre acreditaram em mim, me incentivaram, apoiaram incondicionalmente e torceram pelo meu sucesso.

Agradeço ao meu irmão Alexandre Gonçalves Próspero, por me dar força, por estar ao meu lado durante toda minha vida e ter feito parte de muitas histórias que nos marcaram.

À toda minha família: avós, tios, primos, que sempre me deram energia para conseguir terminar essa caminhada. Em especial à minha avó Marben Ferraz da Porciúncula Gonçalves, que sempre esteve pronta a me ajudar no que fosse necessário.

Ao professor Dr. José Ricardo de Arruda Miranda, meu orientador, à quem tenho grande admiração, por ter uma mente brilhante, por ter o dom de passar seus conhecimentos adiante e por ser um excelente empreendedor da vida acadêmica . Por me proporcionar uma série de oportunidades na carreira acadêmica - aqui destaco meu doutorado sanduíche no exterior, incentivo e apoio para obtenção da vaga de professor bolsista junto ao Dep. de Física e Biofísica, me autorizar contato direto com sua rede de

colaboradores e me permitir adicionar alguns novos colaboradores ao longo desses quatro anos. Por me ensinar muito e principalmente por me fazer descobrir aptidões e gosto pelo ensino e pela pesquisa. Agradeço também à sua esposa, professora Dra. Diana Rodrigues de Pina Miranda, por fazer, junto ao professor José Ricardo, dos grupos de pesquisa Biomag e Lafar uma grande família.

À professora Dra. Patrícia Fidelis de Oliveira, minha co-orientadora, por ter me introduzido em uma nova área do conhecimento científico, por ter uma excelente didática, por ter utilizado seu tempo para retirar minhas dúvidas e por sempre estar disposta a me ajudar no que fosse necessário, principalmente quando chego de última hora com uma série problemas a serem resolvidos. Além disso agradeço também à todas as colaborações intelectuais presentes ao longo deste trabalho, onde sua presença está fortemente marcada nas discussões e interpretações fisiológicas e funcionais, que foram base do desenvolvimento e finalização do trabalho principal aqui apresentado.

À todos os integrantes dos laboratórios Biomag e Lafar, por fazerem deste ambiente de trabalho um lugar onde sinto prazer em estar.

Ao Departamento de Física e Biofísica, por me proporcionar a experiência da docência através de um programa de professor bolsista em três diferentes matérias oferecidas pelo departamento.

Ao professor Dr. Andris Figueiroa Bakuzis, por me proporcionar grandes experiências em seu laboratório, apresentar diferentes técnicas, métodos e instrumentações científicas, além dos constantes questionamentos com alto nível de complexidade, que me motivaram a passar noites em claro debruçado em livros e artigos científicos.

Ao professor Dr. Oswaldo Baffa Filho, por dedicar seu tempo e rede de colaborações a fim de viabilizar meu doutorado sanduíche no exterior, de me

proporcionar aprender sobre temas e instrumentações que estão na vanguarda da pesquisa em biomagnetismo a nível internacional e por me permitir participar do processo de “importação” dessa tecnologia e conhecimento. Além disso, agradeço por ter me proporcionado a oportunidade de fazer parte, futuramente, de seu grupo de pesquisa por meio da possibilidade de um projeto de pós doutorado sob sua supervisão.

Ao doutor Ronald Wakai, por me permitir fazer parte, temporariamente, de seu grupo de pesquisa. Por me receber de braços abertos em seu país, por ser sempre muito atencioso, educado, preocupado e amável. Por me proporcionar a possibilidade de trabalhar com técnicas e instrumentações que eu só conhecia dos livros. Além disso, gostaria de agradecer por, através dessa experiência internacional, me proporcionar um grande auto-conhecimento e me apresentar uma pluralidade de ideias e possibilidades no universo da pesquisa.

Aos amigos Luis Henrique, Luis Marçal e Luis Mauro, que conheci no exterior e criei grande amizade, que me suportaram e fortaleceram durante esse período no exterior. Em especial ao William J. Lutter (Bill) que, mesmo com uma grande distância de idade e cultura, se tornou um amigo a quem tenho muito apreço e carinho; obrigado por me ajudar na rotina do laboratório, por me ensinar suas funções, pelos almoços e longas conversas que muito fortaleceram meu tímido domínio da língua inglesa.

À todo pessoal da UNIPEX, principalmente a Dr. Camila Corrêa, Denise e Leandro, que viabilizaram a preparação e montagem das lâminas, assim como a obtenção das imagens histológicas aqui apresentadas.

Às doutoras Daniela Cristina dos Santos e Vanessa dos Santos Silva, que apesar de termos nos conhecido recentemente, colaboraram imensamente para o enriquecimento deste trabalho e elucidação de vários dados aqui apresentados. Obrigado por disponibilizarem seu tempo e esforços para que estruturassemos um trabalho

multidisciplinar sustentado pela suas experiências em nefrologia e nefropatologia. Aqui destaco a Dra. Daniela, que mesmo com sua intensa rotina no hospital, se desdobrou para nos receber, analisar as lâminas e discutir os resultados obtidos.

Ao doutor Carlos Alexandre Fernandes, à doutora Lucilene Delazari dos Santos e ao professor Marcos Fontes, por estabelecermos uma parceria sólida que possibilitou uma série de novas possibilidades de investigações científicas, além do entendimento de muito do que já haviamos realizado e iremos realizar no futuro. Em especial ao Carlos Alexandre, pelas conversas científicas, políticas e históricas na cozinha do laboratório, que culminaram no desenvolvimento de um projeto de pesquisa em associação com os pesquisadores citados acima.

Ao Guilherme Augusto Soares, ao Caio César Quini, ao Marcos Felipe Calabresi, ao Ronaldo Vitor Reis Matos, à Milena Foltran e à Nurya Pinheiro, pela grande amizade, por terem especial participação em minha vida acadêmica, por terem me ensinado, muitas vezes através de exemplos, como deve ser a postura e atitudes de um pesquisador e de um professor. Por terem trabalhado comigo em muitos projetos e terem tido a paciência e entusiamo necessários, cada qual em seu momento, para que atingíssemos nossos objetivos.

Aos amigos Alan Fattori Alves, Ana Luiza Pavan, Luís Gustavo de Oliveira Simões, Juliana Fernandes Matos, Leonardo Pinto, Gabriela Bittencourt, João Victor Carneiro, Gustavo Serafim, Deivid William Pires e Rodolfo Cicolin pela convivência mais próxima, pelos churrascos, encontros festivos e finalmente pela grande amizade.

À Coordenação de Aperfeiçoamento de Pessoal de Nível Superior (CAPES) pelo financiamento da bolsa que recebi durante esses quatro anos.

Enfim, à todos que me ajudaram de alguma forma, direta ou indiretamente, meu muito obrigado!

RESUMO

A proposta deste trabalho é inédita e consiste na aplicação do sistema de Biosusceptometria AC (BAC), associado à nanopartículas magnéticas (MNPs), a fim de disponibilizar uma nova ferramenta para estudos de função e fisiologia renal, cerebral e efeito corona. Foram realizados experimentos com ratos para o estudo de parâmetros biofísicos da dinâmica de perfusão de MNPs nos rins e cérebro, em situações normais e alteradas, bem como sua biodistribuição no organismo. Além disso empregamos o sistema BAC para avaliar as alterações em propriedades magnéticas e farmacocinéticas das MNPs quando em contato com fluidos biológicos (formação de corona proteica - CP). No estudo de perfusão e dinâmica renal estudamos diferentes fases de lesão renal induzida por doxorrubicina, utilizando o sistema BAC para detectar as MNPs em trânsito nos rins do animal, bem como sua biodistribuição. O trabalho referente à dinâmica de perfusão cerebral utilizou o fármaco manitol, um conhecido disruptor hiperosmótico, para influenciar no fluxo sanguíneo cerebral e permeabilidade da barreira hematoencefálica. Assim, foi possível estudar as alterações que este fármaco causa no cérebro, contribuindo para o desenvolvimento de novas estratégias de diagnóstico e tratamento envolvendo este órgão. Estudamos também a formação da CP nas MNPs, seus impactos em propriedades magnéticas e farmacocinéticas das MNPs. Este trabalho mostra que esses parâmetros são relacionados, uma vez que as MNPs com menor formação de CP apresentam menores alterações nas propriedades magnéticas das MNPs e maiores tempos de circulação.

Este trabalho contempla a aplicação de instrumentação física de baixo custo que subsidia aplicações na pesquisa do sistema renal e cerebral em modelos animais, além de novas aplicações de materiais nano estruturados em angiologia, nefrologia e

neurologia, o que proporcionará futuras inovações em instrumentação biomédica, farmacologia, ciência biomédica, nanomedicina e fisiologia.

ABSTRACT

This work consists in the application of the AC Biosusceptometry (ACB) system, associated with magnetic nanoparticles (MNPs), to provide a new tool for studies of renal and cerebral function and physiology, and corona effect as well. We performed experiments using rats to study biophysical parameters of the MNPs perfusion dynamics in the kidneys and brain, in normal and altered situations, as well as their biodistribution in the animals' body. Also, we applied the ACB system to evaluate changes in the MNPs magnetic and pharmacokinetic properties when in contact with biological fluids (corona protein formation - CP). In the renal perfusion dynamics studies, we accessed three phases of doxorubicin-induced kidney injury, using the ACB system to detect the transit of the MNPs in the animals' kidneys, as well as its biodistribution. In work regarding the dynamics of cerebral perfusion, we used the drug mannitol, a known hyperosmotic disruptor, to influence the cerebral blood flow and permeability of the blood-brain barrier. It was possible to study the changes that this drug causes in the brain, contributing to the development of new strategies for cerebral diagnosis and treatment using nanomedicines. We also studied the CP formation in MNPs, its impacts on the magnetic and pharmacokinetic properties of MNPs. This work shows that these parameters are related, since, the MNPs with lower CP formation, presented smaller differences in the magnetic properties of the MNPs and the greater circulation times.

This work was carried out with the objective of conducting applications of physics instrumentation on the renal and cerebral systems in animals, as well as new applications of nanomaterials in angiology, nephrology, and neurology, which gives innovative perspectives in biomedical instrumentation, pharmacology, biomedical science, nanomedicine, and physiology.

ÍNDICE

INTRODUÇÃO GERAL

Nanopartículas magnéticas (MNPs – do inglês *Magnetic Nanoparticles*) são materiais que possuem grande versatilidade. Seu tamanho reduzido aliado às suas propriedades magnéticas permite que estas estruturas interajam de várias formas diferentes dentro de um sistema biológico (1). Atualmente esses materiais têm grande visibilidade da comunidade científica, devido principalmente ao seu grande potencial teranóstico, isto é, associação de técnicas de terapia e diagnóstico utilizando o mesmo agente. Desta forma, MNPs podem atuar como agentes de contraste em procedimentos de MRI (do inglês – *Magnetic Resonace Imaging*) (2, 3) e imagiamento por fluorescência (4), visando diagnósticos, ou serem utilizadas como sistemas de liberação de fármacos (5) e como agentes de tratamento por hipertemia magnética (6), visando terapias. Pode-se, ainda, associar algumas destas diferentes aplicações, a fim de promover o diagnóstico e terapia com as mesmas MNPs (7, 8).

A farmacocinética das MNPs é uma das principais preocupações quando estas são aplicadas em experimentos *in vivo* e procedimentos clínicos. Características como: potencial Zeta (afinidade eletrônica), diâmetro e revestimento das MNPs possibilitam diferentes alvos e destinos em um sistema biológico. Essas grandezas conferem às MNPs características de afinidade ou repulsão a certas estruturas presentes no plasma sanguíneo, tecidos, órgãos ou sistemas. Nesse sentido, estudos de caracterização pré-clinica, que tem como objetivo elucidar as relações entre a estrutura e a atividade das MNPs dentro de um organismo, são de grande importância na área (9-11).

Além das características das MNPs, outro fator de importância na farmacocinética das partículas são as características morfológicas e fisiológicas dos órgãos, sendo essas intimamente ligadas às suas funções. A relação entre as características dos órgãos e das

MNPs é alvo de vários estudos. Por exemplo, nanopartículas maiores do que 200 nm são seqüestradas por filtração física no baço (12), enquanto que nanopartículas menores do que 6 nm são rapidamente retiradas do sangue via depuração renal (4, 9). Sendo assim, MNPs com diâmetros entre 6 e 200 nm têm como seu principal destino final o sistema retículoendotelial, apresentando maiores acúmulos no fígado (9, 13, 14). Além das características dimensionais das MNPs, outra característica de fundamental importância no destino final das MNPs no organismo é sua interação com entidades presentes no sangue (15, 16).

A partir da administração endovenosa dessas MNPs, existem uma série de proteínas, agentes imunológicos e inflamatórios que podem interagir com as MNPs num processo chamado de formação de corona proteica (CP) (17, 18). Esse processo é basicamente o primeiro contato das MNPs com o organismo, onde as MNPs são envolvidas pelas proteínas e agentes imunológicos. O tipo e quantidade das entidades biológicas que interagem com as partículas dependem de alguns fatores como a quantidade dessas entidades no sangue, revestimento e tamanho das MNPs (19, 20). No geral, as entidades que apresentam maior interação com as MNPs são imunoglobulinas, componentes do sistema complemento e proteínas de alta concentração plasmática como a albumina e apolipoproteínas (20-22). Imunoglobulinas e componentes do sistema complemento são estruturas que reconhecidamente têm uma grande relação com reconhecimento fagocitário, ou seja, atuam como sinalizadores para células fagocitárias (como macrófagos, células de Kuppfer, mastócitos, netrófilos, entre outros) entrarem em ação (23, 24). Devido ao fato de que o fígado e o baço possuem em seu interstíticio um grande número dessas células, e a partir dessa sinalização pelos agentes imunológicos e inflamatórios, o fígado e baço compreendem os órgãos de maior captura de MNPs quando administradas endovenosamente (21, 25-27).

Dessa forma, investigações com o objetivo de relacionar o tipo e quantidade de entidades plasmáticas que interagem com MNPs com parâmetros farmacocinéticos como tempo de circulação, captação hepática e excreção renal, são de fundamental importância. Estudos deste tipo podem disponibilizar importantes informações, que poderão ser utilizadas no desenvolvimento de novas estratégias que visam modular esses parâmetros para obter maior eficácia em tratamentos e diagnósticos envolvendo materiais nanoparticulados.

A captação destas MNPs no fígado tem sido amplamente estudada nas últimas décadas, e as que antes se apresentaram como uma boa opção para a realização de marcação hepática em procedimentos de MRI (28), atualmente tem recebido críticas em relação ao tempo em que permanecem retidas no organismo (29). A fim de solucionar este problema, estudos recentes têm apontado para a utilização de MNPs que apresentem a via de excreção renal como principal via de eliminação das MNPs do organismo (4, 29, 30).

Devido às características morfofisiológicas dos rins, como a presença da unidade de filtração glomerular, da membrana basal e dos podócitos interdigitantes, este órgão tem a habilidade inata de depurar rapidamente nanomateriais com diâmetros menores do que 10 nm (4, 9). Apesar do diâmetro das MNPs ser o principal fator que influencia na depuração renal das MNPs, existem outros fatores que também influenciam neste parâmetro como, por exemplo, o potencial Zeta e a hidrofilicidade das MNPs, já que a seletividade de filtração glomerular é baseada na carga e hidrofilicidade das substâncias a serem depuradas (31). Dentro deste contexto, estudos que visam o melhor entendimento da relação entre os níveis de excreção renal e as características das MNPs, bem como da integridade da unidade de filtração glomerular com esses parâmetros, têm grande importância.

Em virtude dos efeitos deletérios causados nos rins por agentes de contrastes a base de iodo e gadolínio (32-34), MNPs têm sido propostas como uma alternativa segura para contraste, já que em relação aos meios de contraste a base de iodo e gadolínio, não apresenta nefrotoxicidade (34). Além da ausência de toxicidade renal, características das MNPs, como seu tamanho e versatilidade, viabilizaram a utilização destes materiais nanoestruturados em metodologias que visam maior eficácia no imagiamento dos rins via MRI. Hultman, K. L. et al. (2008) utilizaram técnicas de marcação imunológica, tendo como alvo a marcação da medula renal de ratos (35). Este tipo de marcação tem grandes implicações em detecções de doenças específicas que atinjam a medula renal e em entrega de fármacos nesse local. Outros estudos, a fim de diagnosticar Falência Renal Aguda (FRA), mostraram que nanopartículas associadas a técnicas de MRI são capazes de detectar áreas isquêmicas nos rins de animais com FRA (36) e detectar lesões renais antes dos níveis de creatinina sérica se tornarem elevados (37). Estes resultados têm grande importância, uma vez que um aumento progressivo dos níveis de creatinina sérica é um dos principais parâmetros que indicam um possível quadro de FRA.

Um dos principais indicadores de nefropatias é a infiltração de macrófagos no tecido renal (glomérulo e interstício). Hauger, O. et al. (1999) utilizaram MNPs, associadas a técnicas de MRI para localizar macrófagos no tecido renal de animais com síndrome nefrótica previamente induzida (38). A técnica de localização de macrófagos no tecido renal descrita neste estudo ainda pode ser aplicada em diversos outros tipos de disfunções renais, como por exemplo, rejeição de transplantes e glomerulonefrite, que até o momento eram diagnosticadas unicamente por meio de biópsias. Nanopartículas de óxido de ferro associadas a técnicas de MRI também já foram utilizadas para quantificar inflamação renal de nefrite lúpica. Utilizando MNPs funcionalizadas com

recobrimento de fosfolipídios específicos, foi possível quantificar a progressão dos níveis de inflamação renal nos animais doentes por meio da diferença nos tempos de relaxação dos tecidos normais e dos tecidos marcados pelas MNPs funcionalizadas (39).

Nesse contexto, materiais nanoestruturados são de grande valia na área de nefrologia, pois apresentaram bons resultados quando empregadas em estudos de diferentes disfunções renais como nefropatias, progressão de lesões crônicas e detecção precoce de FRA.

Devido às propriedades das MNPs já citadas anteriormente, essas partículas podem acessar locais e estruturas que são pouco acessíveis por meio de outros métodos (40). Neste contexto, outras aplicações das MNPs que têm recebido grande atenção da comunidade científica são a entrega de drogas e realização de tratamentos envolvendo o sistema nervoso central, mais especificamente o tecido cerebral (40, 41). Um grande obstáculo na entrega de agentes terapêuticos no tecido cerebral é a barreira hematoencefálica. Esta barreira, que envolve vasos sanguíneos do sistema nervoso central, tem como principal função impedir a entrada de substâncias tóxicas e agentes patogênicos no cérebro, assim como também manter a homoestase deste órgão (42).

Abordagens que visam alternativas eficientes para melhorar os resultados de diagnóstico e tratamento do tecido cerebral são de grande importância. Recentemente, estudos envolvendo a associação e combinações de técnicas, como a modulação da permeabilidade da barreira hematoencefálica e a aplicação e detecção de nanocarreadores, são fundamentais para atingir este objetivo (43). Uma dessas abordagens é a utilização do fármaco manitol (um disruptor hiperosmótico que modula a permeabilidade da barreira hematoencefálica) associado à MNPs. Utilizando essa abordagem, Kim et al. (2006) conseguiram alcançar concetrações significativas de

MNPs no cérebro com uma admnistração prévia deste fármaco, porém os métodos de avaliação dessa entrega utilizados nesse estudo forneceram apenas dados qualitativos (44). Vale ressaltar que ainda existe uma deficiência de técnicas e métodos capazes de avaliar os resultados de entrega e perfusão cerebral de MNPs de forma quantitativa. Assim, novas tecnologias que são capazes de realizar essas aferições e que apresentem características como baixo custo, fácil manuseio e versáteis são de vital importância para estudos pré-clínicos envolvendo essas abordagens. Tais técnicas podem ser úteis para facilitar as investigações do uso de nanocarreadores magnéticos aplicados ao cérebro, e consequentemente ter impactos tanto no tempo quanto no custo envolvido no desenvolvimento destas novas abordagens que utilizam nanocarreadores magnéticos (45).

Atualmente existem poucas técnicas que são capazes de detectar as MNPs *in vivo* por meio de suas características magnéticas, sendo as principais o MRI (46) e o sistema de Imagiamento de Partículas Magnéticas (MPI – do inglês *Magnetic Particle Imaging*) (47), porém esses sistemas possuem limitações que estimulam a busca por novas instrumentações capazes de detectar as MNPs a partir de suas propriedades magnéticas. As técnicas padrão de MRI e seus protocolos para avaliações funcionais (fMR do inglês – *functional Magnetic Resonance*) apesar de possuírem boa resolução espacial, são técnicas de custo elevado que dependem de um ambiente controlado, o que dificulta sua associação com outros sistemas, limitando as possíveis aplicações terapêuticas das MNPs. Vale ressaltar, ainda, que a fMR é pouco aplicada em regiões como o abdômen e tórax, visto que o movimento de fluidos e estruturas dentro dessas cavidades gera uma série de artefatos na imagem e sua resolução temporal nesses casos é limitada (48). O sistema MPI tem tido muita atenção nos últimos anos devido à sua resolução espacial principalmente, na ordem de milímetros (47), porém esse sistema também limita a

associação de técnicas a fim de explorar as propriedades teranósticas das MNPs. Além disso, esse sistema têm sido aplicado apenas em imagiamento de pequenos animais, devido à sua alta complexidade, sendo que existem apenas estudos de viabilidade, através de simulações, de um sistema com capacidade e segurança para aplicação em humanos (49, 50).

Dessa forma, a busca por novas técnicas e instrumentações mais simples, de baixo custo e que tragam novas perspectivas no estudo de parâmetros relacionados com função renal, cerebral e interação das MNPs com entidades plasmáticas são de grande importância, uma vez que existe a falta de técnicas capazes de interagir com estes materiais nanoestruturados *in vivo* de maneira minimamente invasiva, com alta resolução temporal e custos acessíveis.

Dentro deste contexto, a técnica de Biosusceptometria AC (BAC) aparece como uma valiosa nova ferramenta para a detecção de MNPs *in vivo* e em tempo real. A BAC é uma técnica bem estabelecida na área de gastroenterologia e seus princípios de funcionamento são descritos pelo eletromagnetismo clássico. Em relação a outros sistemas já estabelecidos, a BAC apresenta vantagens como alta resolução temporal, baixo custo, versatilidade, portabilidade e ausência de radiação ionizante.

Desde suas primeiras aplicações, os estudos envolvendo BAC são focados, principalmente, em avaliação de parâmetros envolvendo o trato gastrintestinal de humanos (51-54). Desde o surgimento dessa técnica até os dias atuais, muitas aplicações foram exploradas, como: avaliação de motilidade gástrica (55-57), trânsito gastrintestinal (58-60), esvaziamento gástrico (53, 60, 61) e farmacotécnica (62-64). Até 2012, eram utilizadas partículas de material ferromagnético (ferrita de manganês) como material traçador. As partículas apresentavam diâmetros na ordem de 50 a 100 μm e não

eram absorvidas pelo organismo, sendo excretadas via fezes. Quini et al. (2012) propôs a associação de MNPs com o sistema BAC para avaliar trânsito e esvaziamento de líquidos, o que possibilitou o surgimento de uma nova linha de pesquisa, baseada no monitoramento das MNPs em órgãos e tecidos, o que não era possível até então devido às limitações dimensionais do material e de suas propriedades magnéticas (60, 65).

A associação de MNPs com o sistema BAC se mostra de extrema relevância, já que atuam, respectivamente, como traçador magnético e detector de materiais magnéticos empregados em estudos fisiológicos. Os métodos utilizados até o momento apresentam uma série de inviabilidades, como já citado. A Biosusceptometria AC associada às MNPs fornece, então, uma alternativa versátil de baixo custo para o estudo de parâmetros relacionados com a biofísica renal e cerebral em tempo real e *in vivo* (27, 45, 65, 66), além de ser capaz de realizar aferições sobre a quantidade de material magnético acumulado em cada órgão *ex vivo* (67, 68), e os impactos da formação de corona proteica nas propriedades magnéticas das MNPs. Extrapolando as possibilidades de associação do sistema BAC com MNPs, pode-se, ainda, imaginar soluções para diversos problemas encontrados na clínica médica, como por exemplo o uso de radiação ionizante em angiografias e cintilografias, além de baixa resolução temporal em MRI.

Vale ressaltar que as MNPs que utilizamos aqui, MNPs de ferrita de maganês ($MnFe_2O_4$) possuem propriedades magnéticas muito interessantes. A magnetização dos materiais depende do volume do material magnético, e devido ao fato de que as MNPs aqui utilizadas terem dimensões de aproximadamente 15nm, interagir com materiais nesta dimensão por meios de campos magnéticos pode ser um desafio. Entretanto, as MNPs de ferrita de manganês utilizadas nestes estudos, foram desenvolvidas objetivando melhor sensibilidade pelo sistema BAC, e, devido à sua estrutura e composição, apresentam ótima resposta magnética quando imersas em campos

magnéticos de baixa amplitude, como o caso do sistema BAC, o que nos motivou a aplicá-las como traçador magnético nanoestruturado para o sistema BAC (65, 69).

Desta forma, a presente tese de doutorado envolve a aplicação do sistema de Biosusceptometria AC para a avaliação de parâmetros relacionados a biofísica da dinâmica renal e cerebral, além de estudar os impactos da formação da corona proteica em parâmetros farmacocinéticos e magnéticos das MNPs. Nos últimos anos nosso grupo tem realizado uma série de trabalhos envolvendo o uso do sistema BAC para a detecção de MNPs. Aqui apresentaremos pela primeira vez a utilização deste sistema associado às MNPs para o estudo de disfuncionalidades de órgãos como os rins e o cérebro. A partir da indução de uma lesão renal grave, que se assemelha a uma doença crônica renal (a glomerulo esclerose focal e segmentar) pudemos investigar os parâmetros de perfusão das MNPs pelos rins bem como o acúmulo das MNPs por estes órgãos em animais saudáveis e lesionados. Estudamos também os efeitos do manitol sobre a distribuição de MNPs no cérebro, associando MNPs como traçadores e o sistema BAC como detector *in vivo*. Além disso, o terceiro e último capítulo contempla o estudo da formação da corona proteica e seus impactos no tempo de circulação das MNPs e intensidade de sinal do sistema BAC. Acreditamos que os dados aqui apresentados subsidiem avaliações anteriores já publicados pelo grupo e apresentam novas abordagens que aumentam as aplicabilidades do sistema BAC, fornecendo uma ferramenta alternativa, de baixo custo, fácil manuseio e versátil para estudos pré-clínicos envolvendo materiais magnéticos nanoestruturados.

CHAPTER 1

AC biosusceptometry and magnetic nanoparticles to study doxorubicin-induced kidney injury in rats

PREFÁCIO

O capítulo a seguir nasceu há quatro anos, em meados de fevereiro de 2015, algumas semanas antes da defesa de minha dissertação de mestrado.

Alguns anos antes o Prof. José Ricardo tinha iniciado suas investigações no campo de pesquisa da nanomedicina por meio da dissertação de mestrado do Dr. Caio C. Quini. No período entre o começo dessa nova linha de pesquisa no laboratório Biomag e este dia crucial em minha carreira científica, nosso grupo publicou alguns trabalhos utilizando o sistema de Biosusceptometria AC associado à nanopartículas magnéticas. Um desses trabalhos foi o "*Renal perfusion evaluation by alternating current biosusceptometry of magnetic nanoparticles*", onde aplicamos o sistema BAC para detectar nanopartículas magnéticas perfundindo o rim de ratos, o que nos possibilitou quantificar alguns parâmetros relacionados à dinâmica renal.

No referido dia de fevereiro, o qual não me lembro exatamente, existiu uma visita do Prof. Ricardo Brandt ao nosso laboratório a fim de tomar conhecimento dos trabalhos em andamento, no período em que se encerrava um projeto temático FAPESP do qual ambos o Prof. José Ricardo e o Prof. Ricardo Brandt tinham papel ímpar. Durante as discussões dos trabalhos que foram publicados durante a vigência do projeto, o Prof. Ricardo tomou conhecimento do artigo científico citado no parágrafo acima. Das discussões daquela tarde surgiu a seguinte indagação: "Será que - já que o sistema BAC foi capaz de detectar a perfusão renal de nanopartículas magnéticas em animais saudáveis - ele seria capaz de detectar diferenças em animais com uma doença ou disfunção renal?". Dessa indagação fui incumbido de pesquisar sobre modelos de lesão renal e a viabilidade de desenvolver um projeto com este tema. Na época, ainda me lembro, tínhamos outras perguntas que foram levantadas durante o desenvolvimento de

meu projeto de mestrado, e que poderiam culminar em outra trajetória de meu projeto de pesquisa de doutorado, porém àquele momento essa nova questão foi de maior interesse por parte de meus superiores. O passo seguinte foi levar esta proposta para minha, na época, co-orientadora de mestrado, a Profa. Patrícia Fidelis de Oliveira, a qual foi super receptiva à idéia e foi de fundamental importância desde a fundamentação teórica inicial até a conclusão deste projeto. A Profa. Patrícia teve um papel ímpar no que toca à parte fisiológica e funcional do trabalho.

A partir dessa reunião deu-se o início de minha empreitada no universo dos rins, bexiga, uretéres, glomérulos e túbulos renais. No começo, como quase todo aluno de doutorado, não tinha muito apreço pelo tema, porém ao longo desses quatro anos, por meio de um amadurecimento científico, criei um carinho especial para com este trabalho. Testemunhas disso são o próprio Prof. José Ricardo, que no início teve algumas conversas comigo a fim de me mostrar a importância e beleza do que eu estava fazendo, e a aluna de iniciação científica, Milena Foltran que teve seu projeto de iniciação científica com bolsa FAPESP atrelada a este projeto, e me acompanhou no dia-a-dia do desenvolvimento deste trabalho nos últimos 2 anos. A aluna Milena, apesar de ter como objetivo de sua iniciação científica alcançar apenas a parte inicial deste projeto, fez questão de estar presente em todas as suas etapas e foi fundamental para a parte logística deste trabalho, que diga-se de passagem foi exaustiva, metódica e minuciosa. Sem ela, eu ainda estaria tentando descobrir até hoje qual animal estava com o rim lesionado e qual era saudável. Vale lembra que a aluna Milena foi a primeira a apresentar os dados parciais deste trabalho no Congresso Brasileiro de Física Médica 2017, do qual não pude participar devido ao doutorado sanduíche, e recebeu o prêmio de melhor pôster.

Além de mim, Prof. José Ricardo, Profa Patrícia e Milena, outras pessoas fizeram grande contribuição para este projeto, como o pessoal do laboratório de histologia e microscopia da UNIPEX, as Dras. Daniela Crisitina e Vanessa, que laudaram as lâminas coletadas e contribuiram fortemente para a discussão dos dados coletados, o aluno de doutorado Guilherme Soares que me ajudou em tudo o que era necessário e o Dr. Caio Quini, que me ajudou a estruturar e dar os primeiros passos deste projeto.

Por fim, este capítulo envolve a aplicação de uma instrumentação biomagnética e nanopartículas magnéticas, alternativa aos métodos convencionais que proporcionam dados dinâmicos dos rins. Aqui induzimos uma lesão renal grave no animais, via administração única endovenosa de doxorrubicina, que em seus estágios finais se assemelha a uma glomeruloesclerose focal e segmentar em humanos. Utilizamos as nanopartículas como um traçador magnético e o sistema BAC como detector dessas partículas. Os resultados obtidos apontam a utilização do sistema como uma ferramenta de baixo custo, altamente versátil e portátil para estudos de evolução de doenças renais em modelos animais. Esperamos que este trabalho contribua para o desenvolvimento de novas plataformas de diagnóstico e tratamento destes órgãos tão importantes que são os rins.

ABSTRACT

Chronic kidney diseases are global public health problems. Currently, renal function is evaluated using biochemical procedures, which presents some limitations as the non-specific nature of the tests, the absence of morphological data, and influences of the population habits and diet. In this context, scintigraphy and magnetic resonance imaging represent adjuvant technique employed to detect and for stratification of renal stage damage as well as a follow-up tool. Scintigraphy uses ionizing radiation, and magnetic resonance imaging requires contrast agents, whose are nephrotoxic substances. To provide some alternatives to the standard contrasts, some studies have been investigated the use of nanostructured agents in the detection of kidney diseases. The different etiologies of renal disease include the nephropathy induced by nephrotoxic drugs as the doxorubicin. Since its initial applications, this drug was associated with sever nephrotoxic effects. The Doxorubicin chronic disease model was extensively studied and was of paramount of importance in the elucidation of processes involving kidney injuries progression. Direct detection of magnetic nanoparticles remains restricted to few techniques. At this point, AC Biosusceptometry, a technique that acts as a detector of magnetic materials in biological systems, appears as a versatile and accessible alternative for the detection of magnetic nanoparticles *in vivo* and real time. Our main goal was investigating the doxorubicin chronic kidney disease model using magnetic nanoparticles as a safe tracer, associated with the AC biosusceptometry system for *in vivo* and real-time magnetic nanoparticles detection. Results obtained with AC biosusceptometry system were sustained by biochemical and histological analyses. Also, we studied the magnetic nanoparticles biodistribution (*ex vivo*) in both healthy and kidney-injured animals. The present study provides new applications of

nanostructured materials in angiology, nephrology, biomedical instrumentation, pharmacology, physiology, and nanomedicine.

1. INTRODUCTION

Chronic Kidney Diseases (CKD) are one of the greatest public health problems, defined as abnormalities of kidney structure or function, present for more than three months, with implications for health and increase the risk of cardiovascular diseases and other complications (1). The incidence in the US population was 11%, reaching 47% in more than 70 years old people, from 1999 to 2006 (2). The worldwide prevalence is estimated to be 8-16%. In developing countries, this problem is greater. The population aging-associated with the low investments in public health suggests that the number of cases of end-stage kidney diseases will disproportionately increase in these countries (3).

The identification of CKD relies on, firstly, in some biomedical laboratory procedures, as a measurement of glomerular filtration rate, albuminuria, blood urea nitrogen, and serum creatinine level. Even though these assays are relatively simple and inexpensive, some limitations are inherent to each method. This includes the delay in rising plasmatic substances like the creatinine despite the decreasing in glomerular filtration rate, the nonspecific nature of the tests, the absence of viable techniques capable to monitoring eventual change in renal morphology along the time, variations between populations and ethnic which implies in correction factors (based on the population habits and diet) (3, 4). In this context, scintigraphy and magnetic resonance imaging (MRI) represents adjuvant technique commonly employed to detect and for stratification of renal stage damage as well as a follow-up tool (5-9). These methods present some advantages over the laboratory exams such as the possibility of evaluating

the renal structure and function using dynamical images of the kidney simultaneously to renal perfusion and clearance of contrast agents, respectively. However, the high cost of these equipment associated with shielded environments and the need of using radiotracers and radiation incidence (scintigraphy) or contrast agent (MRI), limits its use in routine clinical practice. Important to note that Gadolinium-based contrasts were widely used and had been considered safe until the last decade. Nowadays the use of gadolinium worsens the patient's condition given the risk of nephrogenic systemic fibrosis (10-12). Given that hindrances found in these methods and the fact that CKD leads to kidney failure, novel, and alternative approaches may be developed to follow up CKD, using a minimally invasive measurement to acquire data in regards to the kidney injury evolution.

Over the last decade, the nanomedicine has been contributed to new possibilities of diagnosis and follow-up and overcoming some barriers in health sciences (13-15). To provide some alternatives to the radiotracers and gadolinium-based contrasts employment, some studies have been investigated the use of nanostructured agents in the detection of kidney diseases (4). Hultman and co-authors (2008) were able to obtain renal medulla images using immunotargeted magnetic nanoparticles and MRI techniques, demonstrating the nanoparticles potential for disease detection and / or drug delivery (16). Acute renal injury was early detected using nanoparticles and MRI, which suggests the efficacious for this noninvasive technique in the diagnosis of acute kidney damage before the serum creatinine is elevated. Macrophages infiltration is an indicator of nephropathy (17). In this way, Hauger and co-authors (1999) used MNPs to detect and localize macrophages in the renal tissue of animals with induced nephrotic syndrome. Their data were unprecedented and can be applied in different studies of renal dysfunction as glomerulonephritis and transplant rejection (18).

The different etiologies of renal disease include the nephropathy induced by nephrotoxic drugs as the Adriamycin®, a doxorubicin-based anti-cancer drug. Doxorubicin (DOX) is a cytotoxic antibiotic which presents a great antitumor efficacy and has been widely used in chemotherapy (19, 20). Unfortunately, its use is associated with several side effects, mainly in the cardiovascular and renal system (21, 22). Since its initial applications in rodents, this drug was associated with sever nephrotoxic effects involving severe glomerular injury, proteinuria, tubular dilatation, fibrosis among others (20, 23, 24). The deleterious effects caused by the DOX administration evolves passing through different progressive stages of injuries leading to focal and segmental glomerulosclerosis (FSGS), which encouraged its use as an inducer model of CKD in rodents (24, 25). The Doxorubicin CKD model was extensively studied and was of paramount of importance in the elucidation of processes involving the CKD progression (25).

Recently our group has applied the alternate current biosusceptometry (ACB) system to detect magnetic nanoparticles (MNPs) *in vivo* and real-time (26, 27). Also, we were able to quantify the MNPs in several different tissues samples and cell culture using the ACB system (28, 29). This system presented good and valuable data regarding the MNP's circulation time, liver uptake, renal perfusion and its biodistribution in healthy animals. The ACB system presents some advantages over the current standard techniques as the portability, low cost, absence of a shielded environment, radiotracers, or contrast agents associated with nephrotoxic effects as gadolinium. Here we applied, for the first time, the ACB and MNPs system to study a kidney injury evolving, induced in rats by a single injection of DOX, in three different stages (14, 28 and 56 days after the CKD induction). Our main goal is investigating the DOX CKD model using MNPs as a safe tracer, associated to the ACB system, *in vivo* and real-time, acting as a low

cost, simple and harmless tool to detect these MNPs and its different perfusion profiles in healthy and doxorubicin-injured kidneys. Results obtained with ACB system were sustained by biochemical and histological analyses, where this last one was performed by a nephropathologist. Also, we studied the MNPs biodistribution (*ex vivo*) in both healthy and kidney-injured animals, for several organs, performed by a biodistribution-optimized ACB system (ACB cavity sensor) in order study the MNPs' potential to act as a magnetic marker of lesions and organ MNPs uptake capability.

2. MATERIAL AND METHODS

2.1. AC Biosusceptometry system

The ACB system is biomagnetic instrumentation that works as a magnetic materials detector. Since its first applications, the ACB system was employed to study several mechanics and physiological parameters of the gastrointestinal tract, pharmacological and pharmaceutical fields (30-35). The system uses a four coils set up to detect magnetic tracers or markers within the body. Several coils configurations were employed in the past. Here we built and applied a conventional mono-channel ACB system. The system contains two pairs of coils, one pair is the reference system, and the other is the measurement system. Each pair is composed by an inductor coil and a detector coil. The inductor coils generate a low amplitude alternating magnetic field (approximately 2mT), which is detected by the detector coils in real time. The reference system is connected to the measurement system in a subtraction configuration, forming an axial first order gradiometer (28). Using this gradiometric configuration is possible to decrease the environmental noise and increase the signal-to-noise ratio of the system. When there is no magnetic material near the measurement system, no signal arises. When is placed a sample containing magnetic material near the measurement system,

there is an imbalance in the total magnetic flux of the system, and a signal arises. The signal recorded is proportional to the amount of magnetic material and its position (26).

We used a lock-in amplifier and an audio amplifier to generate and detect the magnetic signal. The lock-in amplifier generates a signal of 0.7 V at 10 kHz, which is amplified by the audio amplifier (-3 dB – reaching approximately 40 V), and finally is applied in the inductor coils. The magnetic field generated is detected in real time by the detector coils, as a magnetic flux transformer. The electrical signal generated in the detector coils returns to the lock-in amplifier, which processes the output signal to acquire only the 10 kHz component and convert it to a DC signal. Also is possible to use an A/D card and a computer to record and post-process the signal regarding the presence and amount of magnetic material (in our case MNPs). Further details, as the system worksheet and physical model, can be found in our previous publications (26, 34, 35).

2.2. Magnetic nanoparticles

We synthesized, characterized and applied manganese ferrite nanoparticles coated with citrate (Cit-$MnFe_2O_4$). We chose the manganese ferrite due to its good magnetic response at low amplitude magnetic fields. Once the CKD experiment is time-consuming, and was needed that all the animals received MNPs from the same batch, the citrate coating was employed to obtain good colloid stability. The MNPs were synthesized by co-precipitation, as described before (36-39). The MNPs presented a physical core diameter of 15 ± 5 nm and a saturation magnetization of 51.2 emu/g. The magnetization profile study showed no coercive field at DC conditions, that is, a quasi-static superparamagnetic behavior. The MNPs were dispersed in liquid media in a physiological pH, at 25 mg/ml concentration. It is worth to point out that these MNPs

were extensively employed by our group in a series of studies involving animal experimentation, presenting good results and no acute toxic effects (26-28, 37).

2.3. Experimental animals and doxorubicin-induced renal lesion model

In this study we used 60 male rats (*Rattus norvergicus albinus*, Wistar) provided by the UNESP (São Paulo State University) central animal facility (Botucatu, SP, Brazil) maintained in appropriate conditions of temperature (22±1°C), humidity and 12 hours of the light cycle with *ad libitum* feeding. All experiments were conducted according to the UNESP Committee for the use and Care of Animals (protocol no CEUA – IBB 953).

The renal damage was induced in rats weighing 230-280g. In the day 0 the conscious animals were contained in a specific apparatus and received a single intravenous injection (tail vein) of doxorubicin (*Wyeth Pharmaceutical Industry Ltda – São Paulo, Brazil*) or NaCl 0.9% solution (SAL - control group), according to the experimental group. We used a concentration of 15mg/kg of DOX and the same vehicle volume (1 ml/230 g) of saline in the SAL group. Renal injury was evaluated using proteinuria and histological structure at different times after DOX administration: 14, 28 and 56 days. Thus, we established six experimental groups of 10 animals each (Table 1).

Table 1 – Animals groups

Days after injection	DOX or SAL injection	Group label
14	DOX	DOX_14
	SAL	SAL_14
28	DOX	DOX_28
	SAL	SAL_28
56	DOX	DOX_56
	SAL	SAL_56

2.4. Experimental protocol

The experimental protocols were finalized at 14, 28 and 56 days after tail vein injection of DOX or SAL. Before 48h from the end of each experimental protocol period, the animals were taken to individual metabolic cages for urine collection. The first 24h were used for animal adaptation in the cage, and after this period all samples of urine were discarded. After the last 24h of the rat in the metabolic cage, we collected urine samples, weighed the animals and measured water ingestion and waste. Proteinuria was quantified using total protein in the sample by the pyrogallol red method (40). In this method, we used a clinical urine test kit (Bioprot U/LCR – K108 produced by Bioclin®, Belo Horizonte, MG, Brazil) and a spectrophotometer set at 600 nm to read the light absorbance and calculate the total protein content in the sample.

After the urine collection, the animals underwent intraperitoneal anesthesia (Urethane – 1.5 mg/kg), followed by femoral vein catheterization for MNP (25 mg/mL) intravenous administration (0.5mL per animal). Also, we performed a little incision in the lumbar region of the animal to ensure the relative kidney position to the ACB sensor. Each animal was positioned in ventral decubitus, and the ACB sensor was positioned over the kidney region. In this configuration we were able to detect the MNPs reaching, perfusing and washing out from the animals' kidney. After 40 minutes of *in vivo* and in real-time signal acquisition, the animals were sacrificed by decapitation and a blood sample was collected. Laparotomy was made for collecting organs of interest (kidneys, bladder, liver, spleen, lungs, and heart). The left kidney (in which we positioned the ACB sensor) was used for MNPs biodistribution quantification, and the right kidney was prepared for histological analyses. Briefly, we submitted the kidney to a fixative solution (Metacarn – 70% methanol, 20% chloroform and 10 % glacial acetic acid) for 24h, followed by storage in ethanol (70%). The samples were prepared and

included in paraffin and dyed with hematoxylin-eosin for histological analyses, which were qualitatively performed by the pathologist, in a blind analysis, for morphological aspects of the filtration barrier.

For the MNPs ex vivo biodistribution quantification, all the organs were lyophilized and triturated. We randomly collected a sample of 0.1g from each tissue in a 1.5 ml microtube which was positioned in the ACB cavity sensor for electrical signal detection proportional to MNP amount in the sample, as described before (28). Also, we built a calibration curve of the ACB cavity system to calculate the mass of MNPs per gram of tissue (28).

Figure 1 is a representative timeline of the study design, starting from renal injury induction to the final experiment procedures discriminated in details as urine sampling, surgical procedure, MNPs injection, in vivo and real-time detection by BAC, animal sacrifice, organs collection, and biodistribution analyses.

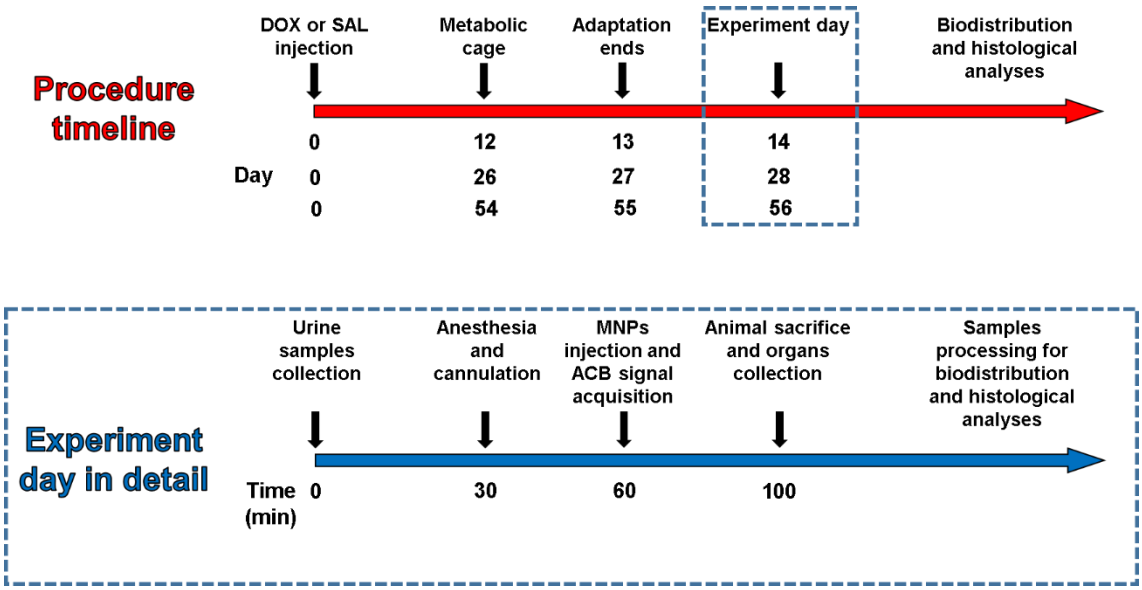

Figure 1 – Procedure timeline. The red arrow is presented the entire procedure, taking into the account from the DOX or SAL injection to the final analyses. The blue arrow presents in details the procedures performed in the day that the animals received the MNPs and we performed an *in vivo* and real-time MNPs detection in the animals' kidney.

2.5. ACB signals acquisition and Quantification

In the *in vivo* experiments, we acquired ACB signals online using a Lock-in amplifier and a Biopac system at 20Hz of the sampling rate. We performed the signal registration and quantification using Acknowledge 4.1.1, MatLab2011 and OriginPro 8 software. All signals were baseline corrected in OriginPro 8, and no filtering processes were applied for quantifications.

The transit time (Δt) of the MNPs in the kidney was measured between the first (t_1) acute peak, and the second (t_2) slow peak registered, respectively, as described previously (27, 41). Also, we quantified the maximum signal intensity (I_{max}), the final signal intensity (I_{final}), after 40 min from the MNPs injection and the arrival time (AT) of the MNPs in the kidney, calculated from the injection until the first peak (t_1) in the ACB signal.

The biodistribution analyses were conducted as described in item 2.4. As this analyses are not online and dynamical, all data were registered manually by the system operator. After the calibration curve built and using a linear fitting model to assess the ACB system transfer function, we were able to calculate the mass of MNPs per gram of tissue in OriginPro 8. Further details for the calibration curve and biodistribution protocol can be found in our previous paper (28).

2.6. Statistical analysis

All data were expressed as mean ± standard deviation. We performed all statistical tests using GraphPad Prism software. We compared the DOX groups with the SAL groups, within the same days after DOX or SAL injection, using a non-paired *t*-test for all quantifications (proteinuria, ACB online signals and *ex vivo* signals). When evaluating a parameter involving different animals under different conditions (groups

periods), we used a two-way analysis of variance followed by Tukey post hoc for comparisons between the groups. Values of $p < 0.1$ were considered statistically significant.

3. RESULTS

3.1 Proteinuria and kidney morphological analyses

The renal damage caused by DOX administration leads to severe proteinuria. To stage the proteinuria levels over the periods, we measured the protein content in the urine samples. Also, we measured the urine volume to calculate the protein quantities excreted in 24h. In figure 2 is presented the protein concentration in urine (figure 2A) and the total excreted protein in 24h (figure 2B) after different times after kidney injury induction by DOX.

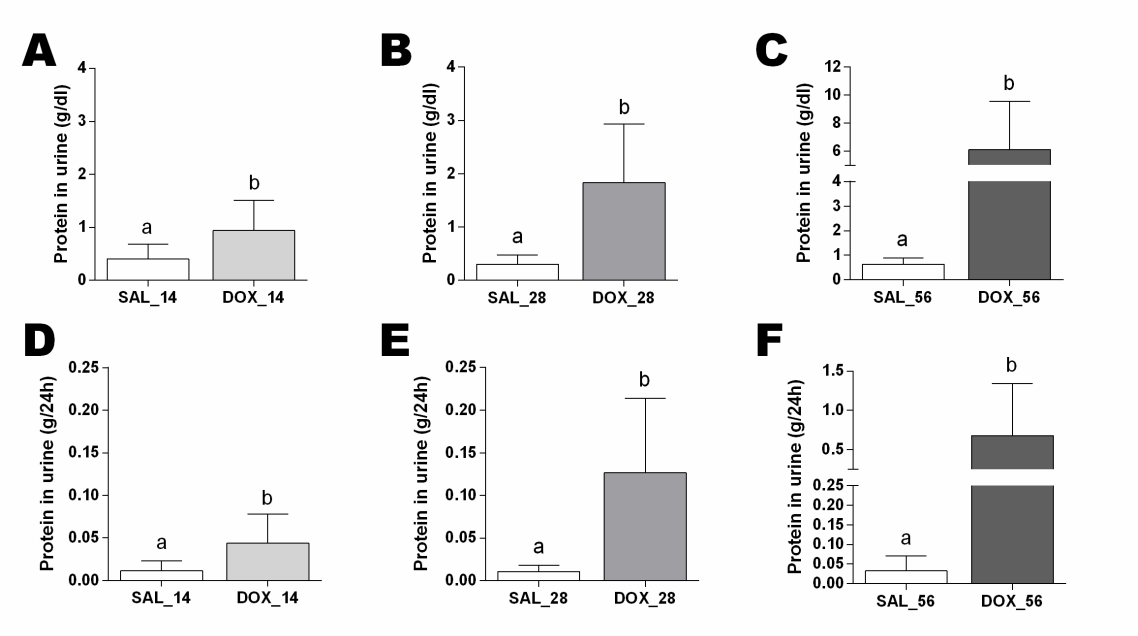

Figure 2 – Proteinuria levels. (A) Protein concentration in the 14 days' period animals' urine. (B) Protein concentration in the 28 days' period animals' urine. (C) Protein concentration in the 56 days' period animals' urine. (D) Total protein excreted in the 24h before the ACB experiment for the 14 days' period animals. (E) Total protein excreted in the 24h before the ACB experiment for the 28 days' period animals. (D) Total protein excreted in the 24h before the ACB experiment for the 56 days' period animals. Different letters represent significant differences between the groups with $p< 0.05$.

DOX-induced kidney injury and proteinuria detected just early (14 days, DOX vs. SAL: $p=0.003$) as longlasting after injection (28 and 56 days, $p < 0.0001$ and $p < 0.001$, respectively). We performed a histological analysis focusing on glomerular structure changes, besides that, some tubular changes were noticed as well. Once the doxorubicin-induced injury in an end-stage leads to a focal and segmental glomerulosclerosis (FSGS), the glomerulus is expected to be the most affected structure in the kidney. These analyses showed the main changes in glomerulus as the mesangial cellularity, reactive and evident podocytes, glomerular hyalinosis, glomerular retraction, periglomerular fibrosis, segmental glomerulosclerosis, adhesion of the glomerular cappilaries in the Bowman's capsule, the presence of polymorphonuclear cells (PMN) and lymphomononuclear cells (LMN). Also, we found some tubular and interstitial changes as the dilated tubules with proteinaceous casts, focal tubular atrophy, interstitial fibrosis, and interstitial mononuclear inflammation. Figure 3 shows an example of the main changes found in the animal's glomerulus. In figure 3 is possible to observe an example of the histology from a SAL group animal and a representative picture from each DOX period showing the injury evolution.

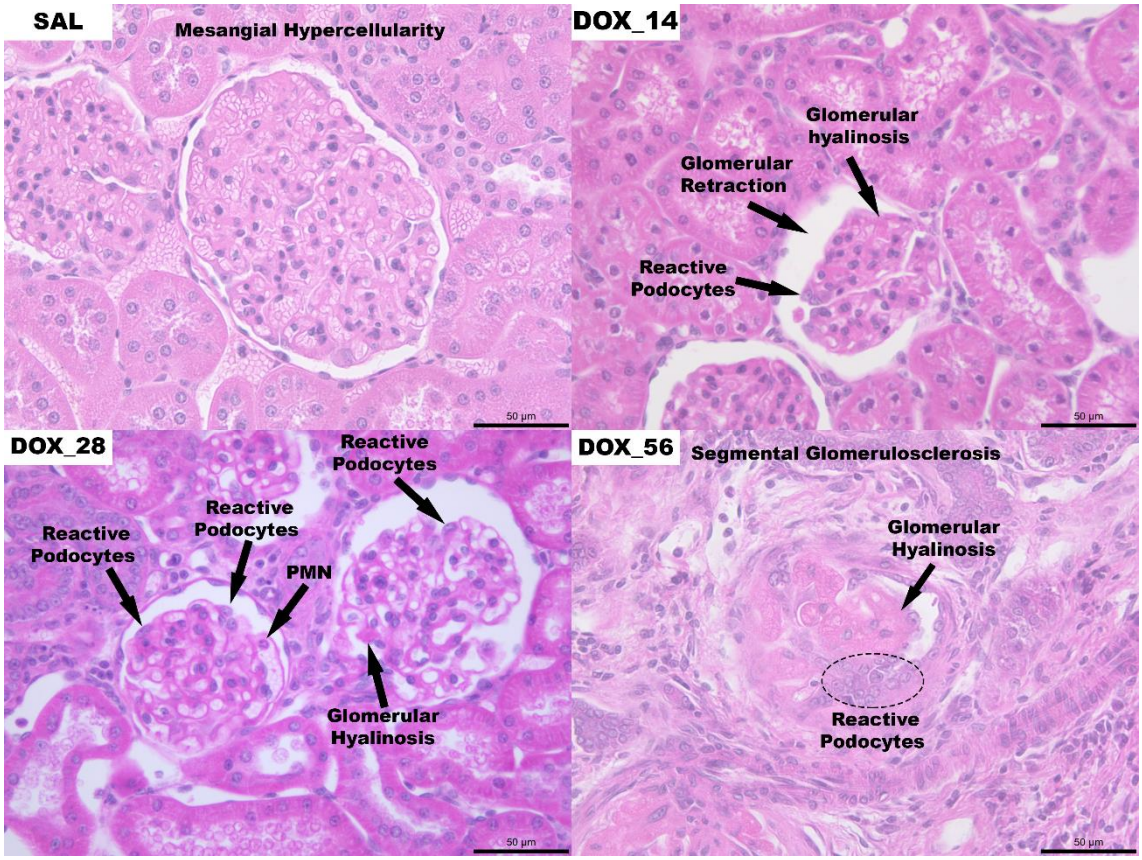

Figure 3 – Examples of a SAL group animal and a representative picture of each DOX period showing the main findings for the glomerulus and its evolution on the periods (400x).

Figure 4 shows some examples of the tubular casts growing over the periods. In this figure is possible to notice no tubular casts in the SAL group, while there are some focal tubular casts in the DOX_14 and DOX_28 groups. In the DOX_56 group, we found the highest tubular casts incidence and affected areas. Note that the figure from DOX_56 in figure 4 is presented on a different scale, once this presence of tubular casts is not focal and takes a great part of the organ. Also in the DOX_56 group is evident the high interstitial inflammatory cells infiltration, where are not present so intense in the other DOX and SAL groups.

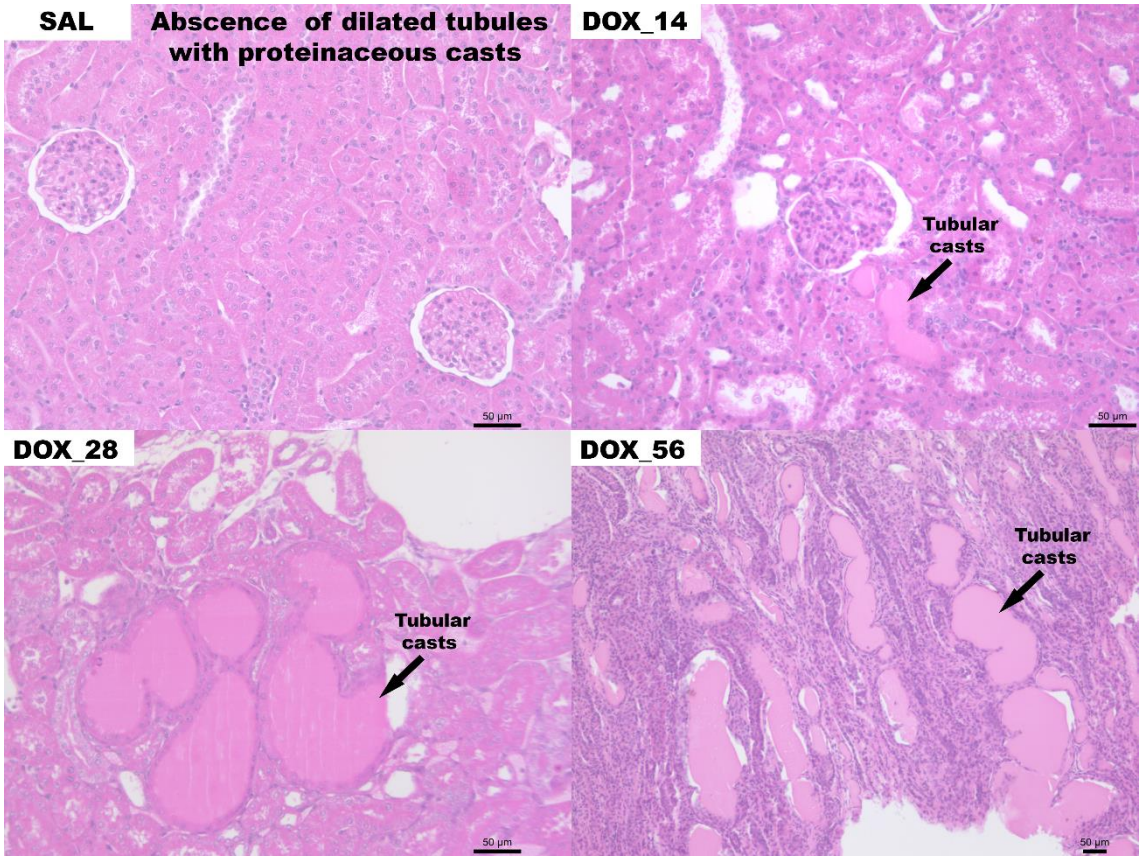

Figure 4 – Examples of a SAL group animal and a representative picture of each DOX period showing the dilated tubules with proteinaceous casts (200x). DOX_56 group is presented on a different scale to show the increasing in the tubular casts area and inflammatory cells infiltration (100x).

Figure 5 shows the LMN and PMN cells infiltration in the peritubular capillaries and interstitial tissue for all DOX groups and a figure showing almost no inflammatory cells infiltration in the SAL group. Also figure 5 shows other significant changes in the DOX_56 histology as the glomerular retraction, adhesion of glomerular capillaries in the Bowman's capsule, the high number atrophied tubules and interstitial inflammatory cells infiltration. This analysis shows that in the 14 and 28 days' periods there are the initial steps of the FSGS, but in the 56 days' period this framework is already established and the kidneys reached the end-stage of the DOX-induced kidney injury.

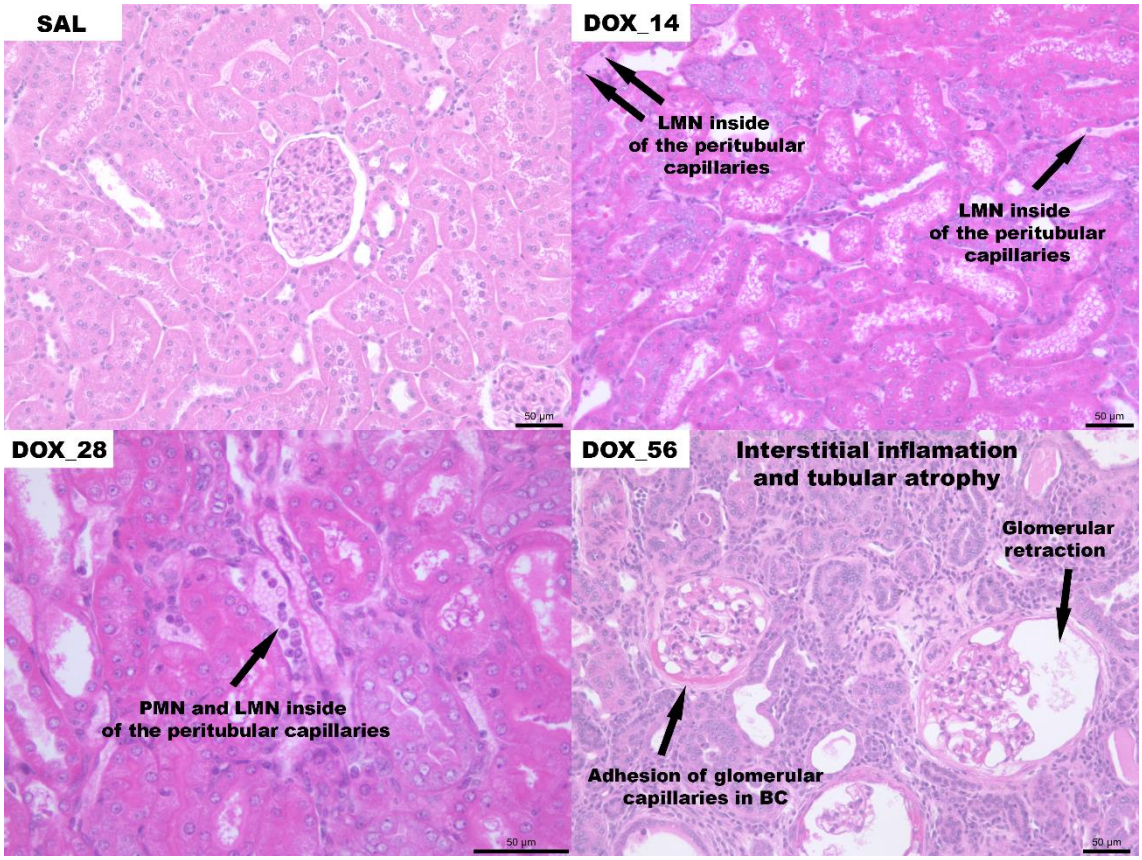

Figure 5 – Examples of a SAL group animal and a representative picture of each DOX period showing the inflammatory cells infiltration and also significant glomerular changes in the DOX_56 group (200x). DOX_28 shows in details the inflammatory cells infiltration (400x).

As mentioned before, all histological data were analyzed by a pathologist, and we built a qualitative table showing the main findings in the groups. Table 2 shows these main findings for all groups. From table 2 is possible to assure that we were able to induce the FSGS by a single DOX injection in the animals. Also it is possible to see that this CKD model has its initial steps with the recruitment of inflammatory cells, glomerulus retraction and tubules dilatation with protein casts. As shown in the figures 3, 4 and 5, and also in table 2, the end-stage of this model is similar to FSGS in humans and presents several severe damages amongst glomerulus, tubules, and interstitial tissue injuries.

Table 2 – Intensity of the histological findings in all groups. *

	SAL_14	DOX_14	SAL_28	DOX_28	SAL_56	DOX_56
Mesangial hypercellularity	+ + +	+	+ + +	+	+++	+
Reactive podocytes	-	+ +	-	+ +	-	+++
PMN cells in glomeruli	+	+ +	+	+ +	+	++
LMN cells in glomeruli	-	+	-	+	+	++
Glomerular hyalinosis[a]	-	+ +	-	+ +	-	+++
Adhesion of glomerular capillaries to BC[b]	-	-	-	-	-	++
Glomerular retraction[c]	-	++	-	++	-	+++
Dilated tubules with proteinaceous casts	-	+	-	+	-	+++
Interstitial mononuclear inflammation	-	-	-	+	-	+++
Focal tubular atrophy	-	-	-	-	-	++
Interstitial fibrosis	-	-	-	-	-	+
Periglomerular fibrosis	-	-	-	-	-	++
Segmental glomerulosclerosis	-	-	-	-	-	++

* the symbols represent the occurrence of the finding. + symbols represent the intensity of that finding occurrence. - Represent absence or very-low occurrence of that finding. [a] portion of glomerular involvement has a smooth glassy (hyaline) appearance; [b] Bowman capsule; [c] increased matrix with obliteration of glomerular capillary lumen.

3.2. *In vivo* ACB signal and *ex vivo* biodistribution of MNPs

The ACB signal showed a different profile for the DOX and SAL groups. The profiles found was very similar in all DOX groups, independent of time after renal injury induction. In SAL groups the signal increases rapidly and the time between the t_1

and t_2 (Δt) was shorter, while the ΔI was higher. DOX groups showed a slower increase (AT) after the injection, the time between passages was higher and ΔI was lower than SAL groups. Figure 6 shows an example of ACB signal acquired in animals from the SAL_14 and DOX_14 groups.

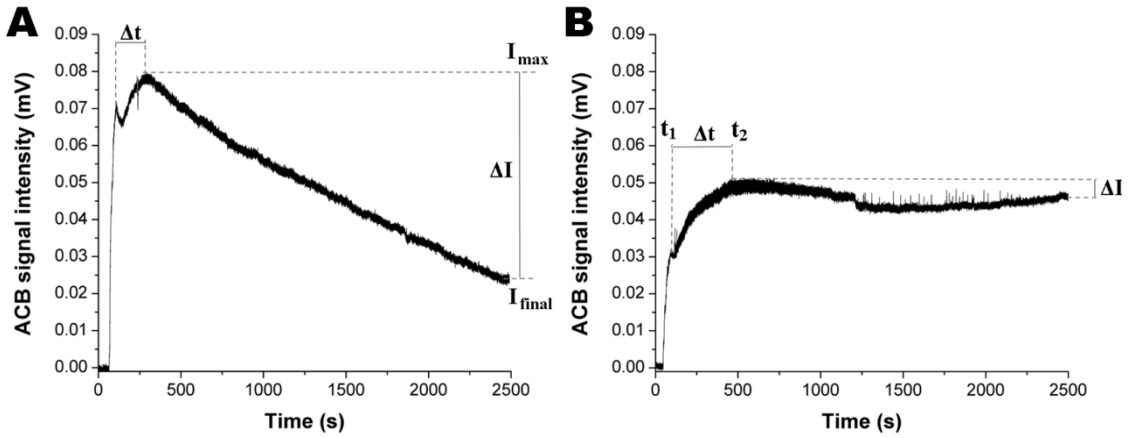

Figure 6 – ACB signal and quantification process examples. (A) Example of a signal acquired in the SAL_14 group, where it is showed the intensity quantification protocol. (B) Example of a signal acquired in the DOX_14 group, where is showed the passage time quantification protocol.

We quantified the signals intensities on regards to the I_{max}, $I_{final,}$ and ΔI module. There was no animal which presented an I_{final} higher than I_{max}. Figure 7 shows the ACB signals intensity quantification. In figure 7A, B and C is presented the I_{max}, which did not present significant differences between the SAL and DOX groups for the 14 and 28 days' period. However, at 56 days after DOX tail vein injection, I_{max} is significantly lower in DOX than in respective SAL group ($p = 0.045$). This difference can be related to the lower MNPs arrival in the kidney, and consequently renal hypoperfusion in the DOX_56 animals due to glomerulosclerosis. Also, these data suggest that until this period there was no influence of DOX renal damage on kidney perfusion. Figure 7D, E and F show I_{final} for the 14, 28 and 56 periods, respectively. In the 14 and 28 days' periods, I_{final} is increased in groups DOX_14 and DOX_28 when compared to respective controls ($p = 0.015$ and $p = 0.014$, respectively) while no difference between groups was

observed 56 days' period, probably due to the initial decreased value of I_{max}. Indeed, ACB signal determined by ΔI (figures 7G, H and I) corroborates the idea that renal damage induced by DOX promoted renal retention of MNPs decreasing ΔI values in all periods (14, 28 and 56 days; p = 0.005, p = 0.044 and p = 0.027, respectively) once the ΔI is calculated from the difference between I_{max} and I_{final}.

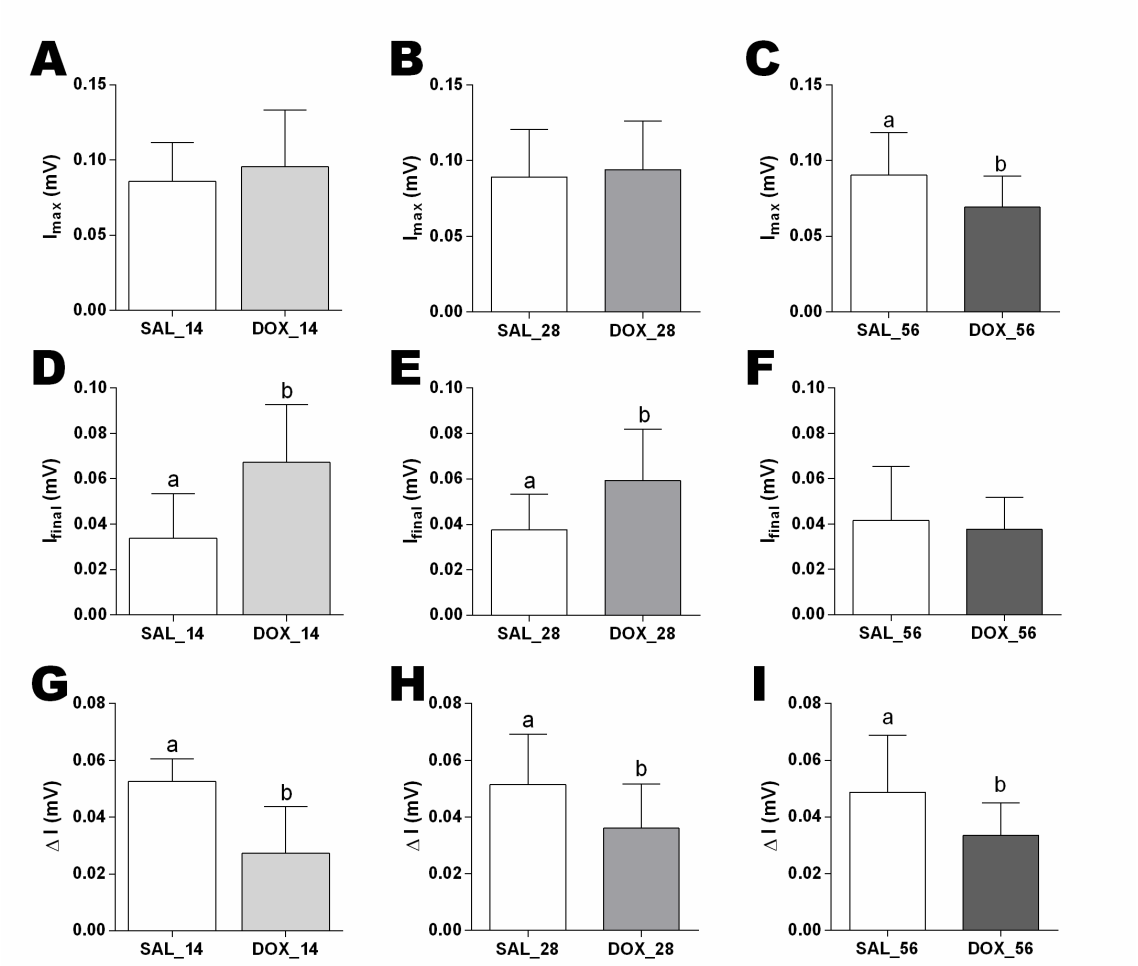

Figure 7 – ACB signal intensity quantifications. (A) I_{max} quantified from the 14 days' period. (B) I_{max} quantified from the 28 days' period. (C) I_{max} quantified from the 56 days' period. (D) I_{final} quantified from the 14 days' period. (E) I_{final} quantified from the 28 days' period. (F) I_{final} quantified from the 56 days' period. (G) ΔI quantified from the 14 days' period. (H) ΔI quantified from the 28 days' period. (I) ΔI quantified from the 56 days' period. Different letters represent a significant difference between groups with $p < 0.05$.

We also quantified the temporal parameters calculated by the interval between the first measurable ACB signal (t_1) and the second (t_2) ACB signal (maximum and stable

value) referent to MNPs passages in the kidney (Δt) and the arrival time (AT, time from the MNPs injection until t_1) of MNPs in the kidney. In figure 8A, B and C is showed the Δt found, respectively, in the 14, 28 and 56 days' period. We found a significant difference between the SAL and DOX groups for the Δt calculated in which in the DOX groups spent more time to reach ACB signal level correspondent to t_2 ($p = 0.025$, $p = 0.005$ and $p = 0.027$ for the 14, 28 and 56 days' period). Similarly, the AT (figures 8D, E and F) for all periods in DOX group was increased around two times when compared to respective SAL groups ($p = 0.049$, $p = 0.005$ and $p = 0.044$ for the 14, 28 and 56 days' period). These data can suggest lower renal perfusion efficiency in the DOX groups.

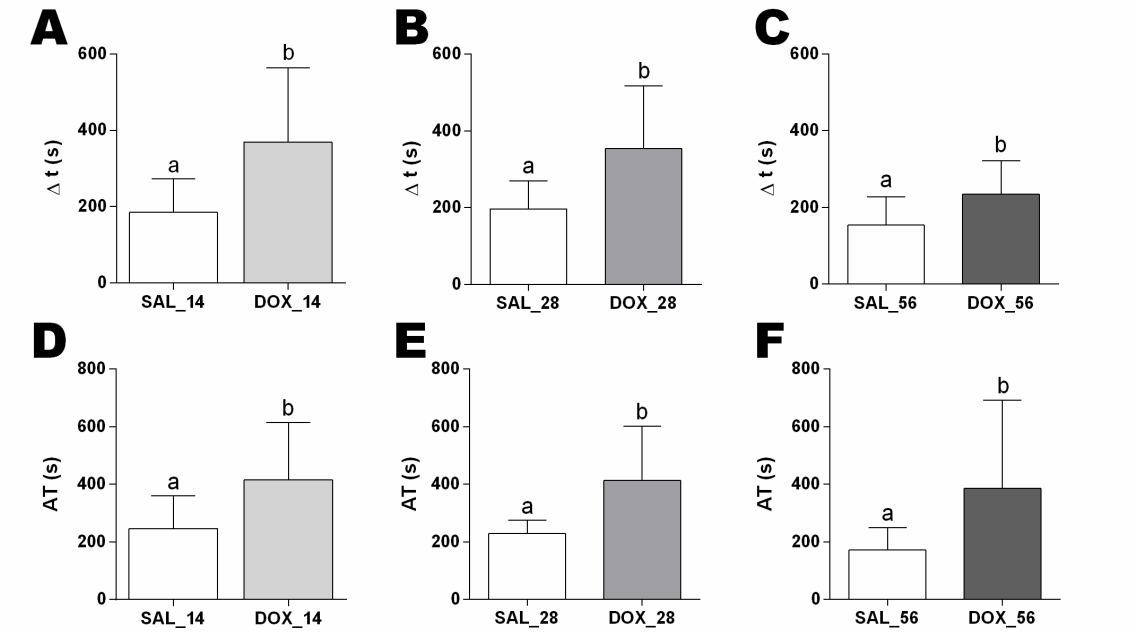

Figure 8 - ACB signal temporal quantifications. (A) Δt quantified from the 14 days' period. (B) Δt quantified from the 28 days' period. (C) Δt quantified from the 56 days' period. (D) AT quantified from the 14 days' period. (E) AT quantified from the 28 days' period. (F) AT quantified from the 56 days' period. Different letters represent a significant difference between groups with $p < 0.05$.

Biodistribution results are shown in figure 9. The overall profile of biodistribution was similar in the three different periods, showing a higher MNPs

retention in spleen, liver, and lungs, respectively. In the 14 and 28 days' periods (figures 9A and B), we found significant differences between the DOX and SAL groups for bladder (14 days: $p = 0.065$; 28 days: $p = 0.058$) and kidney (14 days: $p = 0.086$; 28 days: $p = 0.082$) suggesting lower filterability and more retention of MNPs in the kidneys of DOX groups, resulting in reduced MNPs content in the bladder when compared to respective SAL control groups. Differently from the 14 days' period, we found differences between blood, liver, spleen and lungs in the 28 days' period ($p = 0.0371$, $p = 0.011$, $p = 0.033$ and $p = 0.0140$, respectively) and 56 days' period ($p = 0.021$, $p = 0.0351$ and $p = 0.022$), as is shown in figure 9B and 9C. Although the kidneys and bladder showed significant differences, there was an inversion profile in the DOX_56 group when compared to both previous periods, where the DOX_56 showed a lower MNPs retention by the kidney ($p = 0.004$) and higher accumulation in the bladder ($p = 0.077$) when compared to SAL_56 group. This inversion can be related to the fact that in the 56 days' period the filtration barrier can be lost its size and electrostatic selectivity, allowing the MNPs passage from the kidneys to the bladder. Also, the 56 days' period showed significant differences in the animals' heart, which can be caused by the DOX cardiotoxicity, but this needs further investigations.

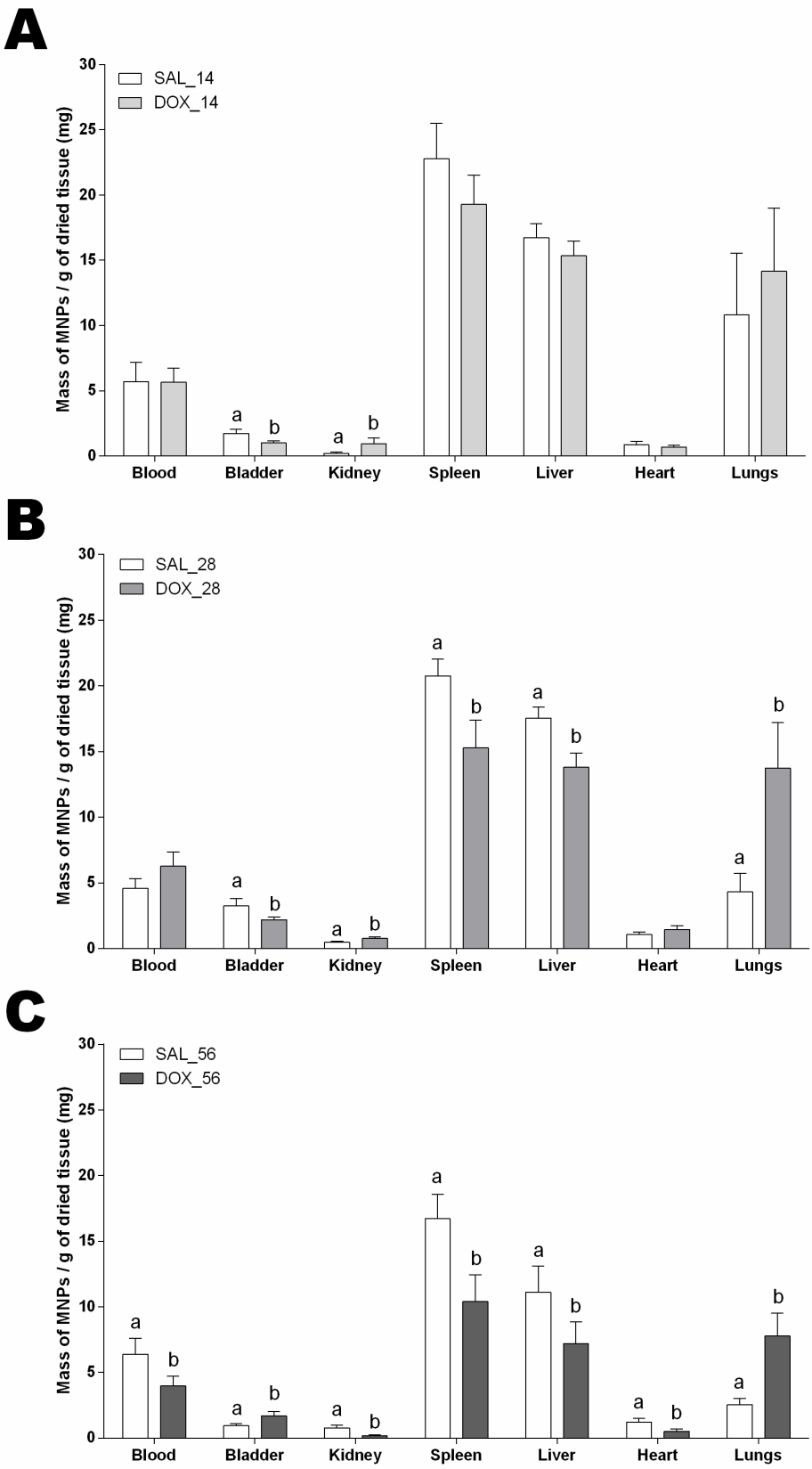

Figure 9 – ACB system biodistribution analyses. (A) Comparison between SAL_14 and DOX_14 groups. (B) Comparison between SAL_28 and DOX_28 groups. (C) Comparison between SAL_56 and DOX_56 groups. Different letters represent a significant difference between groups with $p < 0.1$.

4. DISCUSSION

CKD is a major problem in public health. The use of animal models to elucidate some aspects of kidney injuries evolution is common practice and a well-stablished platform for kidney function and new therapies studies. To optimize the studies involving progressive kidney diseases, it is necessary for new technologies and tools capable of providing dynamically *in vivo* data. Furthermore, technologies able to detecting *in vivo* early abnormal kidney behavior, related to morphology disarrange, without the need of the animals' sacrifice or biopsy sampling, are of paramount importance (42). Here, we reported, for the first time, the use of a magnetic measurement of MNPs kidney perfusion performed by the ACB system, in animals with doxorubicin-induced nephropathy. Although our study has used a level of invasiveness (femoral vein catheterization and a little incision in the lumber region), we believe that these procedures can be modified in further studies. Here we had the care to ensure the fast MNPs delivery to the kidney for sensor-kidney detection of the magnetic signal by the ACB system. Other studies might use a tail vein for MNPs administration (which can cause a delay in MNPs arrival in the organ), and the kidney localization can be assessed in other ways.

Proteinuria data strongly suggests that the doxorubicin administration caused a glomerular macromolecular barrier injury already in the first period, which increased over the periods and presented the highest levels of injury in the 56 days' period. As can be seen in the results section, all DOX groups proteinuria levels presented significant differences when compared to its corresponding SAL groups. Corroborating proteinuria data, our histological analyses showed significant kidney injury in DOX groups, which early manifests at the glomerular level and progressively evolve to tubular interstitial injury which can explain the increase in proteinuria as time last after DOX

administration. In general, doxorubicin administration distorted the normal renal architecture, as shown in histological data. We found prominent differences at the glomerular level including glomerular retraction and adhesion to Bowman's capsule, reduction in mesangial cellularity, the presence of reactive podocytes, LMN and PMN infiltration in DOX groups. The reactive and evident podocytes, associated to glomerular basal membrane changes, strongly suggests a kidney injury, once the main event which characterizes glomerular diseases and proteinuria framework are injuries in glomerular basal membrane, especially in podocytes, which are differentiated glomerular epithelial cells that involve the glomerular membranes (43, 44).

The molecular mechanisms which DOX induce nephrotoxicity, involve an increase in free radicals' production, decrease in the glutathione levels, increase of the lipid peroxides in liver, kidney and heart, and also a decrease in the glomerular ATPase activity, which is the main factor associated with tubular reabsorption process and structural endothelial capillary cell preservation (45). Literature data show that intravenous doxorubicin administration alters progressively the expression of important proteins of the podocytes slit diaphragm disrupting this layer of glomerular filtration barrier and leading to severe proteinuria (46). Furthermore, the hyaline deposits found in the glomerulus and renal tubules in DOX_14 and DOX_28 groups suggest an injury progression which is strongly related to a proteinuria state and the initial steps of an FSGS (47-49). Indeed, we observed a progression of tubular damage demonstrated by increasing in tubular dilation and hyaline deposition, culminating in focal tubular atrophy and interstitial fibrosis in late-stage after DOX. The infiltration of PMN and LMN cells inside of the glomerulus and peritubular capillaries also strongly suggest an inflammatory process, which contributes to the perpetuation of kidney damage until reaching the stage of FSGS (50). Although our histological analyses were not able to

distinguish the specific inflammatory cell types, the presence of PMN can be related to the presence of mastocytes and macrophages, which produce specific chemokines that are active mainly in PMN cells (51). The role of macrophage action, and its inflammatory protein MIP-1, in glomerular injuries and nephropathy caused by doxorubicin administration are well studied, and the reports published suggest a major role of macrophage action in this kidney injury model (50, 52-54).

In our study, we use the ACB system associated with MNPs intravenous administration aiming to investigate if renal damage characterized by morphological disarrangement and proteinuria could be able to generate different patterns of ACB signal detected from the MNPs. The ACB *in vivo* measurements showed different signal profiles between the SAL and DOX groups. The fact that the ΔI was statistically different between SAL and DOX groups is an indicator of a slow MNPs washout profile and its accumulation in the DOX groups animals' kidneys. The differences for ΔI found in 14 and 28 days' periods came from the differences in I_{final} parameter, while for the 56 days' period came from the I_{max} parameter. This might happen due to the fact that in the 14 and 28 days' periods the amount of MNPs that reached the animals' kidney in both SAL and DOX groups were the same, and the only differences were in the ability of the kidney expel the MNPs from its tissue. In the 56 days' period, it is possible to observe a decrease in MNPs amount that reached the kidney. These results suggest a renal hypoperfusion profile in this group, which can be related to elevated renal and systemic Angiotensin II, a potent vasoconstrictor hormone which is increased in doxorubicin nephropathy (55).

Besides the doxorubicin nephrotoxic effects, this drug also is linked to severe cardiotoxic effects as the negative ionotropy and chronotropy (56). As the heart is responsible for blood pumping and distribution, and the blood is the MNPs vehicle, if

the heart activity was compromised, the efficiency of MNPs washout from kidneys could be compromised as well. As the kidney and heart present several and complexes relationships, this issue has to be better addressed in further studies. It is worth to point out that when compared the DOX periods in the proteinuria analyses, the DOX_14 and DOX_28 did not present significant differences between each other, while both groups presented a significant difference when compared to the DOX_56 group. In the ACB signals, it is possible to see a similar profile, where there are no changes in I_{max}, between DOX and its corresponding SAL group, for the 14 and 28 days' period, and this difference arises in the 56 days' period. Comparing the proteinuria and the ACB *in vivo* intensity results, since the initial steps of the doxorubicin action, both proteinuria tests, and ACB system detected a difference between SAL and DOX groups in the same period. When compared over the injury progression, both did not detect differences between the 14 and 28 DOX groups, but this differences emerged in 56 days' period, as the I_{max} for this group.

The use of novel technologies and tracers in studies of kidney injury progression also were studied previously (42). Scarfe L. and co-workers reported the use of a multispectral optoacoustic tomography (MSOT) associated to a near infrared dye, and also a transcutaneous device that measures the clearance of a specific macromolecule related to a glomerular filtration rate, to follow up the doxorubicin kidney injury progression. In their study, it is reported a kinetic curve of the macromolecule clearance and a time-plot signal, extracted from the optoacoustic regions of interest data, very similar to our ACB *in vivo* signals. Just as we, they found that the passage of their tracers was delayed and its half-life in the kidney was longer in the doxorubicin group. They attribute this delay and longer half-life found to a deteriorated glomerular filtration rate. Despite Scarfe L. and co-author suggested that this delay can be associated with

deteriorated glomerular function, our data suggests that this delay can also be an effect of deficient blood supply to the kidney associated with both DOX cardiotoxicity (and consequently a decrease in the cardiac output) and activation of renin-angiotensin system, which can increase the renal vascular resistance (55-57). Although our signals are very similar to them, here we used MNPs with a significant size when compared to their macromolecule tracers, which can explain the slight differences found. In their data, the tracers take more time to be washed out from the doxorubicin-injured kidneys, but it is entirely cleared. Our data show a DOX groups signal profile which suggests there is a lower clearance of the MNPs from kidney, where the signal remains almost constant in DOX groups. Once our particles have a significant size and we found several morphological changes as the hyaline cylinders in renal tubules and fibrosis, the MNPs' size can be a feature that hindrances its total clearance.

The kidney ability to excrete nanostructured materials were subject of several studies. This theme has great importance in the nanomedicine field, once the long-term retention of these materials in organs such liver and spleen are not convenient. Choi and co-authors used a quantum dot to define the maximum size of nanostructured agents to be cleared through the kidneys (58). They found that particles with a size smaller than 6 nm are totally and rapidly cleared by the kidneys, where particles with a size between 7 and 8 nm presented clearance from the bloodstream by both liver and kidney. In general, it is assumed that particles with a size larger than 10 nm are not cleared by the kidneys (13, 59-61). Our MNPs presented size of 15 ±5 nm, which can explain this lack of total clearance in our signal. Also, it is worth to point out that our particles obey a log-normal size distribution, wherein the same batch there were MNPs smaller than 5 nm and larger than 30 nm as well, presenting a mean size of 15 nm (for further details find our previous paper (26)).

The ACB temporal parameters quantified as Δt and AT also showed significant differences between SAL and DOX groups. The Δt, also called as transit time, was longer for the DOX groups when compared to the SAL groups. This parameter can be related to a difficulty of the kidney to clear the MNPs from its tissue from both events: the deficient blood supply and the morphological changes found in the organ. The AT (i.e., the time from the injection that the MNPs take to arrive in the kidney) also showed differences between SAL and DOX groups. These temporal parameters suggest a blood supply reduction in the kidney which corroborates with the reduced delta I presented previously. The results show difficulty in both the MNPs arrival in the kidney and its washout from this organ.

The study published by Scarfe L. and co-workers showed that their technology was able to distinguish the renal cortex from the pelvis, which gave information about the tracer dynamics inside of the kidney. In their data, there is a delay in the tracer time to come out from renal cortex and arrival in the pelvis. Although they have analyzed the regions separately, giving two time-plot signals, and we collected one signal regarding the entire organ, our signals are similar. In a brief visual inspection of their data, is possible to see that summing up both of their signals (cortex and pelvis) will result in a signal very similar to ours. Also, their data showed that this delay increases in the kidney-injured animals and we also found differences between DOX and SAL groups, where the Δt and AT were longer for DOX groups (42). Although they suggested that this increase in the delay happens due to a compromised passage of their tracer through the kidneys tubules, our results also suggest a deficient blood supply related to DOX cardiotoxicity and renin-angiotensin system activation, as commented before. If the heart has reduced contractility to pump the blood to, and through, the kidneys, it is

possible that these temporal parameters can be influenced by this hypoperfusion secondary to heart failure, but this requires further studies.

In another study, focused in the use of iron oxide nanoparticles (hydrodynamic size of 150 nm) as a kidney perfusion contrast agent in MRI, Trillaud and co-workers performed stenosis of the intrarenal aorta to produce a blood flow asymmetry between the animal's kidney (41). Their results showed that the stenotic kidneys presented a significantly delayed and less pronounced maximum signal intensity. They stated that this delay and lower maximum signal intensity found are related to a significant decrease of the relative blood flow in the stenotic kidneys, corroborating our findings. Also, they conclude that the iron oxide nanoparticles are good kidney perfusion contrast agents in MRI, far better than gadolinium-based contrast agents, where the nanoparticles were able to distinguish the stenotic and normal kidneys perfusion. Here we found almost the same. The MNPs and ACB system were also able to distinguish the CKD-induced kidneys from the normal kidneys *in vivo* and in real-time, using both intensity and temporal parameters to do so.

Biodistribution data showed the highest MNPs accumulation in spleen, liver, and lungs for all SAL and DOX groups, as expected. Indeed, these organs are known to be of paramount importance in MNPs uptake and biodegradation processes (28, 62-66). Liver, spleen, and lungs are the main hosts of the mononuclear phagocytic system's cells, which are the main responsible for nanoparticles phagocytosis and clearance route. The literature describes the macrophages as the most important cell playing this role (67). Also, its number in organs as liver, spleen, and lungs are very high, which can explain this high MNPs uptake in these organs. We recently published a paper addressed to the Cit-MNPs biodistribution and liver uptake, and we also found liver, spleen, and lungs as the main responsible for Cit-MNPs uptake (28). In the 14 days'

period, we found significant differences in both kidneys and bladder. The data suggests an accumulation in the kidney and a lower amount of MNPs in the bladder of the DOX_14 group when compared with SAL_14 group. The ACB signal intensity *in vivo* also showed an increase in I_{final} in the DOX_14 group when compared to the SAL_14 group. These data show an MNPs accumulation in the animals DOX-injured kidneys. This can be explained by a kidney difficulty to expel the MNPs from its tissue by both the decreased blood flow in the organ and the presence of PMN cells found in the histology. As commented before, macrophages are strongly related to MNPs uptake and clearance pathways. The presence of PMN cells in the DOX-injured kidneys also has a strong relationship with macrophagocitic activities, where the macrophages are the first cells to arrive in the inflamed tissue and produce the MIP-1 proteins, which is a chemotactic molecule responsible for recruiting PMN cells, more specifically neutrophils (50-52, 54).

In the 28 days' period, we found the same profile for kidney and bladder, but at this period we also found significant differences in spleen, liver, and lungs, where the liver and spleen presented a lower, and the lungs a higher MNPs accumulation in DOX_28 group than in the SAL_28 group. The DOX administration impacts on liver macrophages were studied before. The literature reports that the DOX cause a decrease in the liver macrophages number and activity (68, 69). Furthermore, the DOX effects in the spleen were studied using DOX-loaded nanoparticles and free DOX and shows some DOX effects on the nucleated cells, lymphocytes, erythroblasts and granulocytes (70). Despite the animal model, other studies suggest that DOX administration can cause spleen toxicity in dogs (71). Once DOX causes effects in some immunological cells in spleen, a decrease in liver macrophages number and activity and assuming, from the MNPs point of view, similarity from both organs for phagocytic profile (Kupffer

cells for liver and red pulp macrophages for spleen) and the same progenitor cells type (bone marrow monocytes), we can extrapolate the liver effects of DOX administration for spleen as well. (67). In this way, the lower accumulation of the MNPs in these organs are related to this deficit in macrophages number and activity in these organs. Our *in vivo* and *ex vivo* data suggests that the lungs higher accumulation of MNPs can be related to the cardiotoxicity effects of DOX. As the heart can present a lower strength to pump the blood through the pulmonary microcirculation, and also the lungs present a high microvasculature area, the heart difficulty to pump the blood through the lungs can be a significant factor in the MNPs lung accumulation. Also, the DOX effects on lungs are described in some experimental studies, and case reports in humans as a result of reactive oxygen species overproduced by DOX leading to pleural edema, pulmonary embolism, and fibrosis (72-74). Indeed, lung tissue is singular sensitive to free radical damage due to, among other reasons, its increased oxidative metabolism and reduced antioxidant defense in comparison to other organs, such as the liver.

For the 56 days' periods we also found all differences mentioned above, but this time we found differences for heart and blood, and also an inversion profile, when compared with 14 and 28 days' periods, for kidney and bladder. The lesser accumulation of MNPs in the kidney of DOX_56 group is under accordance with the ACB *in vivo* intensity analyses (reduction in I_{max}). Besides the lower blood supply, and consequently lower MNPs delivery to the kidneys, the late effects of DOX seems to drastically reduce the selectivity of filtration barrier, turning it very permissive not only to protein but even MNPs filtration. This behavior is suggested for different data *in vivo* (progressive proteinuria and reduction in the ACB signal) and postmortem (glomerular and tubular damage; biodistribution inversion with more MNPs in the bladder than in the kidney). Jeansson M. and co-authors studied the effects of the end-stage DOX-

injured kidneys of mice. In such study, they found that the DOX administration can cause an increase in the filtration pores size and a decrease in charge density, which lead to a huge loss of size and charge selectivity of the glomerular barrier (75). Once the DOX induces a severe albuminuria, and the albumin in solution present almost 14 nm of size, and our MNPs present a mean physical core of 15 nm, responding to a log-normal size distribution (ranging from less than 5nm and above 30 nm), we can assume that in this end-stage of CKD DOX-induced model, we reach this loss in size and charge density selectivity which lead to a higher MNPs excretion by kidneys and consequently a higher MNPs presence in bladder(42, 76). This increase in the MNPs clearance by kidneys can explain the lesser quantity of MNPs in the blood of DOX_56 when compared to control SAL. Also, the *in vivo* ACB analyzes showed lower MNPs amount that reached the kidneys, which can help to decrease the amount of MNPs accumulated in the organ.

5. CONCLUSION

In summary, we applied the ACB system *in vivo* and in real-time, and also *ex vivo*, to study a CKD DOX-induced in rats. The system presented a good performance, distinguishing the healthy from the injured animals in both *in vivo* and *ex vivo* analysis. In the biochemical analyzes, our data suggests a severe proteinuria state, which presented the highest value after 56 days from the DOX injection. The morphological analyzes show a progressive kidney injury that reached the FSGS characteristics in the last period, involving severe damage of the glomerular structure, podocytes changes, glomerular retraction, dilated tubules with protein casts, focal tubular atrophy, inflammatory cells infiltration in both glomerulus and interstice, and segmental glomerulosclerosis. The ACB data is strongly in accordance with the biochemical (total protein) results and morphological analyses, showing that the ACB system associated

with MNPs as a magnetic nanotracer, can be a good tool to study kidney injuries. The ACB system is a low-cost, portable and versatile technique to detect MNPs *in vivo* and in real-time. These system's characteristics can help to decrease the costs and time in studies involving kidney progressive diseases opening new possibilities for diagnosis, prognosis and follow-up.

6. REFERENCES

1. Coresh J, Selvin E, Stevens LA, Manzi J, Kusek JW, Eggers P, et al. Prevalence of chronic kidney disease in the United States. Jama. 2007;298(17):2038-47.

2. Fassett RG, Venuthurupalli SK, Gobe GC, Coombes JS, Cooper MA, Hoy WE. Biomarkers in chronic kidney disease: a review. Kidney international. 2011;80(8):806-21. Epub 2011/06/24.

3. Jha V, Garcia-Garcia G, Iseki K, Li Z, Naicker S, Plattner B, et al. Chronic kidney disease: global dimension and perspectives. The Lancet. 2013;382(9888):260-72.

4. Brede C, Labhasetwar V. Applications of nanoparticles in the detection and treatment of kidney diseases. Advances in chronic kidney disease. 2013;20(6):454-65. Epub 2013/11/12.

5. Rushton HG. The evaluation of acute pyelonephritis and renal scarring with technetium 99m-dimercaptosuccinic acid renal scintigraphy: evolving concepts and future directions. Pediatr Nephrol. 1997;11(1):108-20. Epub 1997/02/01.

6. Daniel GB, Mitchell SK, Mawby D, Sackman JE, Schmidt D. Renal nuclear medicine: a review. Veterinary radiology & ultrasound : the official journal of the American College of Veterinary Radiology and the International Veterinary Radiology Association. 1999;40(6):572-87. Epub 1999/12/23.

7. Laissy JP, Faraggi M, Lebtahi R, Soyer P, Brillet G, Mery JP, et al. Functional evaluation of normal and ischemic kidney by means of gadolinium-DOTA enhanced TurboFLASH MR imaging: a preliminary comparison with 99Tc-MAG3 dynamic scintigraphy. Magnetic resonance imaging. 1994;12(3):413-9. Epub 1994/01/01.

8. Grist TM. Magnetic resonance angiography of renal artery stenosis. American journal of kidney diseases : the official journal of the National Kidney Foundation. 1994;24(4):700-12. Epub 1994/10/01.

9. Hricak H, Crooks L, Sheldon P, Kaufman L. Nuclear magnetic resonance imaging of the kidney. Radiology. 1983;146(2):425-32.

10. Perazella MA. Current status of gadolinium toxicity in patients with kidney disease. Clinical Journal of the American Society of Nephrology. 2009;4(2):461-9.

11. Perazella MA, Rodby RA, editors. Gadolinium use in patients with kidney disease: a cause for concern. Seminars in dialysis; 2007: Wiley Online Library.

12. Neuwelt EA, Hamilton BE, Varallyay CG, Rooney WR, Edelman RD, Jacobs PM, et al. Ultrasmall superparamagnetic iron oxides (USPIOs): a future alternative magnetic resonance (MR) contrast agent for patients at risk for nephrogenic systemic fibrosis (NSF)? Kidney international. 2009;75(5):465-74. Epub 2008/10/10.

13. Longmire M, Choyke PL, Kobayashi H. Clearance properties of nano-sized particles and molecules as imaging agents: considerations and caveats. Nanomedicine (Lond). 2008;3(5):703-17. Epub 2008/09/27.

14. Shubayev VI, Pisanic TR, 2nd, Jin S. Magnetic nanoparticles for theragnostics. Advanced drug delivery reviews. 2009;61(6):467-77. Epub 2009/04/25.

15. Singh A, Sahoo SK. Magnetic nanoparticles: a novel platform for cancer theranostics. Drug Discov Today. 2014;19(4):474-81. Epub 2013/10/22.

16. Hultman KL, Raffo AJ, Grzenda AL, Harris PE, Brown TR, O'Brien S. Magnetic resonance imaging of major histocompatibility class II expression in the renal medulla using immunotargeted superparamagnetic iron oxide nanoparticles. ACS nano. 2008;2(3):477-84. Epub 2009/02/12.

17. Kobayashi H, Jo SK, Kawamoto S, Yasuda H, Hu X, Knopp MV, et al. Polyamine dendrimer-based MRI contrast agents for functional kidney imaging to diagnose acute renal failure. J Magn Reson Imaging. 2004;20(3):512-8. Epub 2004/08/28.

18. Hauger O, Delalande C, Trillaud H, Deminiere C, Quesson B, Kahn H, et al. MR imaging of intrarenal macrophage infiltration in an experimental model of nephrotic syndrome. Magnetic resonance in medicine. 1999;41(1):156-62. Epub 1999/02/20.

19. Laginha KM, Verwoert S, Charrois GJ, Allen TM. Determination of doxorubicin levels in whole tumor and tumor nuclei in murine breast cancer tumors. Clinical cancer research. 2005;11(19):6944-9.

20. Okuda S, Oh Y, Tsuruda H, Onoyama K, Fujimi S, Fujishima M. Adriamycin-Induced Nephropathy as a Model of Chronic Progressive Glomerular-Disease. Kidney international. 1986;29(2):502-10.

21. El-Shitany NA, El-Haggar S, El-Desoky K. Silymarin prevents adriamycin-induced cardiotoxicity and nephrotoxicity in rats. Food and Chemical Toxicology. 2008;46(7):2422-8.

22. Von Hoff DD, Layard MW, Basa P, Davis HL, Von Hoff AL, Rozencweig M, et al. Risk factors for doxorubicin-lnduced congestive heart failure. Annals of internal medicine. 1979;91(5):710-7.

23. Pippin JW, Brinkkoetter PT, Cormack-Aboud FC, Durvasula RV, Hauser PV, Kowalewska J, et al. Inducible rodent models of acquired podocyte diseases. American Journal of Physiology-Renal Physiology. 2009;296(2):F213-F29.

24. Weening JJ, Rennke HG. Glomerular permeability and polyanion in adriamycin nephrosis in the rat. Kidney international. 1983;24(2):152-9. Epub 1983/08/01.

25. Lee VWS, Harris DCH. Adriamycin nephropathy: A model of focal segmental glomerulosclerosis. Nephrology. 2011;16(1):30-8.

26. Prospero AG, Quini CC, Bakuzis AF, Fidelis-de-Oliveira P, Moretto GM, Mello FP, et al. Real-time in vivo monitoring of magnetic nanoparticles in the bloodstream by AC biosusceptometry. Journal of nanobiotechnology. 2017;15(1):22.

27. Quini CC, Matos JF, Prospero AG, Calabresi MFF, Zufelato N, Bakuzis AF, et al. Renal perfusion evaluation by alternating current biosusceptometry of magnetic nanoparticles. J Magn Magn Mater. 2015;380:2-6.

28. Quini CC, Prospero AG, Calabresi MFF, Moretto GM, Zufelato N, Krishnan S, et al. Real-time liver uptake and biodistribution of magnetic nanoparticles determined by AC biosusceptometry. Nanomedicine : nanotechnology, biology, and medicine. 2017;13(4):1519-29.

29. Quini CC, Próspero AG, Kondiles BR, Chaboub L, Hogan MK, Baffa O, et al. Development of a protocol to assess cell internalization and tissue uptake of magnetic nanoparticles by AC Biosusceptometry. J Magn Magn Mater. 2019;473:527-33.

30. Cora LA, Americo MF, Oliveira RB, Baffa O, Moraes R, Romeiro FG, et al. Disintegration of magnetic tablets in human stomach evaluated by alternate current Biosusceptometry. European Journal of Pharmaceutics and Biopharmaceutics. 2003;56(3):413-20.

31. Cora LA, Romeiro FG, Stelzer M, Americo MF, Oliveira RB, Baffa O, et al. AC biosusceptometry in the study of drug delivery. Advanced drug delivery reviews. 2005;57(8):1223-41. Epub 2005/06/07.

32. Americo MF, Oliveira RB, Romeiro FG, Baffa O, Cora LA, Miranda JR. Scintigraphic validation of AC Biosusceptometry to study the gastric motor activity and the intragastric distribution of food in humans. Neurogastroenterology and motility : the official journal of the European Gastrointestinal Motility Society. 2007;19(10):804-11. Epub 2007/09/22.

33. Andreis U, Americo MF, Cora LA, Oliveira RB, Baffa O, Miranda JR. Gastric motility evaluated by electrogastrography and alternating current biosusceptometry in dogs. Physiological measurement. 2008;29(9):1023-31. Epub 2008/08/14.

34. Miranda JRA, Oliveira RB, Matsuda NM, Baffa O. Susceptometric Measurement of Gastric-Emptying. Int Congr Ser. 1992;988:635-8.

35. Baffa O, Oliveira RB, Miranda JR, Troncon LE. Analysis and development of AC biosusceptometer for orocaecal transit time measurements. Medical & biological engineering & computing. 1995;33(3):353-7. Epub 1995/05/01.

36. Bakuzis AF, Morais PC, Pelegrini F. Surface and exchange anisotropy fields in MnFe2O4 nanoparticles: Size and temperature effects. J Appl Phys. 1999;85(10):7480-2.

37. Rodrigues HF, Mello FM, Branquinho LC, Zufelato N, Silveira-Lacerda EP, Bakuzis AF. Real-time infrared thermography detection of magnetic nanoparticle hyperthermia in a murine model under a non-uniform field configuration. Int J Hyperther. 2013;29(8):752-67.

38. Bakuzis AF, Branquinho LC, Castro LLE, Eloi MTDA, Miotto R. Chain formation and aging process in biocompatible polydisperse ferrofluids: Experimental investigation and Monte Carlo simulations. Adv Colloid Interfac. 2013;191:1-21.

39. Branquinho LC, Carriao MS, Costa AS, Zufelato N, Sousa MH, Miotto R, et al. Effect of magnetic dipolar interactions on nanoparticle heating efficiency: Implications for cancer hyperthermia. Sci Rep-Uk. 2013;3.

40. Marshall T, Williams KM. Total protein determination in urine: elimination of a differential response between the coomassie blue and pyrogallol red protein dye-binding assays. Clinical chemistry. 2000;46(3):392-8.

41. Trillaud H, Degrèze P, Mesplède Y, Douws C, Palussière J, Grenier N. Evaluation of experimentally induced renal hypoperfusion using iron oxide particles and fast magnetic resonance imaging. Academic radiology. 1995;2(4):293-9.

42. Scarfe L, Rak-Raszewska A, Geraci S, Darssan D, Sharkey J, Huang J, et al. Measures of kidney function by minimally invasive techniques correlate with histological glomerular damage in SCID mice with adriamycin-induced nephropathy. Sci Rep. 2015;5:13601. Epub 2015/09/04.

43. Zhou Y, Kong X, Zhao P, Yang H, Chen L, Miao J, et al. Peroxisome proliferator-activated receptor-α is renoprotective in doxorubicin-induced glomerular injury. Kidney international. 2011;79(12):1302-11.

44. Sharma R, Waller AP, Agrawal S, Wolfgang KJ, Luu H, Shahzad K, et al. Thrombin-induced podocyte injury is protease-activated receptor dependent. J Am Soc Nephrol. 2017:ASN. 2016070789.

45. Barbey MM, Fels LM, Soose M, Poelstra K, Gwinner W, Bakker W, et al. Adriamycin Affects Glomerular Renal-Function - Evidence for the Involvement of Oxygen Radicals. Free Radical Res Com. 1989;7(3-6):195-203.

46. Otaki Y, Miyauchi N, Higa M, Takada A, Kuroda T, Gejyo F, et al. Dissociation of NEPH1 from nephrin is involved in development of a rat model of focal segmental glomerulosclerosis. American Journal of Physiology-Renal Physiology. 2008;295(5):F1376-F87.

47. Bertani T, Cutillo F, Zoja C, Broggini M, Remuzzi G. Tubulo-interstitial lesions mediate renal damage in adriamycin glomerulopathy. Kidney international. 1986;30(4):488-96. Epub 1986/10/01.

48. Gutierrez-Millet V, Nieto J, Praga M, Usera G, Martinez MA, Morales JM. Focal glomerulosclerosis and proteinuria in patients with solitary kidneys. Archives of internal medicine. 1986;146(4):705-9.

49. Lee HS, Spargo BH. Significance of renal hyaline arteriolosclerosis in focal segmental glomerulosclerosis. Nephron. 1985;41(1):86-93.

50. Szalay CI, Erdélyi K, Kökény G, Lajtár E, Godó M, Révész C, et al. Oxidative/nitrative stress and inflammation drive progression of doxorubicin-induced renal fibrosis in rats as revealed by comparing a normal and a fibrosis-resistant rat strain. PloS one. 2015;10(6):e0127090.

51. Wu X, Wittwer AJ, Carr LS, Crippes BA, DeLarco JE, Lefkowith JB. Cytokine-induced neutrophil chemoattractant mediates neutrophil influx in immune complex glomerulonephritis in rat. The Journal of clinical investigation. 1994;94(1):337-44.

52. Vielhauer V, Berning E, Eis V, Kretzler M, Segerer S, Strutz F, et al. CCR1 blockade reduces interstitial inflammation and fibrosis in mice with glomerulosclerosis and nephrotic syndrome. Kidney international. 2004;66(6):2264-78.

53. Wang Y, Wang Y, Zheng G, Lee V, Ouyang L, Chang D, et al. Ex vivo programmed macrophages ameliorate experimental chronic inflammatory renal disease. Kidney international. 2007;72(3):290-9.

54. Wang Y, Wang Y, Cai Q, Zheng G, Lee VW, Zheng D, et al. By homing to the kidney, activated macrophages potently exacerbate renal injury. The American journal of pathology. 2008;172(6):1491-9.

55. Takenaka T, Inoue T, Miyazaki T, Kobori H, Nishiyama A, Ishii N, et al. Klotho suppresses the renin-angiotensin system in adriamycin nephropathy. Nephrology Dialysis Transplantation. 2017;32(5):791-800.

56. Kang YJ, Chen Y, Yu A, Voss-McCowan M, Epstein PN. Overexpression of metallothionein in the heart of transgenic mice suppresses doxorubicin cardiotoxicity. The Journal of clinical investigation. 1997;100(6):1501-6.

57. Kang YJ, Chen Y, Epstein PN. Suppression of doxorubicin cardiotoxicity by overexpression of catalase in the heart of transgenic mice. Journal of Biological Chemistry. 1996;271(21):12610-6.

58. Choi HS, Liu W, Misra P, Tanaka E, Zimmer JP, Itty Ipe B, et al. Renal clearance of quantum dots. Nat Biotechnol. 2007;25(10):1165-70. Epub 2007/09/25.

59. Kobayashi H, Brechbiel MW. Dendrimer-based nanosized MRI contrast agents. Current pharmaceutical biotechnology. 2004;5(6):539-49. Epub 2004/12/08.

60. Yu M, Zheng J. Clearance Pathways and Tumor Targeting of Imaging Nanoparticles. ACS nano. 2015;9(7):6655-74. Epub 2015/07/08.

61. Choi CH, Zuckerman JE, Webster P, Davis ME. Targeting kidney mesangium by nanoparticles of defined size. Proceedings of the National Academy of Sciences of the United States of America. 2011;108(16):6656-61. Epub 2011/04/06.

62. Sun C, Lee JS, Zhang M. Magnetic nanoparticles in MR imaging and drug delivery. Advanced drug delivery reviews. 2008;60(11):1252-65. Epub 2008/06/19.

63. Bengele HH, Palmacci S, Rogers J, Jung CW, Crenshaw J, Josephson L. Biodistribution of an ultrasmall superparamagnetic iron oxide colloid, BMS 180549, by

different routes of administration. Magnetic resonance imaging. 1994;12(3):433-42. Epub 1994/01/01.

64. Lacava LM, Lacava ZGM, Azevedo RB, Chaves SB, Garcia VAP, Silva O, et al. Use of magnetic resonance to study biodistribution of dextran-coated magnetic fluid intravenously administered in mice. J Magn Magn Mater. 2002;252(1-3):367-9.

65. Owens III DE, Peppas NA. Opsonization, biodistribution, and pharmacokinetics of polymeric nanoparticles. International journal of pharmaceutics. 2006;307(1):93-102.

66. Estevanato LL, Lacava LM, Carvalho LC, Azevedo RB, Silva O, Pelegrini F, et al. Long-term biodistribution and biocompatibility investigation of dextran-coated magnetite nanoparticle using mice as the animal model. Journal of biomedical nanotechnology. 2012;8(2):301-8. Epub 2012/04/21.

67. Arami H, Khandhar A, Liggitt D, Krishnan KM. In vivo delivery, pharmacokinetics, biodistribution and toxicity of iron oxide nanoparticles. Chemical Society Reviews. 2015;44(23):8576-607.

68. Daemen T, Regts J, Meesters M, Ten Kate MT, Bakker-Woudenberg IA, Scherphof GL. Toxicity of doxorubicin entrapped within long-circulating liposomes. Journal of Controlled Release. 1997;44(1):1-9.

69. Daemen T, Hofstede G, Ten Kate MT, Bakker-Woudenberg IA, Scherphof GL. Liposomal doxorubicin-induced toxicity: Depletion and impairment of phagocytic activity of liver macrophages. International journal of cancer. 1995;61(5):716-21.

70. Gibaud S, Andreux J, Weingarten C, Renard M, Couvreur P. Increased bone marrow toxicity of doxorubicin bound to nanoparticles. European Journal of Cancer. 1994;30(6):820-6.

71. Herman E, Rahman A, Ferrans V, Vick J, Schein P. Prevention of chronic doxorubicin cardiotoxicity in beagles by liposomal encapsulation. Cancer research. 1983;43(11):5427-32.

72. Injac R, Radic N, Govedarica B, Perse M, Cerar A, Djordjevic A, et al. Acute doxorubicin pulmotoxicity in rats with malignant neoplasm is effectively treated with fullerenol C60 (OH) 24 through inhibition of oxidative stress. Pharmacological reports. 2009;61(2):335-42.

73. Verschoore J, Lagrange J-L, Boublil J-L, Aubanel J-M, Blaive B, Pinto J, et al. Pulmonary toxicity of a combination of low-dose doxorubicin and irradiation for inoperable lung cancer. Radiotherapy and Oncology. 1987;9(4):281-8.

74. Minchin RF, Johnston MR, Schuller HM, Aiken MA, Boyd MR. Pulmonary toxicity of doxorubicin administered by in situ isolated lung perfusion in dogs. Cancer. 1988;61(7):1320-5.

75. Jeansson M, Bjorck K, Tenstad O, Haraldsson B. Adriamycin Alters Glomerular Endothelium to Induce Proteinuria. J Am Soc Nephrol. 2009;20(1):114-22.

76. Miller WG, Bruns DE, Hortin GL, Sandberg S, Aakre KM, McQueen MJ, et al. Current issues in measurement and reporting of urinary albumin excretion. Clinical chemistry. 2009;55(1):24-38.

CHAPTER 2

Dynamic cerebral perfusion parameters and magnetic nanoparticles accumulation accessed by AC biosusceptometry

PREFÁCIO

Este trabalho teve seu início durante meados de 2013, quando eu ainda era aluno de mestrado no PPG em Biologia Geral e Aplicada.

Durante um dia qualquer no laboratório de Biomagnetismo, eu vi o Dr. Matheus Alvarez (na época ainda aluno de doutorado) trabalhando em alguns sinais em seu computador. Ao indagá-lo sobre o que estava fazendo, Matheus me mostrou o projeto no qual estava trabalhando. Aqueles sinais eram uma plotagem temporal de intensidades médias das regiões de interesse coletados de imagens de cintilografia de fluxo cerebral. Ao ver a semelhança de seus sinais, tanto o perfil do sinal quanto a técnica de utilização de traçadores (no sentido genérico da palavra), com alguns sinais anteriormente coletados por nós via sistema BAC, me indaguei se era possível estudar o fluxo cerebral utilizando nanopartículas magnéticas e o sistema BAC. Ao levar essa idéia ao meu orientador, o Prof. José Ricardo, sempre muito receptivo às minhas aventuras científicas, essa idéia culminou, primeiramente, no projeto de mestrado do aluno Gustavo Morlin Moretto, um grande amigo até os dias de hoje.

Infelizmente o aluno Gustavo não seguiu na carreira acadêmica e traçou seu futuro por meio do ingresso no programa de residência em Radioterapia no HC de São Paulo. Uma vez que eu tinha dado os passos iniciais para o desenvolvimento deste projeto, me senti na obrigação de assumí-lo como minha responsabilidade e finalizá-lo. Sob autorização do Prof. José Ricardo, assumi o trabalho com colaboração e ajuda do aluno de doutorado Guilherme Soares e do Dr. Caio Quini. Fizemos uma reavaliação do trabalho, refizemos uma série de experimentos, requantificação dos dados, e demos uma nova roupagem ao trabalho, que até então era apresentado de outra maneira, muito diferente do que tínhamos de idéia inicial e alcançamos agora.

Este trabalho compreende a utilização do sistema BAC como uma ferramenta de estudos de *Cerebral Blood Flow* e perfusão cerebral de nanopartículas. Atualmente existem uma série de trabalhos que envolvem o uso de materiais nanoestruturados (vide o caso do fármaco paclitaxel) para atingir o tecido cerebral. Sendo assim, novas técnicas capazes de avaliar a chegada, saída e acúmulo desses materiais no cérebro, em modelos animais, são de extrema importância para acelerar a experimentação animal e consequentemente a chegada desses agentes nanoestruturados no mercado. Aqui utilizamos um agente modificar do fluxo cerebral e que também têm um efeito conhecido sobre a barreira hematoencefálica, o Manitol. Dessa forma, o sistema foi capaz de avaliar os efeitos do Manitol no fluxo cerebral de nanoparticulas, bem como seu maior acúmulo nos animais que tiveram sua barreira hematoencefálica atingida por este fármaco. Os dados que serão apresentados neste capítulo poderão ter contribuições em áreas como nanomedicina e o desenvolvimento de novos agentes nanoestruturados focados em tratamentos e diagnósticos cerebrais.

ABSTRACT

Cerebral Blood Flow (CBF) assessment is a valuable tool to study several brain disorders. In the past, CBF was mainly accessed by scintigraphy methods that involve ionizing radiation. Therefore, new approaches to assess the CBF through the passage of MNP to BBB are highly necessary. The development of the nanomedicine enabled new approaches to study dynamical parameters regarding the brain blood flow. In this paper, we employed magnetic nanoparticles as a new tracer, and the AC biosusceptometry technique to study the brain perfusion under three different conditions. We utilized the mannitol, a hyperosmotic disruptor, before the MNPs injection to modulate the BBB permeability and study its effects in the circulation time of the MNPs in the brain, *in vivo* and in real-time. Also, we built and characterized a new AC biosusceptometry sensor, called cavity sensor, to increase the systems' applicability to study the MNPs' accumulation, on *ex vivo* situation, in organs, especially in the brain. Our data showed that the previous injection of mannitol increased the MNPs circulation time in the brain. Also, the mannitol increased the MNPs accumulation in these organs. This paper suggests the use of the AC biosusceptometry system as a new tool to study brain dynamical perfusion and accumulation of MNPs in studies involving the development of new nano agents focused in the brain diagnostic and treatment.

1. INTRODUCTION

In the past decades, some methodologies were employed to access dynamic processes in the brain. Cerebral Blood Flow (CBF) assessment is a valuable tool to study cerebral infarction, occlusions of cerebral arteries, insufficiency of cerebral blood flow and many other pathological processes (1-4). The main methods to study the CBF are cerebral scintigraphy, positron emission tomography (PET), arterial spin labeling Magnetic Resonance Imaging (MRI) and phase-contrast MRI (5). When utilizing the scintigraphy method, it is possible to assess the CBF by monitoring the passage of ^{99m}Tc or ^{133}Xe tracers in the brain after intravenous injection (2). The data collected is processed to acquire the signal corresponding to the radioactivity, in a chosen region of interest, over time. In the early stages of development of this method, the acquired signal was interpreted employing a compartmental model, once the signal can be approximated to an exponential decay (1, 2). This technique accesses the circulation time of the radioactive tracer and, consequently, the dynamic parameters associated with the blood flow in the organ.

Among the wide variety of structural possibilities in nanomedicine and, more specifically, nanoagents, one that brings attention is the magnetic nanoparticles (MNPs). Their intrinsic characteristics, such as magnetic behavior, enable their interaction with biological systems and processes. Some of these MNPs, such as the Gastromark®, are already in the clinic, utilized as an MRI tracer, while others are employed in the treatment of diseases, namely the Feraheme®, which is used to treat some specific types of anemia (6, 7). From diagnosis to treatment, or both together, MNPs is a valuable alternative in medicine and health sciences (8).

Since MNPs can be classified as a drug by the FDA(9), their preclinical and pharmacokinetic characterization are of paramount importance (10, 11). The monitoring of biodistribution and circulation time of the MNPs are some of the keys to understand how the MNP act within the body.

Several techniques have been employed for this purpose. Some of those are based on measurements of biological samples (ex vivo analysis) through spectrometry methods (12, 13), which only give snapshots of the entire process. MRI and Magnetic Particle Imaging (MPI), in turn, detect the MNPs due to its intrinsic features (i.e., magnetic behavior) in *vivo* situations (14, 15). Besides their disadvantages, as high costs and complexity, these techniques have been applied successfully to perform *in vivo* monitoring of MNPs.

The alternating current biosusceptometry (ACB) system is a biomagnetic detection technique well established in gastroenterology studies, using both, animal and human models (16, 17). Recently, our group has successfully applied the conventional ACB system to monitor MNPs, after intravenous injection in the bloodstream, liver, and kidneys of rats, *in vivo* and real-time (18-20). Additionally, the technique was compared with Electron Spin Resonance (ESR), measuring lyophilized samples in a biodistribution study for MNPs quantification. The comparison showed good and promising results (18). The ACB system is a relatively inexpensive, versatile and non-invasive technique with high temporal resolution. Such characteristics indicate that the ACB system may be a useful tool for preclinical studies of MNPs.

Once MNPs have dimensions in the order of nanometers, these structures can reach regions of difficult access (21). Recently, one of the most interesting and most explored fields of applications is the delivery of drugs into the central nervous system

(CNS), more specifically, the brain (22). Diseases affecting the CNS are second in the list of most life-threatening diseases, and despite the great number of studies, the development of new diagnostic methods and therapies remains relatively short (23). Taking advantage of the features of the nanosized materials, several drugs were developed to reach brain tissue, such as the Abraxane® and the Nanotherm® (24). Both of these drugs are based on nanostructured agents to treat brain cancer.

The biggest hindrance to deliver drugs in the CNS is the blood-brain barrier (BBB) (22). The BBB is extremely important for the brain homeostasis since it can prevent most drugs to reach the brain tissue. Therefore, there is an additional necessity to find methods that can help to overcome this barrier (25). One solution is to modulate the BBB permeability (26). Using drugs as mannitol, a hyperosmotic disruptor, it is possible to increase the BBB permeability and the microvascular flux of the brain, which can lead to increased delivery of drugs and compounds, as MNPs, in the brain tissue (26-28).

Here we utilized two different ACB sensors to evaluate how a previous injection of mannitol affects the circulation time and further brain accumulation of MNPs. We reported the first characterization study regarding a new ACB sensor setup, called ACB Cavity sensor, in which we were able to increase the sensitivity by one order of magnitude for tissue sample analysis.

2. MATERIAL AND METHODS

2.1. Magnetic Nanoparticles

We employed a manganese ferrite nanoparticle ($MnFe_2O_4$), coated with citrate ($Na_3C_6H_5O_7$), with a core diameter of 13 ± 5 nm, dispersed in liquid solution with pH 7.4 in a concentration of 25 mg/ml. The particles presented a saturation magnetization

of 41.6 emu/g, showing a quasi-static superparamagnetic behavior (any coercive field was observed under direct current conditions) (18). The MNPs were synthesized by co-precipitation method described previously (29, 30). The manganese ferrite was chosen because of its good magnetic response in magnetic fields of low amplitude and interesting features in magnetic hyperthermia applications (31, 32).

2.2. Alternating Current Biosusceptometry

The conventional ACB technique has been previously described and can be approximated to a magnetic material detector (33, 34). Firstly, used in gastroenterology studies, this technique was employed to detect magnetic materials moving through the gastrointestinal tract of humans. In the initial setup, the system was employed to measure gastric contractions, motility, emptying, transit and tablets disintegration (for in pharmaceutical studies) (16, 17, 35, 36).

The system works as a gradiometric magnetic flux transformer, wherein the excitation/detection pair of coils near the magnetic sample works as a detector, while the other coil pair, farther from the sample, acts as a reference system. We utilized a Lock-in amplifier to generate an alternating current in the excitation coils at a constant rate, producing an AC magnetic field of 2 mT at 10 kHz. The field generated in the excitation coils induces a current in the detection coils. When there is no magnetic material near the detector system, the response is minimized due to a first order gradiometric configuration. Once a magnetic material approaches the detector, there is an imbalance in the total magnetic flux of the system and, consequently, on the current generated in the detection coils. These changes can be acquired by the same Lock-in amplifier used to generate the initial current on the excitation coils. With an

analog/digital board, this signal can be acquired, stored, processed, and analyzed on a computer.

The conventional ACB sensor used here was previously developed to optimize the results in animal models (19). The new ACB Cavity sensor was idealized for sample assessment. It was built using two identical excitation coils (200 turns of 24 AWG wire with an average radius of 3 cm) and two identical detection coils (2000 turns of 34 AWG wire with an average radius of 1.5 cm), which enabled a higher amplification factor, never reached before. The tissue samples are then positioned in the center of the detection coil, reaching almost one order of magnitude increase in sensitivity, when compared with the conventional ACB sensor. Both detector and reference pairs are composed by one excitation and one detection coil. Between the detectors and the reference pair, there is a baseline of 120 mm to prevent interference and improve the signal-to-noise ratio (SNR).

The signal acquired is determined by the relationship between the system characteristics (coils specifications and current applied) and the sample features (magnetic susceptibility, volume, concentration and distance from the sensor).

We performed a characterization protocol to compare the sensitivity of the ACB Cavity sensor with the ACB conventional sensor. In this step, we utilized different MNPs concentration to build a calibration curve for both sensors and to compare the smallest MNPs mass that could be detected in both sensors. We also studied the ACB Cavity sensor response regarding the sample position, relative to the detector coil position. This step was performed to determine the optimal detection point inside of the sensor (higher sensitivity) to measure the tissues samples.

2.3. Experimental Set Up

2.3.1. Animal experimentation

We utilized 15 male rats (*Rattus nervegicus albinus*, Wistar), acquired from the São Paulo State University Central Animal House (Botucatu, SP, Brazil), weighing 250-300g. The animals were maintained under suitable conditions with ad libitum feed (all of the animal experimentation were conducted according to the São Paulo State University Committee for Use and Care of Animals). All of the animals underwent urethane anesthesia (1.5 mg/kg), followed by femoral vein cannulation for intravenous MNPs injection, and the ACB sensor was positioned over the animal's head to perform the data acquisition (figure 1).

All of the animals received a dose of 0.2 ml of MNPs at a rate of 0.03 ml/s. Some animals received a previous intravenous dose of mannitol (4 mg/kg) before the MNPs injection, according with the division of the experimental groups: G1 (five animals received only MNPs), G2 (five animals received a previous dose of mannitol 15 minutes before receiving the MNPs dose) and G3 (five animals received a previous dose of mannitol 30 minutes before receiving the MNPs dose).

After MNP injection and online data acquisition, we sacrificed the animals, still under anesthesia, by decapitation (50 minutes after the MNPs injection) and collected a blood sample and brain, heart, lungs, liver, spleen, and kidneys for the biodistribution study.

2.3.2. Acquisition and quantification

We monitored the ACB signal corresponding to the MNPs in the brain, *in vivo* and in real-time, with a Biopac® system, at a sample rate of 20 Hz. The circulation time of the MNPs in the brain was accessed by the $T_{1/2}$ method, calculated by a compartmental

model, approximated to a single-phase exponential decay, as described previously (19). We also quantified the ACB maximum signal intensity after the injection (I_{MAX}) and the MNPs arrival time in the brain (T_A), calculated from the time of injection until the signal's peak. Figure 1 shows an example of the sensor, positioned in the head of the rats and the quantification parameters in the ACB signal.

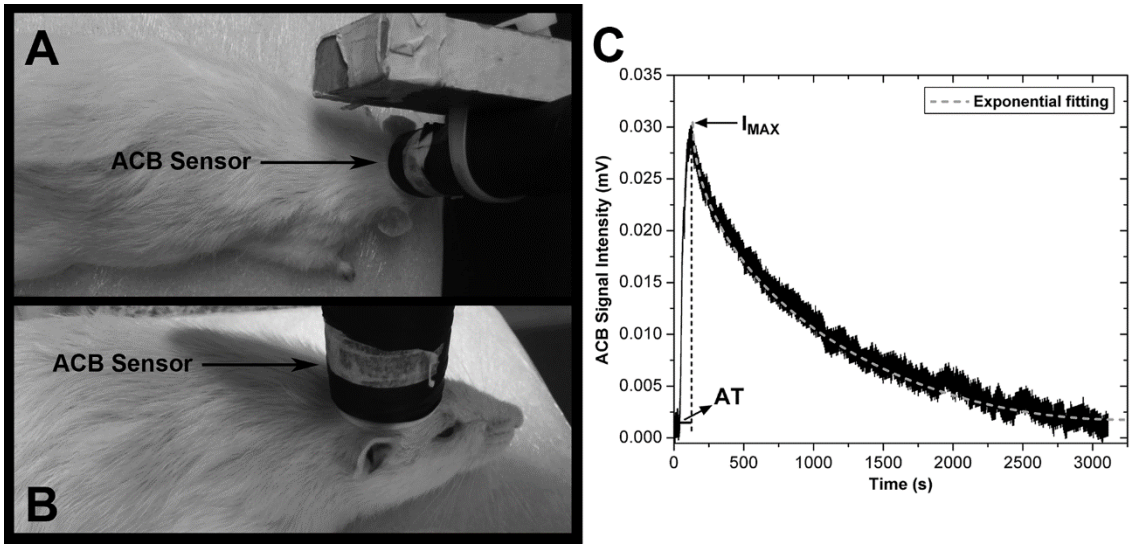

Figure 1 – Animals positioning and signal quantifications. (A) The animal in ventral decubitus with the ACB sensor positioned in the head. (B) Detail of the sensor positioning in the animals' head. (C) Example of a signal detected regarding the MNPs arrival and washout of the brain and the quantifications performed, where I_{MAX} is the maximum signal intensity detected, AT is the time of arrival from the injection until the $I_{MAX,}$ and the exponential fitting performed to quantify the circulation time in the brain.

For the biodistribution study, we utilized 100mg samples of each lyophilized organ, stored in a plastic vial. We placed each sample on the sensor surface and recorded the ACB signal intensity. With the calibration curve results to compare with the results from the organs, we were able to calculate the mass of particles per gram of lyophilized tissue.

The signals were acquired and quantified using Acknowledge 4.1.1, Matlab 2012 and OriginPro 8 software.

2.4. Statistical Analysis

All of the data was expressed as the mean ± standard deviation. We utilized a one-way analysis of variance (ANOVA) followed by the Tukey post hoc test for comparisons between the groups. Values of $p < 0.05$ were considered statistically significant.

3. RESULTS

Figure 2 shows the results obtained from the ACB sensor characterization study. Figure 2A shows the response of the ACB cavity sensor regarding the sample position relative to the center of the detection coil (0 cm). The dashed lines indicate the limits of the detection coil, showing a higher signal intensity when the sample is positioned in the center of the detector. Figure 2A illustrates such profile, which allowed the determination of an optimal detection point, increasing significantly the sensitivity of the technique. The calibration curves built for both ACB Cavity and conventional sensors are shown in Figure 2B, where the ACB Cavity sensor showed higher intensity for greater quantities of MNPs when compared with the conventional one. From figure 2B (inset), it is noticeable that the Cavity sensor showed a detection limit ten times lower than the conventional sensor. Thus, such data encouraged us to employ the technique to measure very small quantities of MNPs in biodistribution studies; such is the case of accumulation of nanoparticles in the brain.

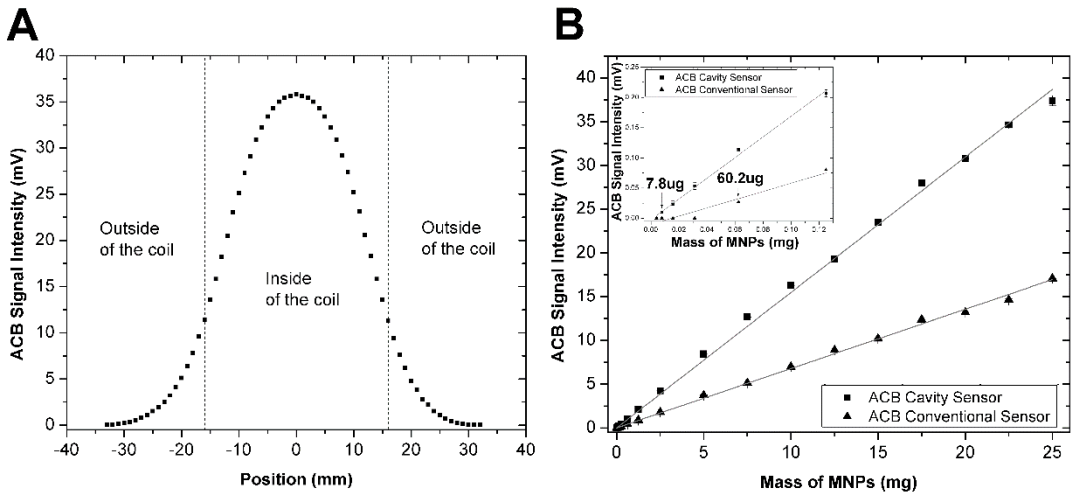

Figure 2 – ACB sensors characterization. (A) ACB Cavity sensor response to the sample position relative to the detector coil position. Dashed line separates the values acquired outside and inside the coil limits. (B) Calibration curves for both ACB Cavity and ACB conventional sensors.

Figure 3 shows the results of the *in vivo* quantification tests for all of the groups (G1 – no mannitol injected previously; G2 – 15 minutes before the MNPs injection, the animals received the previous injection of mannitol; G3 – 30 minutes before the MNPs injection, the animals received the previous injection of mannitol). We found that the arrival time in the brain is almost the same for all groups (no significant differences). In regards to the maximum signal intensity, there was a decrease in the G3 group signal, while circulation time increased for the same group (figure 3B and 3C, respectively). Since the mannitol is an osmotic disruptor, it might influence the vascular pressure in the brain. Therefore, the maximum signal intensity and the circulation time would be affected, the former negatively and the latter, positively.

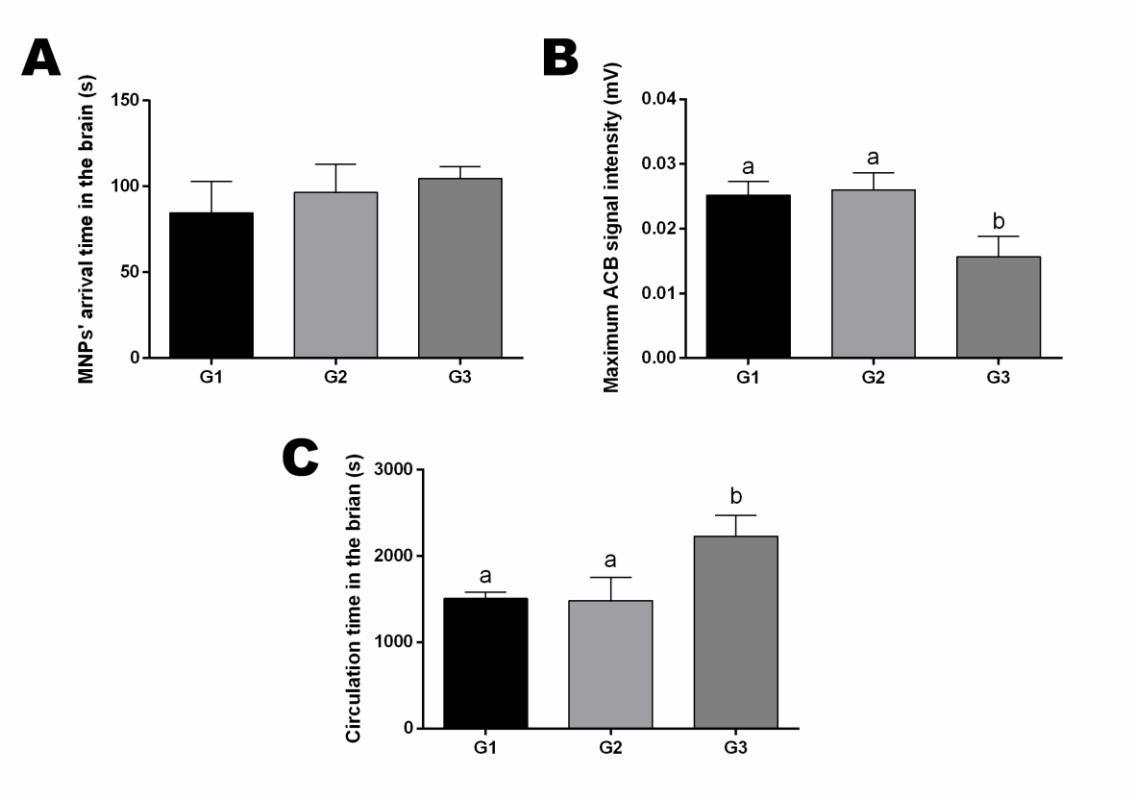

Figure 3 – ACB quantification results for all of the groups. (A) MNPs arrival time in the brain (AT). (B) Maximum signal intensity (I_{MAX}). (C) MNPs circulation time in the brain ($T_{1/2}$). Different letters indicate significant difference with $p<0.01$.

After *in vivo* data acquisition, the animals were sacrificed, and the organs analyzed. Figure 4 shows the data regarding the biodistribution analysis conducted using the ACB Cavity sensor. We found a significant difference in two tissues: blood and brain. While the number of particles in the blood decreases with the previous injection of mannitol, the accumulation in the brain increases. This data corroborates the *in vivo* data since the group G3 presented the highest accumulation in the brain. G3 animals received a previous injection of mannitol (30 minutes) and showed the longer circulation time. Figure 4B (*inset*) shows the concentration of MNPs detected in the brain.

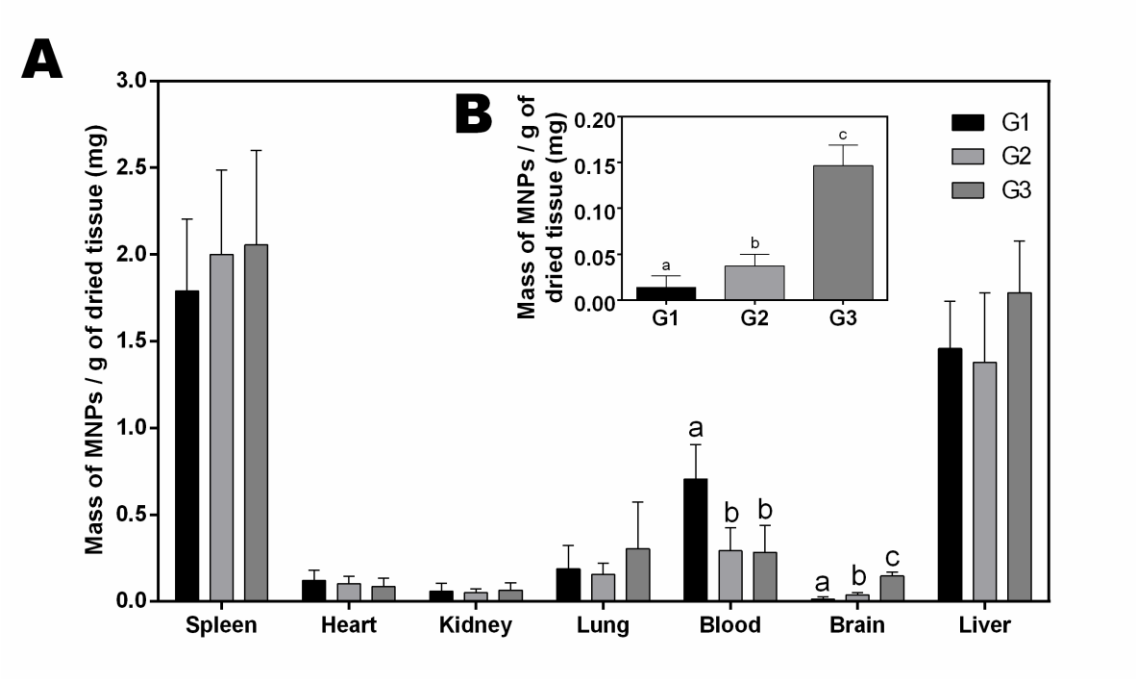

Figure 4 – ACB data for MNPs biodistribution. (A) Comparison between the groups for all of the organs collected. (B) Biodistribution analysis for the brain in detail.

4. DISCUSSION

Cerebral blood flow is a critical physiological parameter with a consistent correlation with other brain functions, which are considerably more complicated to assess. The usual approach for such measurement, the perfusion of radioactive tracers, involve several obstacles to its application, especially due to exposure to ionizing radiation, the need of highly qualified professionals and complex logistics (to acquire, use and discard the radioactive tracers and waste). Additionally, this method demands special infrastructures and, consequently, high costs (37).

The use of MNPs as tracer increased in the past few decades. Some studies previously and usually performed with radiotracers, gadolinium among others, can now be performed using MNPs. As pointed before, the techniques to detect MNPs in vivo presents some disadvantages, mainly due to the high costs and accessibility to conduct the experiments (15, 18, 19).

Our group has shown that the ACB system is a simple tool to detect MNPs *in vivo* and quantify the MNPs accumulation (18). The ACB system has a unique temporal resolution, which can provide real-time analysis (19). Summing up all the features presented above, the ACB system is a low cost, radiation-free, non-invasive and portable technology.

In this study, we applied and adopted two types of ACB sensors to access the MNPs brain perfusion and biodistribution. To quantify lower MNPs quantities in the brain tissue, we characterized and employed an ACB Cavity sensor for the biodistribution analysis. We determined the optimal position of the sample inside the sensor (figure 2A). Placing the sample in the point of the highest signal, the Cavity sensor showed a remarkable increase in sensitivity when compared to the conventional sensor, with a detection limit nearly ten times lower (figure 2B). Such performance gain was expected since the magnetic field amplitude inside of the coil presents higher homogeneity and intensity. Thus, we took advantage of the magnetic field characteristics to enhance the system applicability.

The conventional sensor used has been well described before, developed specifically to detect MNPs in animal models, *in vivo* and in real-time (18-20). The conventional sensor was used to detect the MNPs brain perfusion, *in vivo*, mimicking the scintigraphy methods to study CBF. Furthermore, we used mannitol, a well-known drug to influence the BBB selectivity, to induce variations in the brain perfusion and accumulation of MNPs. Our data showed a good similarity with those previously acquired in CBF studies, by scintigraphy techniques (1, 2). It is possible to observe a peak in the signal, related to the arrival of particles in the brain vasculature, with a sequential exponential decay, related with the MNPs being washed out from this organ.

Similar to the scintigraphy studies, we quantified our data using one-compartmental model, which provides the MNPs circulation time ($T_{1/2}$) in the brain.

Three main parameters were quantified from the in vivo data collected: the arrival time, maximum signal intensity and circulation time of the MNPs in the brain. The arrival time of the MNPs in the brain did not show significant differences between the groups. All of the MNPs injections were conducted with the same injection rate (0.03 ml/s). These data suggest that the mannitol effects did not influence the vasculature that leads the MNPs to the brain. In regards to the maximum signal intensity, both G1 and G2 groups significantly differed from the G3 group and did not differ between each other. The G3 group showed a significantly lower signal when compared with the other groups. These data suggest that the mannitol influence the brain vasculature and permeability, although it only presents perceivable signs after more than 15 minutes from the drug administration, since the G2 (in which the experiments were carried out after 15 min of the mannitol injection) did not show significant differences between the G1 group (which did not receive a previous mannitol injection). The lower signal intensity recorded can be related with the MNPs distribution inside of the brain vasculature. The ACB conventional sensor is sensitive to the magnetic material concentration in a volume. Once the mannitol is an osmotic disruptor, it changes the BBB permeability and brain pressure (26, 27), allowing the MNPs to be more homogeneously distributed in the brain tissue, leading to the decrease of signal intensity detected. The circulation time calculated showed no significant differences between G1 and G2, while both groups showed significant different G3, which presented the highest circulation time. These data also suggest that the mannitol effects happen after more than 15 minutes from the administration. The higher

circulation time might be related to the enhanced permeability of the BBB and the pressure changes in the microvascular flux of the brain (26-28).

Regarding the biodistribution analysis, the spleen and liver showed higher MNPs retention profile, which was expected. Both liver and spleen are organs recognized by their potential to capture and accumulate MNPs, especially the MNPs in size range used here. MNPs smaller than 8 nm are readily excreted through renal clearance, while MNPs larger than 200 nm are not able to pass the spleen barriers (10, 38, 39). Thus, particles between 8 and 200 nm are captured and accumulated in both liver and spleen, mostly (10). We observed significant differences between the groups for both brain and blood samples. We found a higher signal, indicating a greater concentration of MNPs in the blood samples of group G1 (no mannitol injection) when compared with the G2 and G3 groups. In regards to the brain, we observed a linear profile of MNPs accumulation. All of the groups presented a significant difference, where G1 presented the lower MNPs level, the G2 presented an intermediary value and G3 the highest MNPs quantities. It is possible to observe that the G1 and G2 showed nearly the same MNPs quantities, although presenting a significant difference between each other, G3, however, presented the highest value by far. These data corroborate the data acquired in vivo, showing a time-dependent activity of mannitol in the brain tissue.

The enhancement of drug delivery in the brain is an important issue. There is a vast literature reporting the use of mannitol as the main, or adjuvant, a drug to treat or relieve symptoms related to a brain pathology or disorder (40-42). Other studies also used or proposed the mannitol as an agent to enhance the delivery of different types of nanostructured agents in the brain (43, 44). Wadghiri and co-authors (2003) used an intravascular coinjection of mannitol to open the BBB for a brief period and increase the input of a monocrystalline iron oxide nanoparticles. Their MRI data showed an increase

in the nanoparticles input in the brain tissue when mannitol was used as an agent to open de BBB temporally, making possible the detection of amyloid-β plaques (45). Another study, regarding a nanocarrier-mediated transport of a miRNA to the brain parenchyma in vivo, reported the importance of the mannitol in the BBB opening. This study also showed that the injection of mannitol increased the accumulation of the nanocarrier in the studied regions of the brain (46). To investigate the biodistribution and toxicity of silica coated MNP containing rhodamine, Kim and co-authors (2006) used a treatment of 25% of mannitol as a positive control to evaluate the effects of their nanoparticles on BBB integrity (28).

From the diagnosis to the treatment, the association of mannitol with nanostructured agents is a possibility to increase brain assessments. Here we used the mannitol as a modifying agent to study the potential of the ACB system to detect differences in CBF. The ACB system showed good results, once was capable of distinguishing the circulation time and brain tissue accumulation (using different sensors with different configurations) between the animals that did not receive a pre-injection of mannitol and the animals that received a pre-injection of mannitol. The system offers important features, as low-cost, selectivity to the magnetic tracers, and sensitivity to quantify the MNP accumulation in this organ. Furthermore, we propose the use of the ACB system in scientific investigations related to the development of MNPs to reach the brain tissue (among others MNPs studies). As the ACB system state of the art does not present sufficient spatial resolution to differentiate regions in the rat brain or generate images in animal's brain, the present setup is not indicated to perform studies that involve modifications in specific regions, like strokes or Alzheimer disease studies. However, the ACB system is a valuable tool to access organs perfusion, CBF and quantify the biodistribution of MNPs.

5. CONCLUSION

We employed two different ACB sensors, associated with MNPs, to study some parameters regarding the CBF and MNPs brain accumulation. We utilized the mannitol to modify the MNPs circulation time in the brain and its accumulation as well. The cavity sensor showed a significant increase in sensitivity when compared to the conventional sensor, which encouraged us to use this system to perform the biodistribution analysis. The conventional system was able to detect the mannitol influence in the CBF, using the circulation time, and the Cavity sensor was able to quantify MNPs in the organs, especially in the brain. These data suggest the use of the ACB system to study the potential of MNPs to trespass the BBB and can be a suitable tool to increase the MNPs applicability in brain studies, where the MNPs are used as both tracer or delivery systems.

6. REFERENCES

1. Nikolov N, Makeyev S, Yaroshenko O, Novikova T, Globa M. Quantitative evaluation of the absolute value of the cerebral blood flow according to the scintigraphic studies with 99mTc-HMPAO. Naukovi Visti NTUU KPI. 2017(1):61-8.

2. Kuikka J, Ahonen A, Koivula A, Kallanranta T, Laitinen J. An intravenous isotope method for measuring regional cerebral blood flow (rCBF) and volume (rCBV). Physics in Medicine & Biology. 1977;22(5):958.

3. Tolonen U, Ahonen A, Sulg I, Kuikka J, Kallanranta T, Koskinen M, et al. Serial measurements of quantitative EEG and cerebral blood flow and circulation time after brain infarction. Acta Neurologica Scandinavica. 1981;63(3):145-55.

4. Leijenaar JF, van Maurik IS, Kuijer JP, van der Flier WM, Scheltens P, Barkhof F, et al. Lower cerebral blood flow in subjects with Alzheimer's dementia, mild

cognitive impairment, and subjective cognitive decline using two-dimensional phase-contrast magnetic resonance imaging. Alzheimer's & Dementia: Diagnosis, Assessment & Disease Monitoring. 2017;9:76-83.

5. Shi Y, Thrippleton MJ, Makin SD, Marshall I, Geerlings MI, de Craen AJ, et al. Cerebral blood flow in small vessel disease: a systematic review and meta-analysis. Journal of Cerebral Blood Flow & Metabolism. 2016;36(10):1653-67.

6. Bonnemain B. Superparamagnetic agents in magnetic resonance imaging: physicochemical characteristics and clinical applications. A review. Journal of drug targeting. 1998;6(3):167-74. Epub 1999/01/15.

7. Schwenk MH. Ferumoxytol: a new intravenous iron preparation for the treatment of iron deficiency anemia in patients with chronic kidney disease. Pharmacotherapy. 2010;30(1):70-9. Epub 2009/12/25.

8. Cole AJ, Yang VC, David AE. Cancer theranostics: the rise of targeted magnetic nanoparticles. Trends in biotechnology. 2011;29(7):323-32. Epub 2011/04/15.

9. Administration USFaD. FDA Glossary of Terms. https://www.fda.gov/drugs/informationondrugs/ucm079436.htm: FDA; 2017 [updated 11/14/2017; cited 2018]; Available from: https://www.fda.gov/drugs/informationondrugs/ucm079436.htm.

10. Sun C, Lee JS, Zhang M. Magnetic nanoparticles in MR imaging and drug delivery. Advanced drug delivery reviews. 2008;60(11):1252-65. Epub 2008/06/19.

11. Albanese A, Tang PS, Chan WC. The effect of nanoparticle size, shape, and surface chemistry on biological systems. Annual review of biomedical engineering. 2012;14:1-16. Epub 2012/04/25.

12. Lacava LM, Lacava ZG, Da Silva MF, Silva O, Chaves SB, Azevedo RB, et al. Magnetic resonance of a dextran-coated magnetic fluid intravenously administered in mice. Biophysical journal. 2001;80(5):2483-6. Epub 2001/04/28.

13. Huang HS, Hainfeld JF. Intravenous magnetic nanoparticle cancer hyperthermia. International journal of nanomedicine. 2013;8:2521-32. Epub 2013/08/01.

14. Jain TK, Richey J, Strand M, Leslie-Pelecky DL, Flask CA, Labhasetwar V. Magnetic nanoparticles with dual functional properties: Drug delivery and magnetic resonance imaging. Biomaterials. 2008;29(29):4012-21.

15. Weizenecker J, Gleich B, Rahmer J, Dahnke H, Borgert J. Three-dimensional real-time in vivo magnetic particle imaging. Physics in medicine and biology. 2009;54(5):L1-L10. Epub 2009/02/11.

16. Cora LA, Americo MF, Romeiro FG, Oliveira RB, Miranda JR. Pharmaceutical applications of AC biosusceptometry. European journal of pharmaceutics and biopharmaceutics : official journal of Arbeitsgemeinschaft fur Pharmazeutische Verfahrenstechnik eV. 2010;74(1):67-77. Epub 2009/06/02.

17. Quini CC, Americo MF, Cora LA, Calabresi MF, Alvarez M, Oliveira RB, et al. Employment of a noninvasive magnetic method for evaluation of gastrointestinal transit in rats. Journal of biological engineering. 2012;6(1):6. Epub 2012/05/17.

18. Quini CC, Prospero AG, Calabresi MFF, Moretto GM, Zufelato N, Krishnan S, et al. Real-time liver uptake and biodistribution of magnetic nanoparticles determined by AC biosusceptometry. Nanomedicine : nanotechnology, biology, and medicine. 2017;13(4):1519-29.

19. Prospero AG, Quini CC, Bakuzis AF, Fidelis-de-Oliveira P, Moretto GM, Mello FP, et al. Real-time in vivo monitoring of magnetic nanoparticles in the bloodstream by AC biosusceptometry. Journal of nanobiotechnology. 2017;15(1):22.

20. Quini CC, Matos JF, Prospero AG, Calabresi MFF, Zufelato N, Bakuzis AF, et al. Renal perfusion evaluation by alternating current biosusceptometry of magnetic nanoparticles. J Magn Magn Mater. 2015;380:2-6.

21. Schroeder U, Sommerfeld P, Ulrich S, Sabel BA. Nanoparticle technology for delivery of drugs across the blood-brain barrier. Journal of pharmaceutical sciences. 1998;87(11):1305-7. Epub 1998/11/13.

22. Tabatabaei SN, Girouard H, Carret AS, Martel S. Remote control of the permeability of the blood-brain barrier by magnetic heating of nanoparticles: A proof of concept for brain drug delivery. Journal of controlled release : official journal of the Controlled Release Society. 2015;206:49-57. Epub 2015/03/01.

23. Vilella A, Ruozi B, Belletti D, Pederzoli F, Galliani M, Semeghini V, et al. Endocytosis of Nanomedicines: The Case of Glycopeptide Engineered PLGA Nanoparticles. Pharmaceutics. 2015;7(2):74-89. Epub 2015/06/24.

24. von Roemeling C, Jiang W, Chan CK, Weissman IL, Kim BY. Breaking Down the Barriers to Precision Cancer Nanomedicine. Trends in biotechnology. 2017;35(2):159-71. Epub 2016/08/06.

25. Abbott NJ. Blood-brain barrier structure and function and the challenges for CNS drug delivery. Journal of inherited metabolic disease. 2013;36(3):437-49. Epub 2013/04/24.

26. Rapoport SI. Osmotic opening of the blood-brain barrier: principles, mechanism, and therapeutic applications. Cellular and molecular neurobiology. 2000;20(2):217-30. Epub 2000/03/04.

27. Muizelaar JP, Wei EP, Kontos HA, Becker DP. Mannitol causes compensatory cerebral vasoconstriction and vasodilation in response to blood viscosity changes. Journal of neurosurgery. 1983;59(5):822-8. Epub 1983/11/01.

28. Kim JS, Yoon TJ, Yu KN, Kim BG, Park SJ, Kim HW, et al. Toxicity and tissue distribution of magnetic nanoparticles in mice. Toxicological sciences : an official journal of the Society of Toxicology. 2006;89(1):338-47. Epub 2005/10/21.

29. Branquinho LC, Carriao MS, Costa AS, Zufelato N, Sousa MH, Miotto R, et al. Effect of magnetic dipolar interactions on nanoparticle heating efficiency: Implications for cancer hyperthermia (vol 3, 2887, 2013). Sci Rep-Uk. 2014;4.

30. Itri R, Depeyrot J, Tourinho FA, Sousa MH. Nanoparticle chain-like formation in electrical double-layered magnetic fluids evidenced by small-angle X-ray scattering. Eur Phys J E. 2001;4(2):201-8.

31. Atkinson WJ, Brezovich IA, Chakraborty DP. Usable frequencies in hyperthermia with thermal seeds. IEEE transactions on bio-medical engineering. 1984;31(1):70-5. Epub 1984/01/01.

32. Lee JH, Huh YM, Jun Y, Seo J, Jang J, Song HT, et al. Artificially engineered magnetic nanoparticles for ultra-sensitive molecular imaging. Nat Med. 2007;13(1):95-9.

33. Miranda JRA, Oliveira RB, Sousa PL, Braga FJH, Baffa O. A novel biomagnetic method to study gastric antral contractions. Physics in medicine and biology. 1997;42(9):1791-9.

34. Baffa O, Oliveira RB, Miranda JR, Troncon LE. Analysis and development of AC biosusceptometer for orocaecal transit time measurements. Medical & biological engineering & computing. 1995;33(3):353-7. Epub 1995/05/01.

35. Americo MF, Oliveira RB, Romeiro FG, Baffa O, Cora LA, Miranda JR. Scintigraphic validation of AC Biosusceptometry to study the gastric motor activity and the intragastric distribution of food in humans. Neurogastroenterology and motility : the

official journal of the European Gastrointestinal Motility Society. 2007;19(10):804-11. Epub 2007/09/22.

36. Oliveira RB, Baffa O, Troncon LEA, Miranda JRA, Cambrea CR. Evaluation of a biomagnetic technique for measurement of orocaecal transit time. Eur J Gastroen Hepat. 1996;8(5):491-5.

37. Suthummanon S, Omachonu VK, Akcin M. Applying activity-based costing to the nuclear medicine unit. Health services management research. 2005;18(3):141-50.

38. Choi HS, Liu W, Misra P, Tanaka E, Zimmer JP, Itty Ipe B, et al. Renal clearance of quantum dots. Nat Biotechnol. 2007;25(10):1165-70. Epub 2007/09/25.

39. Chen LT, Weiss L. The role of the sinus wall in the passage of erythrocytes through the spleen. Blood. 1973;41(4):529-37. Epub 1973/04/01.

40. Bereczki D, Liu M, do Prado GF, Fekete I. Mannitol for acute stroke. Cochrane Database of Systematic Reviews. 2007(3).

41. Bereczki Dn, Liu M, Prado GFd, Fekete In. Cochrane report: a systematic review of mannitol therapy for acute ischemic stroke and cerebral parenchymal hemorrhage. Stroke. 2000;31(11):2719-22.

42. Alam MI, Beg S, Samad A, Baboota S, Kohli K, Ali J, et al. Strategy for effective brain drug delivery. European journal of pharmaceutical sciences. 2010;40(5):385-403.

43. Sahoo SK, Labhasetwar V. Nanotech approaches to drug delivery and imaging. Drug discovery today. 2003;8(24):1112-20.

44. Singh R, Lillard Jr JW. Nanoparticle-based targeted drug delivery. Experimental and molecular pathology. 2009;86(3):215-23.

45. Wadghiri YZ, Sigurdsson EM, Sadowski M, Elliott JI, Li Y, Scholtzova H, et al. Detection of Alzheimer's amyloid in transgenic mice using magnetic resonance

microimaging. Magnetic Resonance in Medicine: An Official Journal of the International Society for Magnetic Resonance in Medicine. 2003;50(2):293-302.

46. Son S, Jang J, Youn H, Lee S, Lee D, Lee Y-S, et al. A brain-targeted rabies virus glycoprotein-disulfide linked PEI nanocarrier for delivery of neurogenic microRNA. Biomaterials. 2011;32(21):4968-75.

CHAPTER 3

Impacts of the corona protein of three magnetic nanoparticles conjugations on the AC biosusceptometry signal intensity and circulation times

PREFÁCIO

Este trabalho teve seu início no final de 2016 durante uma conversa com o Dr. Carlos Alexandre, na época supervisionado pelo Prof. Marcos Fontes, na cozinha do laboratório Biomag durante uma pausa para um café.

Alguns meses antes tínhamos enviado o artigo fruto de meu mestrado para o Prof. Andris Bakuzis, para que ele avaliasse o trabalho e fizesse suas contribuições. Após ele avaliar o trabalho, fizemos uma vídeo conferência na qual ele me introduziu um novo assunto, do qual nunca tinha ouvido falar, o efeito Corona. Nos dias seguintes à essa conversa, li alguns artigos e descobri que esse tema tinha muito a contribuir com que estávamos desenvolvendo no momento.

Passados alguns meses, e ainda sem saber se poderíamos desenvolver um trabalho envolvendo esse tema, surgiu a referida conversa durante o café. Carlos trabalhava com proteínas de veneno de serpentes e é especialista em purificação de proteínas. Em uma conversa rápida ele me mostrou as possibilidades de realizar alguns experimentos para identificar as proteínas que interagem com as nanopartículas quando em contato com fluidos biológicos. De meus estudos anteriores, já sabia que essa interação era um fator importante para o comportamento das nanopartículas no organismo. No período que se deu entre a vídeo conferência com o Prof. Andris e a conversa com Carlos, tínhamos coletado uma série de dados de tempo de circulação de nanopartículas magnéticas. Na época sabíamos que tinha algo valioso entre esses dados, mas não sabíamos como explicá-los ou discutí-los. Após estudar sobre efeito Corona, e conversar com Carlos, tínhamos a explicação em mãos, mas apenas de maneira sugestiva e sem dados palpáveis para prová-la. Essa foi a parte fácil. A partir daí deram-se início os experimentos para adaptar um protocolo de interação, extração,

identificação e quantificação das proteínas plasmáticas que interagem com as nanopartículas. Durante os primeiros seis meses, aproximadamente, apenas eu e Carlos trabalhávamos nesse projeto. Após um tempo, a aluna de iniciação científica, Nurya Pinheiro, iniciou suas atividades no laboratório Biomag e foi agraciada com uma bolsa de iniciação científica PIBIC atrelada a este projeto. A Nurya foi uma das principais pessoas para que esse trabalho se concretizasse. Durante o período de meu doutorado sanduíche no exterior, foi ela quem assumiu quase que a totalidade dos experimentos que ainda faltavam ser feitos. Após meu retorno, retomei as atividades neste projeto ao lado da Nurya, do Carlos e agora também da Profa. Lucilene, especialista em proteômica e espectrometria de massas, pesquisadora no CEVAP - UNESP.

Infelizmente a aluna Nurya não seguiu a carreira acadêmica e hoje não reside mais em Botucatu. Carlos está realizando um projeto de pós doutoramento na França. Porém, ainda temos contato e os dois permaneceram ativos, mesmo que de longe, no desenvolvimento deste trabalho. Ressalto aqui que a aluna Nurya Pinheiro apresentou os dados referentes à identificação e quantificação das proteínas, no Congresso de Iniciação Científica da UNESP e foi avaliada entre os melhores trabalhos da UNESP Botucatu, sendo convidada a apresentar na segunda fase do Congresso em São Paulo. Além disso, eu também apresentei a parte dos dados *in vivo* e sistema BAC, no Congresso Brasileiro de Engenharia Biomédica, e o trabalho foi selecionado entre os cinco melhores trabalhos para receber o prêmio Cândido Pinto, onde o resultado final foi o terceiro lugar.

Até o momento em que escrevo esse prefácio, ainda não tenho certeza de que todos os dados referentes à este trabalho serão coletados a tempo de estarem apresentados nas páginas a seguir. Entretanto, sei que este é um primeiro trabalho nesta

linha, de muitos que poderão vir, onde foi estabelecida uma metodologia refinada e trabalhosa para a obtenção de dados que poderão ter grandes contribuições na ciência.

Neste capítulo serão apresentados dados referentes ao tempo de circulação de nanopartículas com diferentes recobrimentos e sua relação com os tipos de proteínas plasmáticas que cada revistimento tem afinidade. Por meio deste estudo pudemos ter uma visão crítica e o entendimento de como os revestimentos influenciam no comportamento biológico das nanopartículas. Os dados referentes às nanopartículas revestidas com albumina do soro bovino são interessantes, uma vez que este recobrimento aumenta significativamente o tempo de circulação das partículas, principalmente por essa ser uma proteína muito semelhante com a encontrada no sangue de humanos e ratos, ser de baixo custo e ter características muito interessantes que incentivam a continuidade dos estudos envolvendo sua utilização em nanomedicina e, talvez, no futuro, chegue à clínica médica.

ABSTRACT

Magnetic Nanoparticles (MNPs) are materials with great versatility. Recently, these materials have been proposed for several health applications. From the proposal to use these materials *in vivo* situations, it is necessary, the study their interactions with biological fluids and the impacts in their properties when immersed in a biological environment. The MNPs, when in contact with plasma proteins, undergo an effect known as corona effect, where it occurs the formation of a proteins layer of that involve MNPs. This layer is known as Corona Protein (CP) and which can alter the inherent properties of MNPs, such as magnetization, heat generation efficiency and magnetic relaxation time. Because the coat is the first contact layer of the particle with the biological environment, we used the same MNP core and three different coating protocols. We study the CP formation using electrophoresis gel and mass spectrometry to evaluate the response of the Alternating Current Biosusceptometry (ACB) system to the formation of CP for three different types of MNPs conjugations. Also, we evaluate the impact of CP in the MNPs conjugations' circulation times. The data collected so far suggests a lower CP formation and a longer circulation time for MNPs protein-coated (coated with bovine serum albumin) than for uncoated and citrate-coated MNPs, which presented almost the same circulation times and CP formation (qualitatively evaluated by SD-PAGE gel). Also, the ACB signal intensity presented a lower decrease for the protein-coated MNPs than for all other MNPs conjugation. In this context, this project aimed analyzes quantitatively and qualitatively the CP formation in MNPs of different coating protocols, its impacts on the ACB signal intensity and on the MNPs circulation times.

1. INTRODUCTION

Nanomedicine is a research and clinical field that involves the application of nanostructured agents to organs functions investigations, diagnosis and treatment of several diseases, which can provide to these materials a great theranostic potential (1-5). Within the nanostructures available, magnetic nanoparticles (MNPs) are of paramount importance. Their inherent magnetic properties enable to interact with these MNPs, using magnetic fields, within the body (6-8). In this way, MNPs were employed in several tasks such as the magnetic cancer hyperthermia, magnetic resonance imaging (MRI) contrast, drug delivery system, among others (9-13). Besides the significant number of clinical and preclinical studies involving nanostructured agents, their use in clinical filed is not well established (14).

The use of nanostructured agents in cancer and other diseases treatment efficiency presents a positive relationship with the MNPs circulation times (15). The enhancement of permeability and retention effect that occurs in inflamed tissues, as the tumor tissue, are lacking in the local vasculature that permits the nanostructured agents to leak out from the bloodstream and reach the inflamed tissue. Using this approach, as longer the MNPs circulation time, higher the probability of the MNP escaping from the blood and accumulate in the tissue of interest, increasing the MNPs' treatment efficiency (16). Furthermore, longer circulation time is crucial for its use as a blood pool agent in MRI angiography (17).

When used *in vivo* and clinical situations, these particles are mainly administrated via intravenous injection. Once the MNPs are in the bloodstream, the MNPs' coat is the first layer of contact with biological fluids and its entities, such as proteins and immunological factors. Different MNPs and coat conjugations determine

how the MNPs will interact with such structures in a process where the MNPs are almost entirely covered by these proteins and immunological factors (18). This process, called corona protein (CP) formation, is a factor which can influence in the MNPs' behavior within the body (19, 20). The CP profile (i.e., proteins quantities and types) can play an important role in the MNPs recognition by immune-system cells, macrophage action and removal from the bloodstream (21, 22). Also, the CP formation is a process that evolves along the time, where the highest mobility proteins interact firstly with the MNPs and later are replaced by less motile proteins with higher MNPs' surface affinity (23). Correlate the MNPs CP formation and its evolution over time with its circulation time presents vital importance in the use of MNPs in preclinical and clinical fields.

In the last few years, our group has studied the use of the ACB system as an *in vivo* and real-time MNPs detecting system and also as an MNPs quantifier system for *ex vivo* biodistribution studies. Using the ACB system we were able to study the MNPs circulation time, gastric emptying of liquids, kidney perfusion, liver uptake, biodistribution, and cell culture uptake. The method presented good performance in these analyses which encouraged us to employ the ACB system as a tool to study MNPs pharmacokinetics in the most various investigations (6, 7, 24-26).

In the first ACB system applications to detect MNPs, we used the citrate coated manganese ferrite nanoparticles (Cit-MNPs) as a tracer. Recently our group developed a bovine serum albumin coated manganese ferrite nanoparticle (BSA-MNPs) (27). These BSA-MNPs present some advantages over several MNPs coats described in the literature, as the facility to bind to water and apolar molecules, low costs, easy purification process, high acceptance in the pharmaceutical industry and the similarity

to the human and rat's serum albumin, which can decrease its interaction with plasma proteins and immunological factors (28, 29).

Here our main goal is to study three different coated MNPs' (Cit-MNPs, BSA-MNPs, and Ba-MNPs – an uncoated batch of the same core particles) circulation time assessed by the ACB system, characterize the CP formation of these MNPs over time and study the ACB response over the MNPs CP formation. In this way, we used the ACB system to detect the MNP *in vivo* and in real-time and also *in vitro* signals intensity experimentation, electrophoresis gel techniques, and mass spectrometry to investigate the CP formation over time, its impacts in the ACB signal and in the MNPs' circulation time.

2. MATERIAL AND METHODS

2.1. Magnetic nanoparticles

We synthesized, characterized and applied three conjugations of manganese ferrite ($MnFe_2O_4$) nanoparticles: Bare nanoparticles (Ba-MNPs – uncoated), nanoparticles coated with Citrate (Cit-MNPs) and Bovine Serum Albumin (BSA-MNPs). All the MNPs were synthesized in the same batch by co-precipitation method, as described before (8, 27, 30-33). After the synthesis, the MNPs received, or not, the respective coats.

The MNPs presented a physical core diameter of 13.4 nm and hydrodynamic diameter of 55.1 nm, 133.7 nm and 81.1 nm for the Cit-MNPs, BSA-MNPs, and Ba-MNPs, respectively. The zeta potential was measured and the Cit-MNPs presented a zeta potential of -28mV, the BSA-MNPs presented -5mV and for the Ba-MNPs it was 17mV. In this way we can consider the Cit-MNPs are highly negative charged, the BSA-MNPs are almost neutral and the Ba-MNPs positively charged. The magnetization

profile experiment showed no coercive field at DC conditions, that is, a quasi-static superparamagnetic behavior. The MNPs were dispersed in liquid media, at a concentration of 46 mg/ml. The vibrating sample magnetometer revealed a saturation of magnetization of 49.4 emu/g, 33.7 emu/g and 47.5 emu/g in the powder sample for the Cit-MNPs, BSA-MNPs, and Ba-MNPs, respectively.

2.2. Alternate Current Biosusceptometry

The ACB system is already well established in gastrointestinal and pharmacological studies (34-37). The system basically works as a magnetic tracer detector for *in vivo* studies and as a magnetic material quantifier in *ex vivo* and *in vitro* studies. In its initial applications, it was employed to detect markers and tracers within the stomach and intestine, enabling several physiological studies. As the system presents good features as the portability, low costs, low invasiveness, and versatility, we adapted the original system to optimize its use in studies involving MNPs and animal models (6, 7, 24, 26, 38).

Using two excitation coils, the system generates a low amplitude magnetic field, which is detected in real time by two identical detector coils. The detector coils are connected in a first order gradiometric configuration, to increase the system's signal-to-noise ratio. When there is no magnetic sample near the detection coils, no signal is registered. When a magnetic sample is positioned around the detector coils, there is a change in the system's magnetic flux, and an electrical signal is recorded using an A/D card and a computer (37, 39-41). The system's signal is proportional to the magnetic material quantities and its position, enabling the detection of MNPs acting as tracers inside the body. Further details as the physical model and the system's characterization can be accessed in our previous publications (6, 39, 40).

2.3. Animals experiments

We utilized 30 male Wistar rats (weighing 280 – 350g). All procedures were conducted following the Guide of the Care and Use of Laboratory Animals (Brazilian College of Animal Experimentation) and were approved by the UNESP Committee for use and care of animals (CEUA protocol number 1110). The animals were maintained in appropriate conditions with *ad libitum* feed.

2.3.1. *In vitro* experiments

2.3.1.1. Samples preparation

In the *in vitro* procedures, we utilized 9 of the rats, also divided into three groups according to the MNPs conjugation that it received (3 animals each group). The animals underwent to anesthesia (urethane – 1.5 mg/kg), and we sacrifice the animals by decapitation method to collect enough blood. After the blood collection, we processed all blood samples to acquire the blood plasma, as published before (42). To include the genetic variability in the study and to reduce the experiments costs, we mixed the plasma of each three rats (as a plasma pool). After this mixing, we divided each pool into three equal aliquots, totaling nine plasma samples.

For this experiments, all MNPs samples were diluted using PBS (reaching a final concentration of 23 mg/ml), to optimize the MNPs-plasma interactions. Before the MNPs and plasma incubation, we performed a magnetic measurement of the three samples to future compare with the magnetic measurement after the incubation. For the magnetic measurement, we add 1.5ml of Milli-Q water in each sample, mimetizing the next steps procedure using the plasma. After this, we positioned the samples in the ACB sensor detector surface, and the magnetic signal, proportional to the sample AC

susceptibility, was recorded. We performed this step three times for each sample. For further details of ACB samples measurement, find our previous publications (6, 26).

The different MNPs conjugations were separately incubated with the plasma samples (300µl of MNPs and 1.5ml of plasma) in different incubation times (30 min, 1h, and 2h). Finally, we had nine samples, contemplating three different MNPs incubated for three different periods. Passed the incubation times, the samples containing the blood plasma and MNPs were reread by the ACB system, as before, and we were able to access the impacts of the corona formation in the ACB system signal.

2.3.1.2. Samples preparation and 1D SDS-PAGE gel protocol

After the second ACB measurement, the samples were processed following a protocol published before (42). Briefly, we add 1.5 ml of sucrose (0.5M) in each sample, to form a sucrose cushion around the MNPs and preserve the corona formed in that incubation time. The samples were centrifuged (15 min at 4500rpm and 4°C), and washed. We performed the last step three times to ensure the washing out of all proteins that were not bound to the MNPs. In the end, we obtained the pellets containing only the MNPs and bound proteins (i.e., corona protein). The next step was eluting the proteins from the MNPs by adding 100µl of SDS sample buffer and incubating it for 5 min at 95°C. Following, we pellet the samples by centrifugation (25 min at 15300 rcf and 20°C) and the supernatant, containing only the proteins that were bound to the MNPs' surface, was obtained and stored (-80°C). After this, we ran the samples in a 10% (water/volume) 1D SDS-PAGE gel at 85V and used Coomassie staining for the qualitative analyses and protein spots separation.

2.3.1.3. In-gel digestion and Mass Spectrometry

The in-gel digestion was performed following the protocol published previously (43). We excised the protein bands from the gel (and a control piece containing a spot of the standard molecular marker – 70 kDa) and discolored it with destain solution (methanol 50%, acetic acid 2.5%, and purified water). Sequentially the samples were dehydrated in acetonitrile (100%) and dried in a vacuum centrifuge. Then, for the protein reduction, we added dithiothreitol (10mM), in ammonium bicarbonate solution (100mM), sufficient to cover the gel pieces and the samples were incubated in this solution for 1h at room temperature. After 1h we removed the dithiothreitol solution and replace it with iodoacetamide (50mM), in ammonium bicarbonate (100mM), for the alkylation process, and the samples were incubated for 1h at room temperature in the dark. Using a vortex, we washed the samples with ammonium bicarbonate (100mM) for 10 min, dehydrated adding acetonitrile (100%) for 5 min, removed the acetonitrile and rehydrated it in ammonium bicarbonate (10mM) for 10 min and shrunk again with acetonitrile (100%) for 5 min at room temperature, two times. We removed the acetonitrile and dried the samples in a vacuum centrifuge. Sequentially, the samples were swollen in digestion buffer of trypsin (20 ng/µl), solubilized in ammonium bicarbonate (50mM), in an ice-cold bath for 30 min. With the help of a vortex, we removed the supernatant and replace with ammonium bicarbonate (50mM) for the enzymic cleavage at 37°C overnight. The peptides were extracted adding a solution of formic acid (5% - in purified water) for 10 min, and the supernatant was collected. Sequentially we added a solution of formic acid (5%) in acetonitrile (50%) in the gel samples for 10 min and collected the supernatant. This last step was performed two times, and all three supernatant samples collected of each band were stored in the same vial, dried down and stored at -20°C until the mass spectrometry experiment.

The tryptic digests were reconcentrated and subjected to mass spectrometry followed by a peptide sequencing analyses using an LC/MS/MS system (OrbiTrap with PicoChip source for proteomic analysis). The proteins found in the samples were identified and statistically validated using the *Mascot* bioinformatics tool (Matrix science) and *Rattus Norvegicus* data bank.

2.3.2. *In vivo* experiments

In the *in vivo* experiments, we used 21 of the rats divided into three groups according to the type of MNPs that it received (7 rats each MNPs conjugation – Cit-MNPs, BSA-MNPs, and Ba-MNPs). The animals underwent intraperitoneal urethane anesthesia (99% - 1.5 mg/kg), followed by femoral vein cannulation. After the surgical procedure, the animals were positioned in dorsal decubitus, and the ACB sensor was placed over the animals' cardiac projection, as described before (7). After the animals' positioning, the system started to acquire the data, and we performed the MNPs injection. Each animal received a dose of 0.3 ml of MNPs, according to the experimental group. After the MNPs administration and online data acquisition, we sacrifice all the animals by decapitation while under anesthesia.

The ACB signals from this experiment were collected online in real-time with the help of a Biopac system and a computer at 200Hz of acquisition frequency. All data were processed and quantified using Acknowledge 4.1.1., MatLab2011 and OriginPro 8 software. The circulation time was assessed by the signal half-life ($t_{1/2}$), quantified as a one-compartmental model using a single-exponential decay fitting in the normalized signals, as described before (7). Also, we quantified the ACB maximum signal intensity (I_{max}), corresponding to the signal peak of MNPs arrival in the animals' heart.

2.4. Statistical analyses

All of the results were expressed as mean ± standard deviation. In the analyses comparing the results for different MNPs coats, we used multiple unpaired t-tests. The results were considered statistically significant with $p < 0.05$.

3. RESULTS

3.1. *In Vitro* Experiments

To study the impacts of the CP in the ACB signal intensity, we performed the *in vitro* experiment, already described in the Results section. In figure 1A it is shown the absolute ACB signal intensity for all MNPs conjugations and all incubations times with blood plasma, and Milli-Q water after 30 min of incubation time, which was used as a control. As the Milli-Q water did not influence in the ACB signal intensity for all incubation times (data not shown), we chose the 30 min of MNPs+Milli-Q water incubation time as the control sample, to compare the samples incubated with plasma. Figure 1B shows this impact of the CP in the ACB signal, expressed in percentage of ACB signal variation when compared with the Milli-Q water incubation. When the MNPs were mixed with blood plasma, the ACB signal intensity suffered a significant decrease for the Ba-MNPs (approximately 70%) and Cit-MNPs (approximately 55%) for all incubation times, while for the BSA-MNPs presented a lower decrease, which significantly changed along the time (approximately 27%, 28% and 14% for 30 min, 1 h and 2 h, respectively).

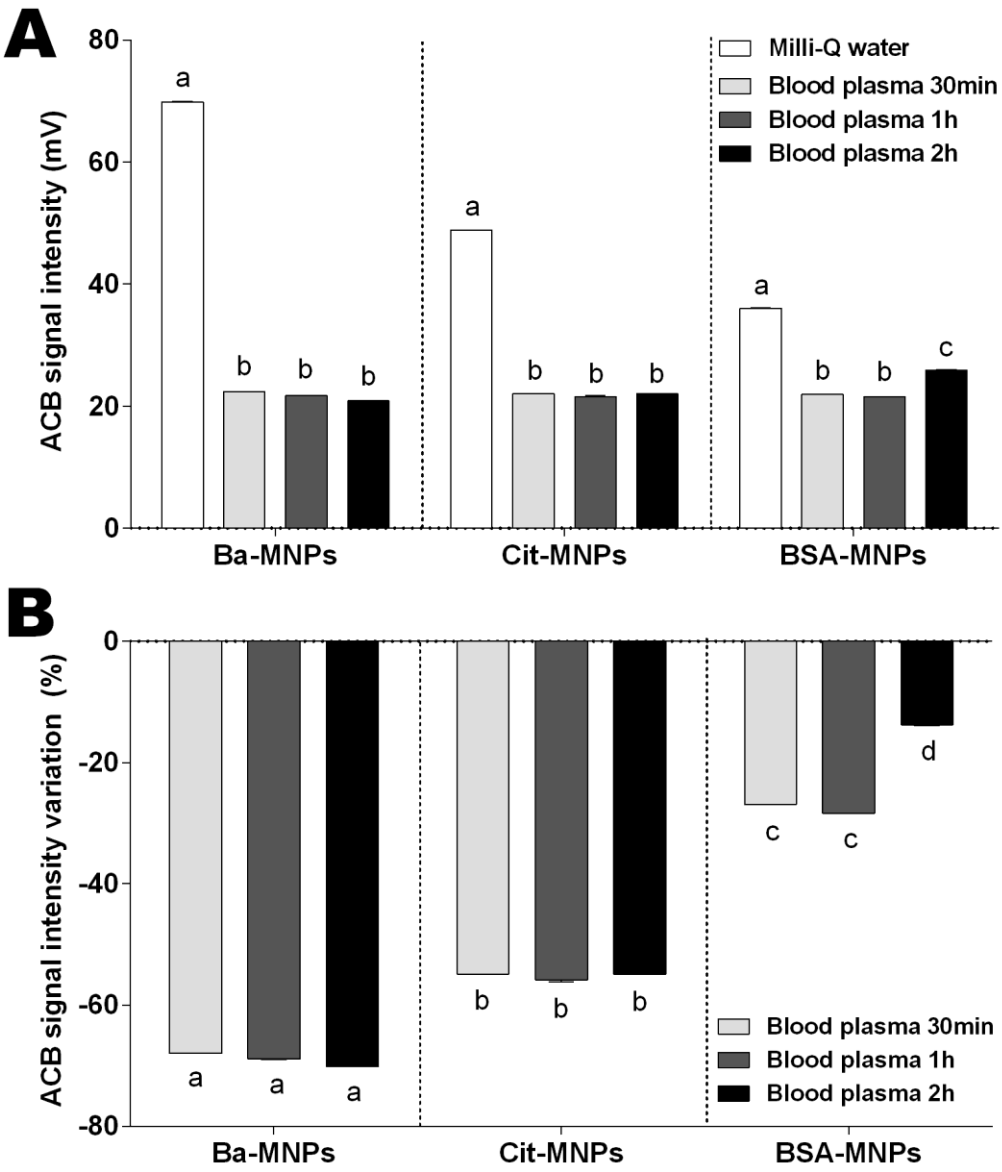

Figure 1 – Impacts of the CP in the ACB signal intensity. (A) ACB absolute signal intensity for the Ba-MNPs, Cit-MNPs, and BSA-MNPs after 30min, 1h, and 2h of incubation, and their respective controls with Milli-Q water after 30 min of incubation time. (B)Percentage of ACB signal decrease for the Ba-MNPs, Cit-MNPs, and BSA-MNPs after 30min, 1h, and 2h of incubation.

After the second magnetic measurement by the ACB system, we processed the samples to elute the proteins from the MNPs, as described in the Results section and applied the supernatant in SDS-PAGE gels. Figure 2 shows the gels containing the protein spots found in each incubation time for each MNPs coat. As expected we found a different weight proteins profile that interacts with each MNPs coat. Although it is a

semi-quantitative analysis, it is possible to notice that in the Ba-MNPs interacted more intensive with heavier proteins, where the spots are between 180 kDa and 55 kDa, in which the 70 kDa and 55 kDa were the most pronounced spots. The Cit-MNPs also presented a heavier proteins profile, but this time the most pronounced spots were between 100 kDa (marker just above 70kDa) and 70 kDa. For BSA-MNPs we found the pronounced spots between 100 kDa and 55 kDa. Beside all MNPs showed a heavier proteins profile, it is possible to notice a slight difference between them. In Ba-MNPs the 70 kDa and 55 kDa are well separated and composes most of all proteins that interact with the MNPs, and in 1h and 2h of incubation times appears 10 kDa spots, that are not present in the 30 min incubation time. In the Cit-MNPs this occurs with the spots between 100 kDa and 70 kDa, where the 55 kDa shows a lower intensity when compared with heavier proteins spots. For the BSA-MNPs the spots are not clearly separated, but we can see that the amount of bound proteins changed along the time, wherein the first 30 min there is a higher protein concentration in the gel than in other times. Also, after 30 min of incubation, there is a 10 kDa and a 25 kDa spots that are not present, or less intense, in the 1h and 2h of incubation. Furthermore, the BSA-MNPs presented the lower proteins in the gel analysis. These data suggest that the CP formation evolves and some proteins can be unlinked to the MNPs surface, and replaced by other proteins of higher affinity along the time.

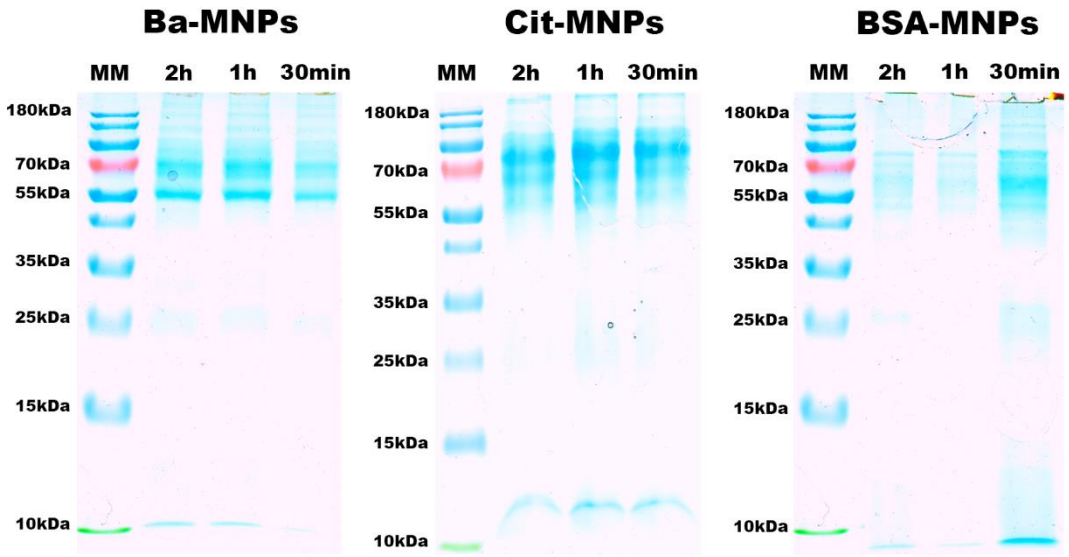

Figure 2 – 10% 1D SDS-PAGE and Coomassie Blue staining of the eluted proteins for each MNPs conjugation. In the first gels' wells, MM represents the standard molecular marker and the 2h, 1h and 30min, the incubation times. At left are presented the molecular weights of the MM spots for control.

Unfortunately, in this version, we were able to apply in the LC/MS/MS system and analyze only the Cit-MNPs CP pilot sample for 2h of incubation time. All other samples have already been processed and prepared to be applied in the system, but there was unexpected maintenance in the system's facilities that delayed our schedule. We expect that these data will be collected until the presentation of this thesis, and if we can collect and analyze all data, it will be included in the presentation and final version. Table 1 shows the identification of the proteins found in the LC/MS/MS system and *Mascot* software analysis with hit probability higher than 95%.

Table 1 – Proteins found and their identification code for each spot from the Cit-MNPs CP sample for 2h of incubation time.

Spot	Protein found	Identification code (UNIPROT)
1	Plasminogen, Isoform CRA_d	EDL83068.1
2	Plasminogen, plasmin heavy chain A	Q01177.2
3	Complement C4-like Complement component 4, gene 2	CAE83956.1
4	Complement C4-like	XP_008770996.1
5	Gamma-2a immunoglobulin heavy chain	AAA91896.1
6	Plasminogen, plasmin heavy chain A	Q01177.2
7	Complement C1q, subcomponent subunit B	P31721.2
8	No proteins hit above 95%	--
9	Chain A, Hemoglobin	3DHT_A
10	No proteins hit above 95%	--

From table 1 it is possible to observe that the Cit-MNPs presented a considerable affinity with proteins related to coagulation processes (plasminogen), immunological

(Gamma Immunoglobulin – IgG) and inflammatory (C1, C4, and C4-like components) responses. In the future mass spectrometry analyzes, involving all MNPs conjugation and incubation times samples, the Ba-MNPs samples will possibly present almost the same behavior than Cit-MNPs samples, and the BSA-MNPs present less, or none interactions with inflammatory and immunological factors, which can explain its longer circulation time. Also, until this version we were not able to quantify these proteins, but in the future analyzes, just before of the samples application in the LC/MS/MS system, we will perform a protein quantification in all samples, which can give us not only the protein identity profile, but also the amount of protein bound in each MNPs conjugation sample.

3.2. *In Vivo* Experiments

Figure 3 shows examples of the ACB normalized signals acquired for the three groups. All the *in vivo* signals showed a similar profile, with a rapid peak, related to the MNPs arrival in the animals' heart, and an exponential-like decay, related to the withdrawal of the MNPs from the bloodstream. To compare the MNPs circulation time, we plotted an example of each MNPs conjugation in the same time scale, but the acquisition time was longer than presented in figure 3 for the BSA-MNPs. We stopped the acquisition when there was stabilization in the ACB signal. In this way, for the Cit-MNPs and Ba-MNPs groups, the ACB signal stabilized we performed approximately 30 min of signal acquisition, while for the BSA-MNPs group this period was not sufficient, and we acquired the signals for approximately 80 min (figure 3 inset).

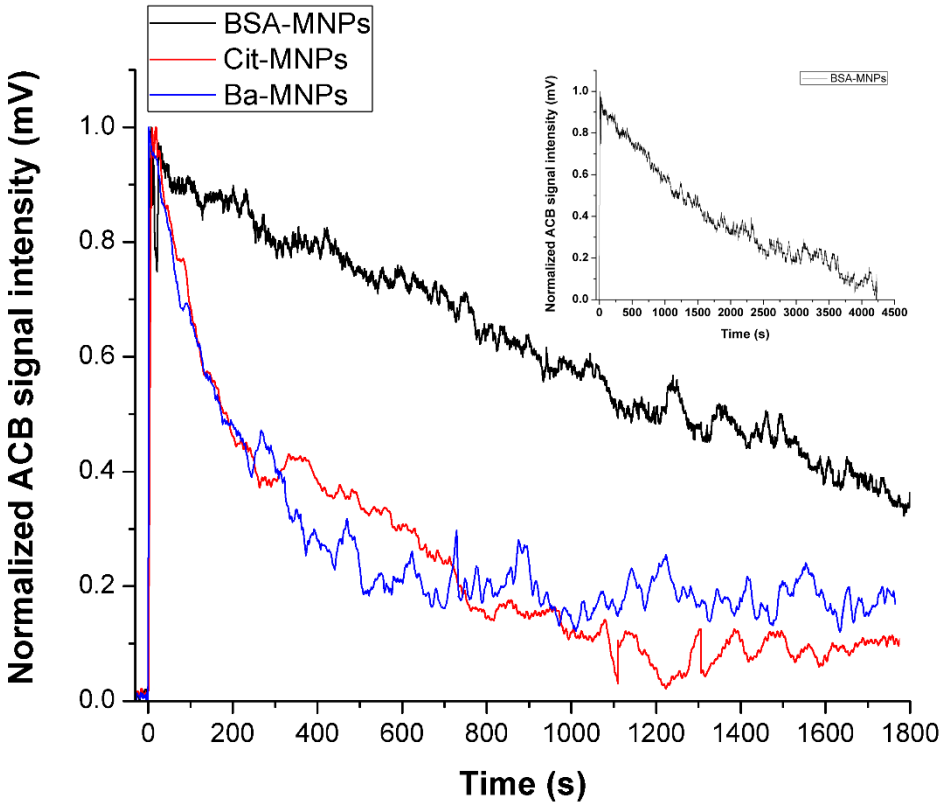

Figure 3 – Magnetic signal acquired by the ACB system. The black line is an example of an animal from the BSA-MNPs group, the red line is an example of an animal from the Cit-MNPs group, and the blue line is an example of an animal from the Ba-MNPs group. Inset shows the entire acquired signal from BSA-MNPs.

As described before, we used a single exponential decay to quantify the MNPs' circulation times ($t_{1/2}$). Figure 4 shows the $t_{1/2}$ and the I_{max} values found in each group. In figure 4A is possible to see that the BSA-MNPs presented the longer circulation time among all MNPs. Statistical analyses showed significant differences between BSA-MNPs and all other groups, while Cit-MNPs and Ba-MNPs did not differ between each other. Figure 4B shows the I_{max} for the three groups. It is possible to see that there was a significant difference only between Cit-MNPs and BSA-MNPs, where the Ba-MNPs showed no differences when compared with both Cit-MNPs and BSA-MNPs.

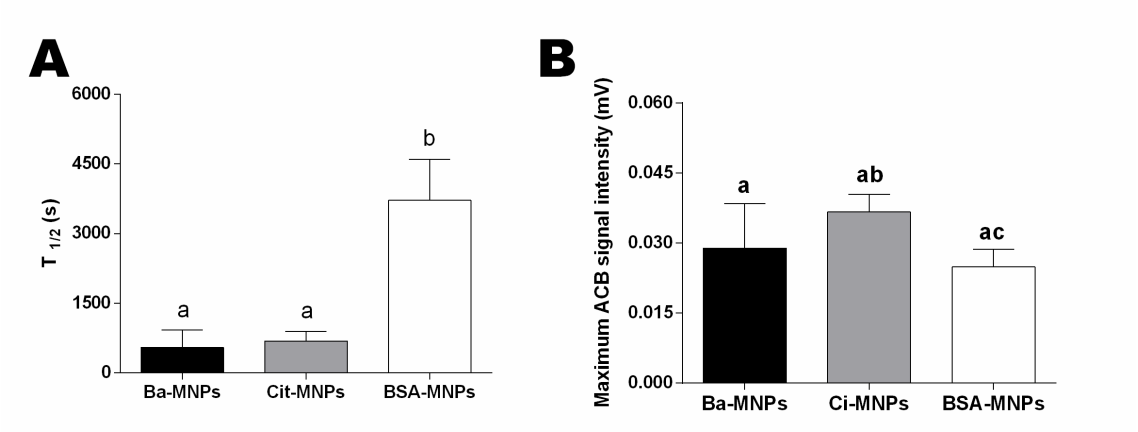

Figure 4 – ACB *in vivo* signals quantification. (A) Circulation time for the Ba-MNPs, Cit-MNPs, and BSA-MNPs. (B) Maximum signal intensity detected in each group. Different letters show a significant difference between groups with $p < 0.05$.

4. DISCUSSION

Here we studied the CP formation of three different manganese ferrite MNPs conjugations: uncoated (positively charged), coated with citrate (negatively charged) and BSA (almost neutral) its impacts in the ACB signal intensity and in MNPs circulation time. Correlate the MNPs' circulation time with the CP formation is of paramount importance and can help to facilitate the establishment of certain MNPs in preclinical and clinical routine. Also studying these parameters is possible to develop specific coating protocols to assuring the MNPs intravenous injection safety and efficiency.

The *in vitro* experiments showed that the ACB signal intensity suffered a significant variation of the CP formation in all MNPs conjugations. Once the ACB system is based on the MNPs' AC susceptibility, these results suggest that when there is an MNPs-blood serum interaction, the MNPs' AC susceptibility decreases. Salvador and co-authors also found this effects in the MNPs' magnetic susceptibility (44). They performed Monte Carlo simulations and an extensive MNPs characterization process, and their findings showed that the MNPs presented a lower magnetic susceptibility

when the particles were coated with liposomes than when the particles were coated with citrate. In nanostructured materials, the number of atoms in the surface is higher than in bulk material, which gives to these materials a series of interesting properties, as its superparamagnetic behavior. Since there are other structures interacting with these surface's atoms, it can change the electronic configuration of the MNPs surface, and consequently its anisotropy axis and interparticle interactions, that are two of the main factors in the MNPs magnetic properties (45). This fact also can have effects in the MNPs' heat generation for magnetic cancer hyperthermia, and when these particles are detected by a magnetic system as the MRI or magnetic particle imaging system. Since these detecting systems are calibrated using different concentrations of MNPs before the CP formation, its quantification process can be influenced by the CP formation impacts on the MNPs' magnetic properties. The implications of CP formation on MRI contrast efficiency were studied before (46, 47). Using a fetal bovine serum as a representative biological fluid, Amiri and co-workers found that the CP layer affected the MRI contrast efficiency in a way that was dependent on the characteristics of the MNPs coating. Also, they found that the CP compositions were strongly related to the MNPs surface composition and charge. For their MNPs, the positively charged ones were the batch that presented the lower proteins interaction, while the negatively charged were the most protein-reactive batch (46).

In our data, the BSA-MNPs presented the lower ACB signal intensity variation. In this way, when compared with the literature data, the BSA-MNPs might be the MNPs conjugation that less interact with plasma proteins among the MNPs conjugations studied here. The highest ACB signal intensity variation was found for the Ba-MNPs. These particles are not coated, and because of that, they are strongly dependent on the ionic forces in the liquid media to stay stable in the colloid suspension (31). When we

mixed these MNPs in plasma, or the bloodstream, the pH media changes, and also the ionic forces, that sustain the MNPs well dispersed in the colloid, forming complexes structures as spherical-like aggregates. Spherical-like aggregates can have a flux closures moment configurations, and a low amplitude magnetic field, as the ACB excitating magnetic fields, would not excite the particles inside the aggregate, decreasing the ACB signal more intensively (6). In regards to the Cit-MNPs, they also are stable due to ionic interactions, but in their case, the stability is greater than the Ba-MNPs, probably because of the surface charge intensity (-28mV for Cit-MNPs and 17mV for Ba-MNPs). We recently published a paper involving the Cit-MNPs and the ACB system (7). In such article, we performed a dynamic light scattering (DLS) analyzes, and the Cit-MNPs presented only one peak of size distribution, around 30 nm of a hydrodynamic radius. In the same study, when mixed these particles whit biological fluids, the DLS analyzes presented two peaks of hydrodynamic radius, where one of those peaks presented its original size and the second presented a size increase (reaching around 100 nm). In this way, some of the Cit-MNPs can suffer the pH changes more intensively than others, and the flux closures are less present in Cit-MNPs than in the Ba-MNPs, but this issue might be addressed in other studies.

The SDS-PAGE gels showed the proteins weight profile for each MNPs conjugation and incubation times. From the gel analysis, it is possible to see that all MNPs conjugations presented a heavy proteins interaction profile. Besides that, there are some slight differences between the MNPs conjugations and the incubation times for the same MNPs conjugation. Also, the Cit-MNPs (negatively charged) presented more intense staining (related to the concentration of the proteins) and a heavier proteins profile when compared with both Ba-MNPs and BSA-MNPs, which was also found previously (46). For the Cit-MNPs and Ba-MNPs, the proteins profile almost no changed along the time,

where the only changes were on the 10kDa spots for 1h and 2h in the Ba-MNPs, which were not present in the 30 min of incubation. This BSA-MNPs behavior is related to the fact that the CP formation is a dynamical process, and the more motile proteins bind to the MNPs in the first moment, but with the time these proteins can be unlinked of the proteins' surface. Two main factors can play this role: enzymatic action, which can break the link between the MNPs and the proteins; and the binding kinetics, where the less motile proteins present a higher MNPs surface's affinity, and them can replace the more motile but of less-affinity proteins (48). A study, focused in the nanoparticles-protein binding kinetics, found that the human serum albumin (HSA) is rapidly adsorbed in the polymer-coated nanoparticles surface, but they showed that the HSA resides on the nanoparticles' surface for approximately 100s (49). They also stated that both the nanoparticle and proteins should adapt their surfaces to find a stable interface, and even should exist a rearrangement of the firstly bound proteins to make available some spaces for the binding of proteins that reach the particles in a second moment. Other works showed, both by experiments and by simulations that the besides the high binding rates of HSA with copolymer nanoparticles the HSA is rapidly replaced by other proteins with higher affinity and lower exchange rate (48, 50).

As stated before, we were able to collect the LC/MS/MS data for just one CP sample. In this sample (Cit-MNPs after 2h of incubation) we found several proteins related to coagulation process, inflammatory and immunological factors as plasminogen, C1q, and C4 complement, and gamma IgG. Note that the plasminogen is a factor associated with negative feedback in the coagulation process, it is one of the most abundant proteins in the blood and consequently is expected to find these proteins in MNPs' CP due non-specific interactions (50, 51). Components of the complement system as the C3, C4, and C5, and also immunoglobulins, are known to be common

structures that act as opsonins (i.e., produce an opsonization process, also called as CP formation for nanoparticles). Generally speaking, these components are the most common opsonins related to phagocytic recognition (52, 53). Also, IgG and complement proteins are known to be associated with large particles and hydrophobic surfaces (54, 55). Lundqvist and co-authors performed an extensive CP characterization in differently functionalized copolymer nanoparticles (56). They also found C1q and C4 complement, plasminogen, and IgG in the CP formed in nanoparticles carboxyl functionalized. The Cit-MNPs that we used here are citrate coated and the citrate presents carboxyl groups in its structure, which can explain these factors found in the LC/MS/MS analysis.

The *in vivo* data showed a longer circulation time for the BSA-MNPs, where was almost five times longer than for Cit-MNPs and Ba-MNPs. The lower circulation time for the Cit-MNPs can be related to the CP that we found in the first analysis, and this can also be extrapolated to the Ba-MNPs, which presented more staining and similar (besides slight differences) proteins profile. The immunological factors and components of the complement system are known to act as signaling molecules for phagocytic recognition (52, 53). Recently we published a paper in regards to the liver uptake of the Cit-MNPs. In such study, we demonstrated that most of the injected MNPs is uptake by the liver and spleen, organs are known by their high numbers of phagocytic cells like macrophages and Kuppfer cells (6). In this way, the CP formed in these particles could activate the phagocytic action, and the particles were rapidly uptake in the liver and spleen, which explain its fast withdrawal from the bloodstream. Besides we were not able to collect the LC/MS/MS data for the Ba-MNPs, we expect almost the same behavior for these particles, presenting immunological and complement system factors, once we found a short circulation time.

The BSA coating presents an excellent potential for nanomedicine since they are biodegradable, non-toxic and non-antigenic (27, 57, 58). The high BSA-MNPs' circulation time can be related to the fact that the bovine serum albumin presents high sequence homologies above 70% for the rat serum albumin (RSA), and also, aiming clinical applications, for human serum albumin (59, 60). Although we did not perform the LC/MS/MS analyzes for the BSA-MNPs samples, since this high similarity presented by the BSA with the RSA, we expect that these particles will show a different CP profile, where the immunological and inflammatory blood components would not recognize the MNPs as an exogenous compound so fast, which could increase its circulation time. Furthermore, we expect a different CP profile along the time, once the SDS-PAGE gel showed a significant difference of staining for the different incubation times samples. It is worth to point out that some drugs, as Paclitaxel, presented a higher efficiency and lower toxicity when are formulated with albumin (61). Also, the use of BSA as a drug and nanoparticulated carrier represents an interesting strategy. The BSA carrier enables a significant amount of drug in the carrier matrix, different and numerous drug binding sites, which can allow the adsorption of positively or negatively charged molecules without the need of an intermediary substance (29). In this way, the use of BSA-MNPs can also be associated with chemotherapeutic agents, leading to a multi-modal cancer imaging and treatment approach. As the BSA-MNPs presented a longer circulation time, these particles present a good advantage over several MNPs conjugations described in the literature, once the high circulation time can improve the enhanced permeability and retention effect for cancer treatment and its potential as a blood pool contrast agent for MRI.

In this way, we present several data showing some relationships between the ACB signal intensity, CP formation and circulation time. Our data suggest that the negatively

charged MNPs interact more with plasma proteins than positively and neutral particles. Also, the positively charged particles can form aggregates, which can explain the ACB signal intensity decrease. Both Cit-MNPs and Ba-MNPs presented an intense CP formation, where the LC/MS/MS data collected so far showed immunological and inflammatory factors linked to the MNPs, higher ACB signal intensity decrease, and also lower circulation times. The protein coat (BSA) present an almost neutral charge, lower ACB signal intensity decrease and longer circulation times. These data suggest that the BSA-MNPs can be a good choice in regards to biocompatibility, influences of its CP in the MNPs magnetic behavior, and circulation times.

5. CONCLUSION

Summary, we employed a biomagnetic, electrophoresis gel and mass spectrometry techniques to study the CP formation for three different MNPs conjugations, its impacts on the ACB signal intensity and its circulation times. For the data that we collected so far, we can conclude that the Cit-MNPs presented a CP mainly formed by immunological and inflammatory plasma components which can be linked to their short circulation time. Also, we expect similar results for the Ba-MNPs, which presented almost the same circulation time than the Cit-MNPs. The BSA-MNPs presented the highest circulation time among the three conjugations studied here. From the future LC/MS/MS analyses, we expect a different CP profile for the BSA-MNPs, with less immunological and inflammatory components interactions. The results obtained *in vivo* and by the SDS-PAGE for the BSA-MNPs suggests its use as a new nanomedicine agent. This MNPs conjugation already presented a good performance as magnetic cancer hyperthermia heat generators (27), can also be associated with chemotherapeutic agents, and now presented good results as a nanotracer for the ACB system, providing a good platform for cancer theranostics.

6. REFERENCES

1. Shubayev VI, Pisanic TR, 2nd, Jin S. Magnetic nanoparticles for theragnostics. Advanced drug delivery reviews. 2009;61(6):467-77. Epub 2009/04/25.

2. Huang HS, Hainfeld JF. Intravenous magnetic nanoparticle cancer hyperthermia. International journal of nanomedicine. 2013;8:2521-32. Epub 2013/08/01.

3. Singh A, Sahoo SK. Magnetic nanoparticles: a novel platform for cancer theranostics. Drug Discov Today. 2014;19(4):474-81. Epub 2013/10/22.

4. von Roemeling C, Jiang W, Chan CK, Weissman IL, Kim BY. Breaking Down the Barriers to Precision Cancer Nanomedicine. Trends in biotechnology. 2017;35(2):159-71. Epub 2016/08/06.

5. Cole AJ, Yang VC, David AE. Cancer theranostics: the rise of targeted magnetic nanoparticles. Trends in biotechnology. 2011;29(7):323-32. Epub 2011/04/15.

6. Quini CC, Prospero AG, Calabresi MFF, Moretto GM, Zufelato N, Krishnan S, et al. Real-time liver uptake and biodistribution of magnetic nanoparticles determined by AC biosusceptometry. Nanomedicine : nanotechnology, biology, and medicine. 2017;13(4):1519-29.

7. Prospero AG, Quini CC, Bakuzis AF, Fidelis-de-Oliveira P, Moretto GM, Mello FP, et al. Real-time in vivo monitoring of magnetic nanoparticles in the bloodstream by AC biosusceptometry. Journal of nanobiotechnology. 2017;15(1):22.

8. Rodrigues HF, Mello FM, Branquinho LC, Zufelato N, Silveira-Lacerda EP, Bakuzis AF. Real-time infrared thermography detection of magnetic nanoparticle hyperthermia in a murine model under a non-uniform field configuration. Int J Hyperther. 2013;29(8):752-67.

9. Reimer P, Balzer T. Ferucarbotran (Resovist): a new clinically approved RES-specific contrast agent for contrast-enhanced MRI of the liver: properties, clinical

development, and applications. European radiology. 2003;13(6):1266-76. Epub 2003/05/24.

10. Kobayashi H, Brechbiel MW. Dendrimer-based nanosized MRI contrast agents. Current pharmaceutical biotechnology. 2004;5(6):539-49. Epub 2004/12/08.

11. Lubbe AS, Bergemann C, Huhnt W, Fricke T, Riess H, Brock JW, et al. Preclinical experiences with magnetic drug targeting: tolerance and efficacy. Cancer research. 1996;56(20):4694-701. Epub 1996/10/15.

12. Schroeder U, Sommerfeld P, Ulrich S, Sabel BA. Nanoparticle technology for delivery of drugs across the blood-brain barrier. Journal of pharmaceutical sciences. 1998;87(11):1305-7. Epub 1998/11/13.

13. Sahoo SK, Labhasetwar V. Nanotech approaches to drug delivery and imaging. Drug discovery today. 2003;8(24):1112-20.

14. Caracciolo G, Farokhzad OC, Mahmoudi M. Biological identity of nanoparticles in vivo: clinical implications of the protein corona. Trends in biotechnology. 2017;35(3):257-64.

15. Yoo J-W, Chambers E, Mitragotri S. Factors that control the circulation time of nanoparticles in blood: challenges, solutions and future prospects. Current pharmaceutical design. 2010;16(21):2298-307.

16. Prabhakar U, Maeda H, Jain RK, Sevick-Muraca EM, Zamboni W, Farokhzad OC, et al. Challenges and key considerations of the enhanced permeability and retention effect for nanomedicine drug delivery in oncology. AACR; 2013.

17. Xiao W, Lin J, Li M, Ma Y, Chen Y, Zhang C, et al. Prolonged in vivo circulation time by zwitterionic modification of magnetite nanoparticles for blood pool contrast agents. Contrast media & molecular imaging. 2012;7(3):320-7.

18. Docter D, Bantz C, Westmeier D, Galla HJ, Wang Q, Kirkpatrick JC, et al. The protein corona protects against size-and dose-dependent toxicity of amorphous silica nanoparticles. Beilstein journal of nanotechnology. 2014;5:1380.

19. Safi M, Courtois J, Seigneuret M, Conjeaud H, Berret JF. The effects of aggregation and protein corona on the cellular internalization of iron oxide nanoparticles. Biomaterials. 2011;32(35):9353-63. Epub 2011/09/14.

20. Monopoli MP, Aberg C, Salvati A, Dawson KA. Biomolecular coronas provide the biological identity of nanosized materials. Nature nanotechnology. 2012;7(12):779-86.

21. Deng ZJ, Liang M, Monteiro M, Toth I, Minchin RF. Nanoparticle-induced unfolding of fibrinogen promotes Mac-1 receptor activation and inflammation. Nature nanotechnology. 2011;6(1):39.

22. Mahon E, Salvati A, Bombelli FB, Lynch I, Dawson KA. Designing the nanoparticle–biomolecule interface for "targeting and therapeutic delivery". Journal of Controlled Release. 2012;161(2):164-74.

23. Casals E, Pfaller T, Duschl A, Oostingh GJ, Puntes V. Time evolution of the nanoparticle protein corona. ACS nano. 2010;4(7):3623-32.

24. Quini CC, Matos JF, Próspero AG, Calabresi MF, Zufelato N, Bakuzis AF, et al. Renal perfusion evaluation by alternating current biosusceptometry of magnetic nanoparticles. J Magn Magn Mater. 2014.

25. Quini CC, Matos JF, Prospero AG, Calabresi MFF, Zufelato N, Bakuzis AF, et al. Renal perfusion evaluation by alternating current biosusceptometry of magnetic nanoparticles. J Magn Magn Mater. 2015;380:2-6.

26. Quini CC, Próspero AG, Kondiles BR, Chaboub L, Hogan MK, Baffa O, et al. Development of a protocol to assess cell internalization and tissue uptake of magnetic nanoparticles by AC Biosusceptometry. J Magn Magn Mater. 2019;473:527-33.

27. Zufelato N. Construção, caracterização e otimização da magnetohipertermia de nanocarreadores multifuncionais fluorescentes: a importância da relaxação coletiva na geração de calor. 2018.

28. Farrugia A. Albumin usage in clinical medicine: tradition or therapeutic? Transfusion medicine reviews. 2010;24(1):53-63.

29. Elzoghby AO, Samy WM, Elgindy NA. Albumin-based nanoparticles as potential controlled release drug delivery systems. Journal of Controlled Release. 2012;157(2):168-82.

30. Bakuzis AF, Morais PC, Pelegrini F. Surface and exchange anisotropy fields in MnFe2O4 nanoparticles: Size and temperature effects. J Appl Phys. 1999;85(10):7480-2.

31. Bakuzis AF, Branquinho LC, Castro LLE, Eloi MTDA, Miotto R. Chain formation and aging process in biocompatible polydisperse ferrofluids: Experimental investigation and Monte Carlo simulations. Adv Colloid Interfac. 2013;191:1-21.

32. Branquinho LC, Carriao MS, Costa AS, Zufelato N, Sousa MH, Miotto R, et al. Effect of magnetic dipolar interactions on nanoparticle heating efficiency: Implications for cancer hyperthermia. Sci Rep-Uk. 2013;3.

33. Nunes AD, Ramalho LS, Souza ÁP, Mendes EP, Colugnati DB, Zufelato N, et al. Manganese ferrite-based nanoparticles induce ex vivo, but not in vivo, cardiovascular effects. International journal of nanomedicine. 2014;9:3299.

34. Cora LA, Americo MF, Oliveira RB, Baffa O, Moraes R, Romeiro FG, et al. Disintegration of magnetic tablets in human stomach evaluated by alternate current

Biosusceptometry. European Journal of Pharmaceutics and Biopharmaceutics. 2003;56(3):413-20.

35. Cora LA, Romeiro FG, Stelzer M, Americo MF, Oliveira RB, Baffa O, et al. AC biosusceptometry in the study of drug delivery. Advanced drug delivery reviews. 2005;57(8):1223-41. Epub 2005/06/07.

36. Americo MF, Oliveira RB, Romeiro FG, Baffa O, Cora LA, Miranda JR. Scintigraphic validation of AC Biosusceptometry to study the gastric motor activity and the intragastric distribution of food in humans. Neurogastroenterology and motility : the official journal of the European Gastrointestinal Motility Society. 2007;19(10):804-11. Epub 2007/09/22.

37. Andreis U, Americo MF, Cora LA, Oliveira RB, Baffa O, Miranda JR. Gastric motility evaluated by electrogastrography and alternating current biosusceptometry in dogs. Physiological measurement. 2008;29(9):1023-31. Epub 2008/08/14.

38. Quini CC, Americo MF, Cora LA, Calabresi MF, Alvarez M, Oliveira RB, et al. Employment of a noninvasive magnetic method for evaluation of gastrointestinal transit in rats. Journal of biological engineering. 2012;6(1):6. Epub 2012/05/17.

39. Baffa O, Oliveira RB, Miranda JR, Troncon LE. Analysis and development of AC biosusceptometer for orocaecal transit time measurements. Medical & biological engineering & computing. 1995;33(3):353-7. Epub 1995/05/01.

40. Miranda JRA, Oliveira RB, Sousa PL, Braga FJH, Baffa O. A novel biomagnetic method to study gastric antral contractions. Physics in medicine and biology. 1997;42(9):1791-9.

41. Cora A, Andreis U, Romeiro FG, Americo MF, Oliveira RB, Baffa O, et al. Magnetic images of the disintegration process of tablets in the human stomach by ac biosusceptometry. Physics in medicine and biology. 2005;50(23):5523-34.

42. Docter D, Distler U, Storck W, Kuharev J, Wünsch D, Hahlbrock A, et al. Quantitative profiling of the protein coronas that form around nanoparticles. Nature protocols. 2014;9(9):2030.

43. Shevchenko A, Wilm M, Vorm O, Mann M. Mass spectrometric sequencing of proteins from silver-stained polyacrylamide gels. Analytical chemistry. 1996;68(5):850-8.

44. Salvador MA, Costa AS, Gaeti M, Mendes LP, Lima EM, Bakuzis AF, et al. Characterization, nanoparticle self-organization, and Monte Carlo simulation of magnetoliposomes. Physical review E. 2016;93(2-1):022609. Epub 2016/03/18.

45. Peddis D, Orrù F, Ardu A, Cannas C, Musinu A, Piccaluga G. Interparticle interactions and magnetic anisotropy in cobalt ferrite nanoparticles: influence of molecular coating. Chemistry of Materials. 2012;24(6):1062-71.

46. Amiri H, Bordonali L, Lascialfari A, Wan S, Monopoli MP, Lynch I, et al. Protein corona affects the relaxivity and MRI contrast efficiency of magnetic nanoparticles. Nanoscale. 2013;5(18):8656-65.

47. Yallapu MM, Chauhan N, Othman SF, Khalilzad-Sharghi V, Ebeling MC, Khan S, et al. Implications of protein corona on physico-chemical and biological properties of magnetic nanoparticles. Biomaterials. 2015;46:1-12.

48. Dell'Orco D, Lundqvist M, Oslakovic C, Cedervall T, Linse S. Modeling the time evolution of the nanoparticle-protein corona in a body fluid. PloS one. 2010;5(6):e10949.

49. Röcker C, Pötzl M, Zhang F, Parak WJ, Nienhaus GU. A quantitative fluorescence study of protein monolayer formation on colloidal nanoparticles. Nature nanotechnology. 2009;4(9):577.

50. Aggarwal P, Hall JB, McLeland CB, Dobrovolskaia MA, McNeil SE. Nanoparticle interaction with plasma proteins as it relates to particle biodistribution, biocompatibility and therapeutic efficacy. Advanced drug delivery reviews. 2009;61(6):428-37. Epub 2009/04/21.

51. Sakulkhu U, Mahmoudi M, Maurizi L, Coullerez G, Hofmann-Amtenbrink M, Vries M, et al. Significance of surface charge and shell material of superparamagnetic iron oxide nanoparticle (SPION) based core/shell nanoparticles on the composition of the protein corona. Biomaterials science. 2015;3(2):265-78.

52. Owens III DE, Peppas NA. Opsonization, biodistribution, and pharmacokinetics of polymeric nanoparticles. International journal of pharmaceutics. 2006;307(1):93-102.

53. Moghimi SM, Patel H. Serum-mediated recognition of liposomes by phagocytic cells of the reticuloendothelial system–the concept of tissue specificity. Advanced drug delivery reviews. 1998;32(1-2):45-60.

54. Thode K, Lück M, Semmler W, Müller RH, Kresse M. Determination of plasma protein adsorption on magnetic iron oxides: sample preparation. Pharmaceutical research. 1997;14(7):905-10.

55. Gessner A, Waicz R, Lieske A, Paulke B-R, Mäder K, Müller R. Nanoparticles with decreasing surface hydrophobicities: influence on plasma protein adsorption. International journal of pharmaceutics. 2000;196(2):245-9.

56. Lundqvist M, Stigler J, Elia G, Lynch I, Cedervall T, Dawson KA. Nanoparticle size and surface properties determine the protein corona with possible implications for biological impacts. Proceedings of the National Academy of Sciences. 2008.

57. Jun JY, Nguyen HH, Chun HS, Kang B-C, Ko S. Preparation of size-controlled bovine serum albumin (BSA) nanoparticles by a modified desolvation method. Food Chemistry. 2011;127(4):1892-8.

58. Jahanshahi M, Najafpour G, Rahimnejad M. Applying the Taguchi method for optimized fabrication of bovine serum albumin (BSA) nanoparticles as drug delivery vehicles. African Journal of Biotechnology. 2008;7(4).

59. Stehle G, Wunder A, Schrenk HH, Hartung G, Heene DL, Sinn H. Albumin-based drug carriers: comparison between serum albumins of different species on pharmacokinetics and tumor uptake of the conjugate. Anti-Cancer Drug. 1999;10(8):785-90.

60. Majorek KA, Porebski PJ, Dayal A, Zimmerman MD, Jablonska K, Stewart AJ, et al. Structural and immunologic characterization of bovine, horse, and rabbit serum albumins. Molecular immunology. 2012;52(3-4):174-82.

61. Sparreboom A, Scripture CD, Trieu V, Williams PJ, De T, Yang A, et al. Comparative preclinical and clinical pharmacokinetics of a cremophor-free, nanoparticle albumin-bound paclitaxel (ABI-007) and paclitaxel formulated in Cremophor (Taxol). Clinical cancer research. 2005;11(11):4136-43.

CONCLUSÃO GERAL

A presente tese de doutorado envolve a aplicação do sistema de Biosusceptometria AC para a avaliação de parâmetros relacionados a biofísica da dinâmica renal e cerebral, além de estudar os impactos da formação da corona proteica em parâmetros farmacocinéticos e magnéticos das MNPs. Aqui apresentamos pela primeira vez a utilização deste sistema associado às MNPs para o estudo de disfuncionalidades de órgãos como os rins e o cérebro.

A partir da indução de uma lesão renal grave, induzida por administração única de doxorrubicina, pudemos investigar os parâmetros de perfusão das MNPs pelos rins bem como o acúmulo das MNPs por estes órgãos em animais saudáveis e lesionados. Os resultados obtidos das análises realizadas pelo sistema BAC, tanto *in vivo* quanto *in vitro*, se apresentaram fortemente em concordância com os dados obtidos via teste bioquímico padrão e análises morfológicas. Esses dados fortalecem o uso do sistema BAC e MNPs para estudos que envolvem o estudo e acompanhamento de disfunções relacionadas com alterações no perfil de perfusão e fluxo sanguíneo nos rins. O desenvolvimento de novas tecnologias de baixo custo e que forneçam dados mais rapidamente de parâmetros ligados à evolução de doenças renais se mostra de grande valia, uma vez que pode diminuir custos e acelerar o processo de desenvolvimento de novas estratégias de diagnósticos e tratamentos envolvendo os rins. Sendo assim, esse trabalho viabiliza o uso de uma tecnologia simples, de baixo custo e versátil para investigações e desenvolvimento de nanocarreadores e nanotraçadores magnéticos como uma alternativa aos meios de contraste e instrumentações padrão utilizados para avaliações funcionais dos rins, que como já citado, apresentam algumas desvantagens.

Estudamos também os efeitos do manitol sobre a distribuição de MNPs no cérebro, associando MNPs como traçadores e o sistema BAC como detector *in vivo*. Para os estudos *in vitro,* aplicamos uma nova variação do sensor padrão do sistema BAC, o "sensor de cavidade". Apresentamos aqui, pela primeira vez, a caracterização deste sensor, que foi capaz de quantificar o depósito de MNPs nos tecidos com uma sensibilidade de quase uma ordem de grandeza maior do que o sensor convencional. Sendo assim, o sistema BAC e as MNPs foram capazes de detectar variações na dinâmica de perfusão cerebral, bem como o acúmulo de MNPs no cérebro. Acreditamos que o uso da BAC associada à MNPs possa também contribuir nas áreas de desenvolvimento de MNPs específicas para aplicações como traçadores ou sistemas de liberação de drogas focados neste órgão tão importante e difícil de acessar, que é o cérebro.

O terceiro e último capítulo contemplou o estudo da formação da corona proteica e seus impactos no tempo de circulação das MNPs e intensidade de sinal do sistema BAC. Apesar de que ainda faltam alguns dados a serem coletados, os dados obtidos até o momento indicam que a formação de corona proteica pode influenciar em propriedades magnéticas das MNPs. Além disso, as MNPs com cargas superficiais mais intensas (tanto negativas quanto positivas) apresentaram maior formação e densidade de corona proteica do que as MNPs mais próximas da neutralidade de cargas superficiais (BSA-MNPs), como mostraram as análises de eltroforese em gel SDS-PAGE. As partículas revestidas com citrato que foram analisadas pela espetrometria de massas, apresentaram interações com uma série de agentes imunológicos e inflamatórios, provavelmente por interações inespecíficas, o que refletiu no tempo de circulação dessas MNPs. Os tempos de circulação das três conjugações de MNPs aparecem fortemente relacionados com a formação de corona proteica, onde as MNPs que mostraram

formação de corona proteica mais intensa foram os que apresentaram os menores tempos de circulação. Ainda deveremos finalizar este estudo com os dados que ainda serão obtidos da espectrometria de massas, porém os dados obtidos até o momento sugerem que as BSA-MNPs são a conjugação que apresenta perfil diferente de corona proteica e menor interação com proteínas do que as outras partículas que tinham maior densidades de cargas superficiais. Os dados obtidos para as BSA-MNPs foram muito interessantes, onde essa conjugação foi a que apresentou menor efeito corona e consequentemente maior tempo de circulção, o que sugere uma maior biocompatibilidade e eficácia quando usada em tratamentos de tumores (quando usada a estratégia de *targeting* passivo, baseada no efeito de aumento de permeabilidade e retenção) ou como agentes de contraste em angiografias em procedimentos de MRI.

Acreditamos que os dados aqui apresentados subsidiem avaliações anteriores já publicados pelo grupo e apresentam novas abordagens que aumentam as aplicabilidades do sistema BAC, fornecendo uma ferramenta alternativa, de baixo custo, fácil manuseio e versátil para estudos pré-clínicos envolvendo materiais magnéticos nanoestruturados.

REFERÊNCIAS INTRODUÇÃO E CONCLUSÃO GERAL

1. Pankhurst QA, Connolly J, Jones SK, Dobson J. Applications of magnetic nanoparticles in biomedicine. J Phys D Appl Phys. 2003;36(13):R167-R81.

2. Chertok B, Moffat BA, David AE, Yu FQ, Bergemann C, Ross BD, et al. Iron oxide nanoparticles as a drug delivery vehicle for MRI monitored magnetic targeting of brain tumors. Biomaterials. 2008;29(4):487-96.

3. Taupitz M, Schnorr J, Abramjuk C, Wagner S, Pilgrimm H, Hunigen H, et al. New generation of monomer-stabilized very small superparamagnetic iron oxide particles (VSOP) as contrast medium for MR angiography: Preclinical results in rats and rabbits. J Magn Reson Imaging. 2000;12(6):905-11.

4. Choi HS, Liu W, Misra P, Tanaka E, Zimmer JP, Itty Ipe B, et al. Renal clearance of quantum dots. Nat Biotechnol. 2007;25(10):1165-70. Epub 2007/09/25.

5. Pradhan P, Giri J, Rieken F, Koch C, Mykhaylyk O, Doblinger M, et al. Targeted temperature sensitive magnetic liposomes for thermo-chemotherapy. Journal of controlled release : official journal of the Controlled Release Society. 2010;142(1):108-21. Epub 2009/10/13.

6. Huang HS, Hainfeld JF. Intravenous magnetic nanoparticle cancer hyperthermia. International journal of nanomedicine. 2013;8:2521-32. Epub 2013/08/01.

7. Shubayev VI, Pisanic TR, 2nd, Jin S. Magnetic nanoparticles for theragnostics. Advanced drug delivery reviews. 2009;61(6):467-77. Epub 2009/04/25.

8. Singh A, Sahoo SK. Magnetic nanoparticles: a novel platform for cancer theranostics. Drug Discov Today. 2014;19(4):474-81. Epub 2013/10/22.

9. Sun C, Lee JS, Zhang M. Magnetic nanoparticles in MR imaging and drug delivery. Advanced drug delivery reviews. 2008;60(11):1252-65. Epub 2008/06/19.

10. Lubbe AS, Bergemann C, Huhnt W, Fricke T, Riess H, Brock JW, et al. Preclinical experiences with magnetic drug targeting: tolerance and efficacy. Cancer research. 1996;56(20):4694-701. Epub 1996/10/15.

11. Albanese A, Tang PS, Chan WC. The effect of nanoparticle size, shape, and surface chemistry on biological systems. Annual review of biomedical engineering. 2012;14:1-16. Epub 2012/04/25.

12. Chen LT, Weiss L. The role of the sinus wall in the passage of erythrocytes through the spleen. Blood. 1973;41(4):529-37. Epub 1973/04/01.

13. Ruoslahti E, Bhatia SN, Sailor MJ. Targeting of drugs and nanoparticles to tumors. J Cell Biol. 2010;188(6):759-68.

14. Gamarra LF, daCosta-Filho AJ, Mamani JB, de Cassia Ruiz R, Pavon LF, Sibov TT, et al. Ferromagnetic resonance for the quantification of superparamagnetic iron oxide nanoparticles in biological materials. International journal of nanomedicine. 2010;5:203-11. Epub 2010/05/14.

15. Yallapu MM, Chauhan N, Othman SF, Khalilzad-Sharghi V, Ebeling MC, Khan S, et al. Implications of protein corona on physico-chemical and biological properties of magnetic nanoparticles. Biomaterials. 2015;46:1-12.

16. Caracciolo G, Farokhzad OC, Mahmoudi M. Biological identity of nanoparticles in vivo: clinical implications of the protein corona. Trends in biotechnology. 2017;35(3):257-64.

17. Monopoli MP, Aberg C, Salvati A, Dawson KA. Biomolecular coronas provide the biological identity of nanosized materials. Nature nanotechnology. 2012;7(12):779-86.

18. Docter D, Distler U, Storck W, Kuharev J, Wünsch D, Hahlbrock A, et al. Quantitative profiling of the protein coronas that form around nanoparticles. Nature protocols. 2014;9(9):2030.

19. Lundqvist M, Stigler J, Elia G, Lynch I, Cedervall T, Dawson KA. Nanoparticle size and surface properties determine the protein corona with possible implications for biological impacts. Proceedings of the National Academy of Sciences. 2008.

20. Sakulkhu U, Mahmoudi M, Maurizi L, Coullerez G, Hofmann-Amtenbrink M, Vries M, et al. Significance of surface charge and shell material of superparamagnetic iron oxide nanoparticle (SPION) based core/shell nanoparticles on the composition of the protein corona. Biomaterials science. 2015;3(2):265-78.

21. Aggarwal P, Hall JB, McLeland CB, Dobrovolskaia MA, McNeil SE. Nanoparticle interaction with plasma proteins as it relates to particle biodistribution, biocompatibility and therapeutic efficacy. Advanced drug delivery reviews. 2009;61(6):428-37. Epub 2009/04/21.

22. Thode K, Lück M, Semmler W, Müller RH, Kresse M. Determination of plasma protein adsorption on magnetic iron oxides: sample preparation. Pharmaceutical research. 1997;14(7):905-10.

23. Owens III DE, Peppas NA. Opsonization, biodistribution, and pharmacokinetics of polymeric nanoparticles. International journal of pharmaceutics. 2006;307(1):93-102.

24. Moghimi SM, Patel H. Serum-mediated recognition of liposomes by phagocytic cells of the reticuloendothelial system–the concept of tissue specificity. Advanced drug delivery reviews. 1998;32(1-2):45-60.

25. Chertok B, Cole AJ, David AE, Yang VC. Comparison of Electron Spin Resonance Spectroscopy and Inductively-Coupled Plasma Optical Emission

Spectroscopy for Biodistribution Analysis of Iron-Oxide Nanoparticles. Mol Pharmaceut. 2010;7(2):375-85.

26. Estevanato LL, Lacava LM, Carvalho LC, Azevedo RB, Silva O, Pelegrini F, et al. Long-term biodistribution and biocompatibility investigation of dextran-coated magnetite nanoparticle using mice as the animal model. Journal of biomedical nanotechnology. 2012;8(2):301-8. Epub 2012/04/21.

27. Quini CC, Prospero AG, Calabresi MFF, Moretto GM, Zufelato N, Krishnan S, et al. Real-time liver uptake and biodistribution of magnetic nanoparticles determined by AC biosusceptometry. Nanomedicine : nanotechnology, biology, and medicine. 2017;13(4):1519-29.

28. Reimer P, Balzer T. Ferucarbotran (Resovist): a new clinically approved RES-specific contrast agent for contrast-enhanced MRI of the liver: properties, clinical development, and applications. European radiology. 2003;13(6):1266-76. Epub 2003/05/24.

29. Yu M, Zheng J. Clearance Pathways and Tumor Targeting of Imaging Nanoparticles. ACS nano. 2015;9(7):6655-74. Epub 2015/07/08.

30. Longmire M, Choyke PL, Kobayashi H. Clearance properties of nano-sized particles and molecules as imaging agents: considerations and caveats. Nanomedicine (Lond). 2008;3(5):703-17. Epub 2008/09/27.

31. Brede C, Labhasetwar V. Applications of nanoparticles in the detection and treatment of kidney diseases. Advances in chronic kidney disease. 2013;20(6):454-65. Epub 2013/11/12.

32. Cigarroa RG, Lange RA, Williams RH, Hillis LD. Dosing of contrast material to prevent contrast nephropathy in patients with renal disease. The American journal of medicine. 1989;86(6 Pt 1):649-52. Epub 1989/06/01.

33. Manske CL, Sprafka JM, Strony JT, Wang Y. Contrast nephropathy in azotemic diabetic patients undergoing coronary angiography. The American journal of medicine. 1990;89(5):615-20. Epub 1990/11/01.

34. Neuwelt EA, Hamilton BE, Varallyay CG, Rooney WR, Edelman RD, Jacobs PM, et al. Ultrasmall superparamagnetic iron oxides (USPIOs): a future alternative magnetic resonance (MR) contrast agent for patients at risk for nephrogenic systemic fibrosis (NSF)? Kidney international. 2009;75(5):465-74. Epub 2008/10/10.

35. Hultman KL, Raffo AJ, Grzenda AL, Harris PE, Brown TR, O'Brien S. Magnetic resonance imaging of major histocompatibility class II expression in the renal medulla using immunotargeted superparamagnetic iron oxide nanoparticles. ACS nano. 2008;2(3):477-84. Epub 2009/02/12.

36. Kobayashi H, Jo SK, Kawamoto S, Yasuda H, Hu X, Knopp MV, et al. Polyamine dendrimer-based MRI contrast agents for functional kidney imaging to diagnose acute renal failure. J Magn Reson Imaging. 2004;20(3):512-8. Epub 2004/08/28.

37. Dear JW, Kobayashi H, Brechbiel MW, Star RA. Imaging acute renal failure with polyamine dendrimer-based MRI contrast agents. Nephron Clinical practice. 2006;103(2):c45-9. Epub 2006/03/18.

38. Hauger O, Delalande C, Trillaud H, Deminiere C, Quesson B, Kahn H, et al. MR imaging of intrarenal macrophage infiltration in an experimental model of nephrotic syndrome. Magnetic resonance in medicine. 1999;41(1):156-62. Epub 1999/02/20.

39. Serkova NJ, Renner B, Larsen BA, Stoldt CR, Hasebroock KM, Bradshaw-Pierce EL, et al. Renal Inflammation: Targeted Iron Oxide Nanoparticles for Molecular MR Imaging in Mice. Radiology. 2010;255(2):517-26.

40. Schroeder U, Sommerfeld P, Ulrich S, Sabel BA. Nanoparticle technology for delivery of drugs across the blood-brain barrier. Journal of pharmaceutical sciences. 1998;87(11):1305-7. Epub 1998/11/13.

41. Tabatabaei SN, Girouard H, Carret AS, Martel S. Remote control of the permeability of the blood-brain barrier by magnetic heating of nanoparticles: A proof of concept for brain drug delivery. Journal of controlled release : official journal of the Controlled Release Society. 2015;206:49-57. Epub 2015/03/01.

42. Wohlfart S, Khalansky AS, Gelperina S, Maksimenko O, Bernreuther C, Glatzel M, et al. Efficient chemotherapy of rat glioblastoma using doxorubicin-loaded PLGA nanoparticles with different stabilizers. PLoS One. 2011;6(5):e19121.

43. Mangraviti A, Gullotti D, Tyler B, Brem H. Nanobiotechnology-based delivery strategies: New frontiers in brain tumor targeted therapies. Journal of controlled release : official journal of the Controlled Release Society. 2016.

44. Kim JS, Yoon TJ, Yu KN, Kim BG, Park SJ, Kim HW, et al. Toxicity and tissue distribution of magnetic nanoparticles in mice. Toxicological sciences : an official journal of the Society of Toxicology. 2006;89(1):338-47. Epub 2005/10/21.

45. Prospero AG, Quini CC, Bakuzis AF, Fidelis-de-Oliveira P, Moretto GM, Mello FP, et al. Real-time in vivo monitoring of magnetic nanoparticles in the bloodstream by AC biosusceptometry. Journal of nanobiotechnology. 2017;15(1):22.

46. Jain TK, Richey J, Strand M, Leslie-Pelecky DL, Flask CA, Labhasetwar V. Magnetic nanoparticles with dual functional properties: Drug delivery and magnetic resonance imaging. Biomaterials. 2008;29(29):4012-21.

47. Weizenecker J, Gleich B, Rahmer J, Dahnke H, Borgert J. Three-dimensional real-time in vivo magnetic particle imaging. Physics in medicine and biology. 2009;54(5):L1-L10. Epub 2009/02/11.

48. Marciani L. Assessment of gastrointestinal motor functions by MRI: a comprehensive review. Neurogastroent Motil. 2011;23(5):399-407.

49. Saritas EU, Goodwill PW, Zhang GZ, Yu W, Conolly SM. Safety Limits for Human-Size Magnetic Particle Imaging Systems. Springer Proceedings in Physics. 2012;140(Magnetic Particle Imaging):325-30.

50. Lyu X, Wang Z, Wei SF, Deng L, Yang WH. Design and Optimization for a Novel Field Free Line Generation Magnet for Human Target Clinical MPI-A Preliminary Study. Ieee T Magn. 2014;50(11).

51. Wenger MA, Henderson EB, Dinning JS. Magnetometer Method for Recording Gastric Motility. Science. 1957;125(3255):990-1.

52. Wenger MA, Clemens TL, Cullen TD, Engel BT. Stomach Motility in Man as Recorded by Magnetometer Method. Gastroenterology. 1961;41(5):479-&.

53. Benmair Y, Dreyfuss F, Fischel B, Frei EH, Gilat T. Study of Gastric-Emptying Using a Ferromagnetic Tracer. Gastroenterology. 1977;73(5):1041-5.

54. Benmair Y, Fischel B, Frei EH, Gilat T. Evaluation of a Magnetic Method for Measurement of Small Intestinal Transit-Time. Am J Gastroenterol. 1977;68(5):470-5.

55. Americo MF, Oliveira RB, Romeiro FG, Baffa O, Cora LA, Miranda JR. Scintigraphic validation of AC Biosusceptometry to study the gastric motor activity and the intragastric distribution of food in humans. Neurogastroenterology and motility : the official journal of the European Gastrointestinal Motility Society. 2007;19(10):804-11. Epub 2007/09/22.

56. Miranda JRA, Oliveira RB, Sousa PL, Braga FJH, Baffa O. A novel biomagnetic method to study gastric antral contractions. Physics in medicine and biology. 1997;42(9):1791-9.

57. Andreis U, Americo MF, Cora LA, Oliveira RB, Baffa O, Miranda JR. Gastric motility evaluated by electrogastrography and alternating current biosusceptometry in dogs. Physiological measurement. 2008;29(9):1023-31. Epub 2008/08/14.

58. Baffa O, Oliveira RB, Miranda JR, Troncon LE. Analysis and development of AC biosusceptometer for orocaecal transit time measurements. Medical & biological engineering & computing. 1995;33(3):353-7. Epub 1995/05/01.

59. Miquelin CA, Braga FJ, Dantas RO, Oliveira RB, Baffa O. Pharyngeal clearance and pharyngeal transit time determined by a biomagnetic method in normal humans. Dysphagia. 2001;16(4):308-12. Epub 2001/11/27.

60. Quini CC, Americo MF, Cora LA, Calabresi MFF, Alvarez M, Oliveira RB, et al. Employment of a noninvasive magnetic method for evaluation of gastrointestinal transit in rats. Journal of biological engineering. 2012;6(1).

61. Miranda JRA, Oliveira RB, Matsuda NM, Baffa O. Susceptometric Measurement of Gastric-Emptying. Int Congr Ser. 1992;988:635-8.

62. Cora A, Andreis U, Romeiro FG, Americo MF, Oliveira RB, Baffa O, et al. Magnetic images of the disintegration process of tablets in the human stomach by ac biosusceptometry. Physics in medicine and biology. 2005;50(23):5523-34.

63. Cora LA, Americo MF, Oliveira RB, Baffa O, Moraes R, Romeiro FG, et al. Disintegration of magnetic tablets in human stomach evaluated by alternate current Biosusceptometry. European Journal of Pharmaceutics and Biopharmaceutics. 2003;56(3):413-20.

64. Cora LA, Americo MF, Romeiro FG, Oliveira RB, Miranda JRA. Pharmaceutical applications of AC Biosusceptometry. European Journal of Pharmaceutics and Biopharmaceutics. 2010;74(1):67-77.

65. Quini CC, Matos JF, Próspero AG, Calabresi MF, Zufelato N, Bakuzis AF, et al. Renal perfusion evaluation by alternating current biosusceptometry of magnetic nanoparticles. J Magn Magn Mater. 2014.

66. Quini CC, Matos JF, Prospero AG, Calabresi MFF, Zufelato N, Bakuzis AF, et al. Renal perfusion evaluation by alternating current biosusceptometry of magnetic nanoparticles. J Magn Magn Mater. 2015;380:2-6.

67. Quini CC. Análise dinâmica da perfusão e biodistribuição de nanopartículas magnéticas por biosusceptometria AC. Botucatu - SP: Universidade Estadual Paulista "Júlio de Mesquita Filho"; 2015.

68. Quini CC, Próspero AG, Kondiles BR, Chaboub L, Hogan MK, Baffa O, et al. Development of a protocol to assess cell internalization and tissue uptake of magnetic nanoparticles by AC Biosusceptometry. J Magn Magn Mater. 2019;473:527-33.

69. Lee JH, Huh YM, Jun Y, Seo J, Jang J, Song HT, et al. Artificially engineered magnetic nanoparticles for ultra-sensitive molecular imaging. Nat Med. 2007;13(1):95-9.